

# Shaping manifolds in equivariant recurrent neural networks

Arianna Di Bernardo<sup>1</sup>, Adrian Valente<sup>1</sup>, Francesca Mastrogiovanni<sup>2</sup>, and Srdjan Ostojic<sup>1</sup>

<sup>1</sup>Laboratoire de Neurosciences Cognitives et Computationnelles, INSERM U960, École Normale Supérieure - PSL Research University, 75005 Paris, France

<sup>2</sup>SISSA - Theoretical and Scientific Data Science, Via Bonomea 265, 34136 Trieste, Italy

November 10, 2025

## ABSTRACT

Recordings of increasingly large neural populations have revealed that the firing of individual neurons is highly coordinated. When viewed in the space of all possible patterns, the collective activity forms non-linear structures called neural manifolds. Because such structures are observed even at rest or during sleep, an important hypothesis is that activity manifolds may correspond to continuous attractors shaped by recurrent connectivity between neurons. Classical models of recurrent networks have shown that continuous attractors can be generated by specific symmetries in the connectivity. Although a variety of attractor network models have been studied, general principles linking network connectivity and the geometry of attractors remain to be formulated. Here, we address this question by using group representation theory to formalize the relationship between the symmetries in recurrent connectivity and the resulting fixed-point manifolds. We start by revisiting the classical ring model, a continuous attractor network generating a circular manifold. Interpreting its connectivity as a circular convolution, we draw a parallel with feed-forward convolutional neural networks. Building on principles of geometric deep learning, we then generalize this architecture to a broad range of symmetries using group representation theory. Specifically, we introduce a new class of *equivariant recurrent neural networks*, where the connectivity is based on group convolution. Using the group Fourier transform, we reduce such networks to low-rank models. This formulation gives us a low-dimensional non-linear description that can be fully analyzed to determine the symmetry, dimensionality and stability of fixed-point manifolds. Our results underline the importance of stability considerations: for a connectivity with a given symmetry, depending on parameters, several manifolds with different symmetry subgroups can coexist, some stable and others consisting of saddle points. Our framework unifies a variety of existing models and offers a principled approach to build new types of continuous attractor models of neural systems.

## Introduction

Neural computations rely on the collective dynamics of populations of neurons, which exhibit rich structure in their coordinated activity (Vyas et al. 2020, Chung & Abbott 2021, Ostoic & Fusi 2024, Duncker & Sahani 2021). Large scale recordings in a variety of species and brain areas have identified a prominent type of structure, in which population activity is organized along low-dimensional manifolds in the space of all possible firing patterns (Jazayeri & Ostoic 2021, Perich et al. 2025). Such neural manifolds have in particular been observed in systems representing and manipulating continuous variables, such as the oculo-motor integrator (Seung et al. 2000, Seung 1996), the head direction system (Chaudhuri et al. 2019, Rubin et al. 2019), the entorhinal cortex (Gardner et al. 2022, Hermansen et al. 2024), the primary visual cortex (Blumenfeld et al. 2006, Dipoppa et al. 2025), motor cortex (Churchland et al. 2012, Gallego et al. 2017) or working memory (Wimmer et al. 2014, Cueva et al. 2021). Because they are often observed even when the animal is at rest or sleeping (Chaudhuri et al. 2019, Trettel et al. 2019), an important hypothesis posits that these manifolds of activity may correspond to continuous sets of stable states - or attractors - generated by recurrent connectivity in the underlying networks (Khona & Fiete 2022, Langdon et al. 2023). To identify the underlying mechanisms, a range of continuous attractor network (CAN) models have been developed for various systems that encode continuous variables (Amari 1977, Ben-Yishai et al. 1995, Zhang 1996, Compte et al. 2000, Burak & Fiete 2009, Stringer et al. 2002, Wu et al. 2016, Couey et al. 2013, Ságodi et al. 2024, Si et al. 2014, Xie et al. 2002, Romani & Tsodyks 2010, Spalla et al. 2021). In these models, the geometry of the resulting activity manifolds is naturally linked to the symmetries of the continuous variable being encoded, and arises from either explicit or implicit symmetries in the recurrent connectivity (Darshan & Rivkind 2022, Clark et al. 2025). General, unifying principles linking the properties of encoded variables to the symmetry in network connectivity and the geometry of the resulting attractor manifolds however remain to be formulated.

Remarkably, a set of such unifying principles has been proposed in the adjacent field of artificial neural networks, and assembled within the framework of Geometric Deep Learning (Bronstein et al. 2021). Starting from the premise that classical convolutional neural networks (CNNs) extract invariant features from images based on the symmetries of the physical world, GDL developed an abstract formulation of CNNs using the language of group theory. This broad generalization of CNNs then enabled GDL to derive feed-forward network architectures based on the symmetries and invariances present in a vast set of problems beyond classical image classification. These principles were in particular applied to derive spherical CNNs (Cohen, Geiger, Köhler & Welling 2018), different types of graph neural networks (Scarselli et al. 2009, Monti et al. 2017), or networks operating on arbitrary sets (Segol & Lipman 2020). More recently, these principles have been extended beyond static transformations to recurrent architectures that handle temporal symmetries, addressing scaling equivariance (Zuo et al. 2023) and flow equivariance (Keller 2025) in sequence processing.

Here we build on the theory of Geometric Deep Learning to formalize the general relationship between the symmetries in connectivity of a recurrent neural network and the resulting manifolds of fixed points. We start by revisiting the classical ring model, a continuous attractor network which generates a circular manifold (Ben-Yishai et al. 1995), and extract the key underlying ingredients: (i) neurons are indexed by a one-dimensional angular variable; (ii) the recurrent connectivity has the structure of a circular convolution (Zhang et al. 2022); (iii) this confers translational symmetry to the set of attractors of the dynamics; (iv) expanding the convolutional connectivity on Fourier modes leads to a low-dimensional description that allows for an analysis of the stability and dimensionality of fixed-point solutions (Mastrogiuseppe & Ostoic 2018). By formulating the classical ring model in the GDL language, we then generalize it to a broad range of continuous variables and symmetries using the theory of group representations. Specifically, we introduce a new class of *equivariant recurrent neural networks*, where the connectivity is defined via a group convolution (Kondor & Trivedi 2018), which confers group symmetry to the manifolds of fixed points. Using the concept of group Fourier transform, the network can then be reduced to a low-dimensional model, which preserves the original symmetries and determines the manifold's dimensionality, geometry and stability. As concrete examples, we apply this approach to derive toroidal and spherical RNN models. Analyzing the low-dimensional dynamics, we show that connectivity with the same symmetry can generate a variety of manifolds with different dimensionalities and geometries. More generally, our framework reveals the importance of non-linearity for relating connectivity to emerging manifolds, and offers a new method to generate models of neural systems.

## 1 Recurrent neural networks

Throughout this manuscript, we consider recurrent neural networks (RNNs) consisting of  $N$  interacting neurons evolving in discrete time. The activation of neuron  $i$  at time  $t$  is denoted as  $x_i^t \in \mathbb{R}$ , and the dynamics are given by:

$$x_i^{t+1} = x_i^t + \Delta t(-x_i^t + F_i^t) \quad i = 0, \dots, N-1, \quad (1)$$

where

$$F_i^t = \frac{1}{N} \sum_{j=0}^{N-1} J_{ij} \Phi[x_j^t] \quad (2)$$

is the recurrent input to neuron  $i$  at time-step  $t$ , with  $J_{ij} \in \mathbb{R}$  the connection strength from neuron  $j$  to neuron  $i$ , and  $\Phi : \mathbb{R} \rightarrow \mathbb{R}$  the non-linear function transforming the activation of each unit into its firing rate. The general framework is independent of the form of  $\Phi$ , but for specific examples we use  $\Phi[x] = 1 + \tanh[x]$ .

## 2 Ring models as convolutional RNNs

In this section, we revisit ring models, the most fundamental type of continuous attractor networks (Amari 1977, Ben-Yishai et al. 1995, Zhang 1996). We formulate this class of models within the language of geometric deep learning (Bronstein et al. 2021), and outline their relation with convolutional neural networks (CNNs). We outline how the symmetry properties of CNNs - in particular their equivariance (Cohen & Welling 2016) - induce structure in the sets of fixed points in ring models that we denote as *fixed point manifolds*. Expanding the recurrent connectivity on Fourier modes, we then introduce *low-rank ring models*, and show how this subset of ring models leads to an explicit parametrization of fixed point manifolds.

### 2.1 Convolutional structure of ring models

Ring models are a subclass of recurrent neural networks in which each neuron  $i$  is labeled by an angle  $\theta_i = \frac{2\pi i}{N}$  for  $i = 0, \dots, N-1$ , so that the network can be visualised as lying on a ring (Fig. 1 A). Following the language of geometric deep learning (Bronstein et al. 2021), here we formalize the collective activation in the network as a function of neural labels. Writing  $\Omega = \{\theta_i = \frac{2\pi i}{N} | i = 0, \dots, N-1\}$ , we represent the network activity at time  $t$  as a function  $x^t : \Omega \rightarrow \mathbb{R}$  such that the activation of neuron  $i$  is obtained by applying  $x^t$  to its angular label  $\theta_i$ :

$$x^t : \theta \mapsto x^t(\theta) \quad \text{such that} \quad x^t(\theta_i) = x_i^t.$$

The firing rate and the collective recurrent input in the network can be similarly expressed as functions  $\Phi^t$  and  $F^t : \Omega \rightarrow \mathbb{R}$  such that, for neuron  $i$  at time  $t$ , the firing rate is given by  $\Phi^t(\theta_i) = \Phi[x^t(\theta_i)] = \Phi[x_i^t]$  and the recurrent input is  $F^t(\theta_i) = F_i^t$  defined in Eq. (2). Since  $\Phi^t$  and  $F^t$  depend intrinsically on the neural activity at time  $t$ , they can be expressed in terms of time-independent operators  $\mathcal{P}$  and  $\mathcal{F}$  applied to  $x^t$ :

$$\mathcal{P} : x^t \mapsto \Phi^t \quad \Phi^t = \mathcal{P}[x^t] \quad (3)$$

$$\mathcal{F} : x^t \mapsto F^t \quad F^t = \mathcal{F}[x^t]. \quad (4)$$

Denoting as  $L_{\mathbb{R}(\Omega)}$  the space of square-integrable functions  $\{f : \Omega \rightarrow \mathbb{R}\}$ , we have  $x^t, F^t \in L_{\mathbb{R}(\Omega)}$  and  $\mathcal{P}, \mathcal{F} : L_{\mathbb{R}(\Omega)} \rightarrow L_{\mathbb{R}(\Omega)}$ . In the following, we identify the set of  $2\pi$ -periodic functions  $\mathbb{R} \rightarrow \mathbb{R}$  with the set  $L_{\mathbb{R}(\Omega)}$  of functions  $\Omega \rightarrow \mathbb{R}$ . Because the functional  $\mathcal{P}$  is obtained by applying  $\Phi$  "pointwise" to  $x^t$  (i.e. the value of  $\Phi^t$  at  $\theta_i$  depends only on the value of  $x^t$  at  $\theta_i$ ), in the following we write  $\Phi^t = \Phi[x^t]$ .

With these notations, the network dynamics in Eq. (1) can therefore be formulated as a temporal evolution within  $L_{\mathbb{R}(\Omega)}$ :

$$x^{t+1} = x^t + \Delta t(-x^t + \mathcal{F}[x^t]). \quad (5)$$

A key ingredient of ring models is that the connection strength  $J_{ij}$  from neuron  $j$  to neuron  $i$  depends only on the difference  $\theta_i - \theta_j$  between their angular variables:

$$J_{ij} = c(\theta_i - \theta_j), \quad (6)$$

where  $c : \mathbb{R} \rightarrow \mathbb{R}$  is a  $2\pi$ -periodic function, which we call the *connectivity kernel*. Classical examples for  $c$  are a shifted cosine (Ben-Yishai et al. 1995) or a circular Gaussian (Amari 1977). We moreover assume that  $c$  is even, which is equivalent to having a symmetric connectivity matrix and ensures the existence of fixed points.

The specific connectivity structure in Eq. (6) confers a periodicity and symmetry to ring models: each neuron  $i$  in the network receives connections from other neurons through the same set of weights, translated by an angle  $\theta_i$  (Fig. 1 C). Equivalently, the connectivity matrix  $J$  is circulant, meaning that each row is obtained by shifting the previous row (Fig. 1 B).

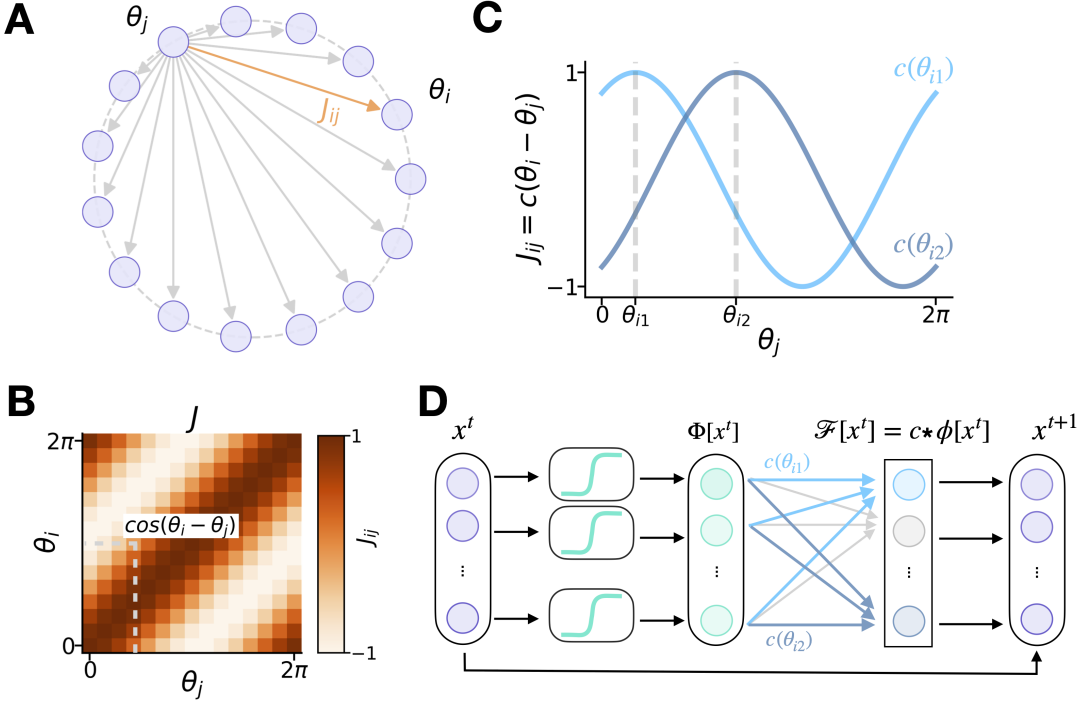


Figure 1: A) Ring structure of neurons with recurrent connectivity where the weight  $J_{ij}$  between neurons  $i$  and  $j$  only depends on their angular distance. B) Connectivity matrix showing cosine-shaped weights as a function of neuron indices. C) Connectivity weights of selected neurons share the same connectivity profile, but shifted according to their preferred angle. D) Feed-forward implementation of recurrent dynamics. The recurrent input is computed by applying point-wise non-linearity  $\Phi$  to input  $x$ , then convolving with shifted connectivity profiles  $c(\theta_i)$  corresponding to each neuron's preferred angle.

The recurrent input  $F_i^t$  to neuron  $i$  in Eq. (2) can therefore be written as

$$F_i^t = \frac{1}{N} \sum_{j=0}^{N-1} J_{ij} \Phi[x_j^t] \quad (7)$$

$$= \frac{1}{N} \sum_{\theta' \in \Omega} c(\theta_i - \theta') \Phi[x^t(\theta')] \quad (8)$$

$$= \frac{1}{N} \sum_{\theta' \in \Omega} c(\theta_i - \theta') \Phi^t(\theta')$$

$$= F^t(\theta_i)$$

$$= \mathcal{F}[x^t](\theta_i)$$

so that  $\mathcal{F}[x^t]$  is given by the *convolution* between the kernel  $c$  and the firing rate  $\Phi^t$  of the network:

$$\mathcal{F}[x^t] = c * \Phi^t. \quad (9)$$

The convolution between two functions  $f_1, f_2 \in L_{\mathbb{R}(\Omega)}$ , is a function  $f_1 * f_2 : \Omega \rightarrow \mathbb{R}$  defined as

$$(f_1 * f_2)(\theta) = \frac{1}{N} \sum_{\theta' \in \Omega} f_1(\theta - \theta') f_2(\theta').$$

In Eq. (9),  $f_1 = c$  and  $f_2 = \Phi^t = \Phi[x^t]$ .

The recurrent input  $F^t$  at time-step  $t$  is therefore obtained by applying to the activation  $x^t$  the point-wise non-linear function  $\Phi$ , followed by a convolution with the kernel  $c$ . This is equivalent to applying to the set of activities  $\{x_i^t\}_{i=0, \dots, N-1}$  a single-layer feed-forward convolutional neural network, in which the order of the convolution and point-wise non-linearity are reversed with respect to standard CNNs. The output of that CNN is the set of recurrent inputs  $\{F_i^t\}_{i=0, \dots, N-1}$  (Fig. 1 D).

In the limit  $N \rightarrow \infty$ ,  $x^t, \Phi^t, c$  and  $F^t$  become functions on the continuous set  $\Omega = [0, 2\pi]$ . In that limit, the discrete sum over  $\Omega$  in Eq. (8) is replaced by an integral (Gerstner et al. 2014).

$$F^t(\theta) = \frac{1}{2\pi} \int_{\theta' \in \Omega} c(\theta - \theta') \Phi[x^t(\theta')] d\theta'. \quad (10)$$

For  $N \rightarrow \infty$ , the recurrent input is obtained by applying to  $x^t$  the point-wise non-linearity  $\Phi$ , followed by a continuous convolution with the kernel  $c$ . Following the formalism of geometric deep learning (Bronstein et al. 2021), this sequence of operations can be interpreted as a continuous-valued CNN (Monti et al. 2017). Throughout this study we will assume that this limit is well-defined, and we will interchangeably consider domains  $\Omega$  corresponding to finite and infinite  $N$ .

Altogether, the recurrent input in ring models has the form of a single layer CNN that can be either discrete or continuous. Ring models are therefore closely related to feed-forward convolutional neural networks and form a class of models that we denote as convolutional RNNs. In particular, ring models directly inherit the symmetry properties of convolutional neural networks.

## 2.2 Equivariance under angular translations

A central property of feed-forward convolutional networks is that a translation of their input leads to an equivalent translation of their output. This property is more generally called *equivariance* (Cohen & Welling 2016). Since the recurrent input  $\mathcal{F}$  in ring models has the form of a CNN, it directly inherits the equivariance property. Using the language of geometric deep-learning (Bronstein et al. 2021), here we formulate more formally the equivariance of the recurrent input  $\mathcal{F}$  under translations of the activity in the network.

The operator  $\mathcal{F}$  defined in Eqs. (4) and (8) takes as input the activation  $x^t$  of the network, and outputs the recurrent input  $F^t$ . As  $x^t$  is a function of an angle  $\theta \in \Omega$ , an angular translation by an angle  $\phi \in \Omega$  is obtained by mapping any  $\theta \in \Omega$  to  $\theta + \phi$  modulo  $2\pi$ . More formally, we represent this angular translation by the function  $g_\phi : \Omega \rightarrow \Omega$  defined by

$$g_\phi : \theta \mapsto \theta' \quad \theta' = \theta + \phi \bmod(2\pi).$$

For later reference, it is important to note that the set of all angular translations  $G = \{g_\phi | \phi \in \Omega\}$  has some remarkable properties, which confer to it the structure of a *group* (Kosmann-Schwarzbach 2009). In particular, composing any pair of angular translations  $g_{\phi_1}, g_{\phi_2}$  yields an angular translation by the angle  $\phi_1 + \phi_2$ :

$$g_{\phi_1} g_{\phi_2} = g_{\phi_1 + \phi_2}. \quad (11)$$

Moreover, any translation  $g_\phi$  can be inverted by a translation  $g_{-\phi}$ , so that

$$g_\phi^{-1} = g_{-\phi}. \quad (12)$$

Angular translations on  $\Omega$  naturally induce transformations of functions in  $L_{\mathbb{R}(\Omega)}$ . Indeed any translation  $g_\phi$  maps any function  $f \in L_{\mathbb{R}(\Omega)}$  to a translated function  $S_\phi[f] : \Omega \rightarrow \mathbb{R}$  defined by

$$S_\phi[f] : \theta \mapsto f(g_{-\phi}(\theta)) = f(\theta') \quad \text{with} \quad \theta' = \theta - \phi \bmod(2\pi). \quad (13)$$

The operator  $S_\phi : L_{\mathbb{R}(\Omega)} \rightarrow L_{\mathbb{R}(\Omega)}$  is more generally called the *action* of the translation  $g_\phi$  on functions in  $L_{\mathbb{R}(\Omega)}$ . In particular, applying  $S_\phi$  to  $x^t$  yields the network activation profile translated by  $\phi$ , while applying  $S_\phi$  to the kernel  $c$

translates the connectivity by  $\phi$  and therefore yields the profile of incoming connection strengths to the neuron indexed by  $\phi$  (Eq. (6)).

With these definitions, we can formulate more formally the equivariance property of  $\mathcal{F}$ , which states that a translation of the activation profile  $x^t$  by  $\phi$  leads to a translation of the recurrent input  $F^t$  by the same angle  $\phi$ . Using the operator  $S_\phi$  to express an angular translation by  $\phi$ , the equivariance of  $\mathcal{F}$  corresponds to the fact that the operators  $\mathcal{F}$  and  $S_\phi$  commute for any  $\phi$ :

$$\mathcal{F}S_\phi = S_\phi\mathcal{F} \quad \forall\phi \in \Omega. \quad (14)$$

This property stems directly from the fact that  $\mathcal{F}$  has the form of a convolution, i.e. an angular translation of the kernel  $c$  (Eq. (10)). Indeed,  $\forall x \in L_{\mathbb{R}(\Omega)}$  and  $\forall\theta, \phi \in \Omega$ , we have

$$\begin{aligned} \mathcal{F}[S_\phi[x]](\theta) &= c * \Phi[S_\phi[x]](\theta) \\ &= \frac{1}{N} \sum_{\theta' \in \Omega} c(\theta - \theta') \Phi[S_\phi[x](\theta')] \\ &= \frac{1}{N} \sum_{\theta' \in \Omega} c(\theta - \theta') \Phi[x(\theta'')] \quad \text{with } \theta'' = \theta' - \phi \bmod(2\pi) \\ &= \frac{1}{N} \sum_{\theta'' \in \Omega} c((\theta - \theta'') - \phi) \Phi[x(\theta'')] \\ &= \frac{1}{N} \sum_{\theta'' \in \Omega} S_\phi[c](\theta - \theta'') \Phi[x(\theta'')] \\ &= S_\phi[\mathcal{F}[x]](\theta). \end{aligned}$$

Here we used the definition of  $\mathcal{F}$  (Eq. (8)), the definition of  $S_\phi$  (Eq. (13)), and the fact that  $c$  is  $2\pi$ -periodic.

### 2.3 Structure of fixed points

The equivariance of the recurrent input has direct consequences on the structure of fixed points in the ring model. Indeed from Eqs. (1) and (5), an activation profile  $x^* \in L_{\mathbb{R}(\Omega)}$  is a fixed point of the dynamics if it obeys

$$x^*(\theta) = \mathcal{F}[x^*](\theta) \quad \forall\theta \in \Omega. \quad (15)$$

The equivariance of  $\mathcal{F}$  directly implies that, if  $x^*$  is a fixed point, then the translated activation profile  $S_\phi x^*$  is also a fixed point. Indeed

$$\begin{aligned} \mathcal{F}(S_\phi x^*) &= S_\phi \mathcal{F}(x^*) \\ &= S_\phi x^*, \end{aligned}$$

where the first equality follows from the equivariance property of  $\mathcal{F}$  (Eq. (14)), and the second one follows from the fact that  $x^*$  is a fixed point (Eq. (15)). Intuitively, because the interactions depend only on the difference between angular labels, shifting the activation profile  $x^*$  by an angle  $\phi$  leads to an activation profile  $S_\phi x^*$  that is equivalently a fixed point. Unless the activation profile  $x^*$  is uniform over  $\Omega$ ,  $S_\phi x^*$  will correspond to a distinct fixed point. This means that if a given bump of activations is a fixed point of the dynamics, any shift of that bump will also be a fixed point of the dynamics.

The convolutional structure of ring models therefore induces the existence of sets of fixed points, within which different fixed points are related by angular translations. Each such set is obtained by starting from a fixed point  $x^*$  and applying shift operators  $S_\phi$  for  $\phi \in \Omega$ . Denoting  $x^*$  as the seed, the corresponding set of fixed points  $\mathcal{M}_{x^*}$  is defined by

$$\mathcal{M}_{x^*} = \{S_\phi x^* \mid \phi \in \Omega\}. \quad (16)$$

If  $x^*$  is non-uniform over  $\Omega$ ,  $\mathcal{M}_{x^*}$  consists of more than one fixed point. For finite  $N$ ,  $\mathcal{M}_{x^*}$  is in general a finite set because  $\Omega$  is finite (but see [Noorman et al. \(2024\)](#)). For  $N \rightarrow \infty$ ,  $\mathcal{M}_{x^*}$  becomes a manifold of intrinsic dimension 1, parametrized by the angular parameter  $\phi \in [0, 2\pi)$ . By abuse of language, we will denote  $\mathcal{M}_{x^*}$  as a *fixed-point manifold* for both finite and infinite networks.

## 2.4 Fourier transform of convolutional RNNs

The equivariance of ring models can give rise to fixed-point manifolds parametrized by an angle  $\phi \in \Omega$ . The specific shape of these manifolds in general depends on the connectivity kernel  $c$  and the seed fixed point  $x^*$ . To characterize in more detail the shape of the manifolds, we will turn to a restricted class of ring models that we denote as *low-rank convolutional RNNs*. To define this class of models, we start by introducing the Fourier representation of general ring models.

Any function  $f : \Omega \rightarrow \mathbb{R}$  can be expressed in terms of its Fourier components  $\hat{f}_r$  for  $r = 0, 1, \dots$ . Distinguishing even and odd indices as  $r = 2k$  and  $r = 2k - 1$  for  $k = 0, 1, \dots$ , we write the Fourier components as :

$$\hat{f}_0 = \frac{1}{2\pi} \int_{\Omega} f(\theta) d\theta, \quad (17)$$

$$\hat{f}_{2k-1} = \frac{1}{2\pi} \int_{\Omega} f(\theta) \cos(k\theta) d\theta, \quad (18)$$

$$\hat{f}_{2k} = \frac{1}{2\pi} \int_{\Omega} f(\theta) \sin(k\theta) d\theta. \quad (19)$$

Denoting as  $\hat{c}_r, \kappa_r, \hat{\Phi}_r^t, \hat{F}_r^t$  the Fourier components of the connectivity kernel  $c$ , the activation  $x^t$ , the firing rate  $\Phi(x^t)$  and the recurrent input  $F^t$  at time  $t$ , we next express the dynamics in the ring network in terms of these quantities.

Since we assumed that the connectivity kernel  $c$  is even, only cosine terms have non-zero coefficients, i.e.  $\hat{c}_r = 0$  for  $r$  even. Since  $F^t$  is a convolution between  $c$  and  $\Phi^t$  (Eq. (10)), from the convolution theorem (Bracewell & Kahn 1966) we have

$$\hat{F}_{2k-1}^t = \hat{c}_{2k-1} \hat{\Phi}_{2k-1}^t \quad (20)$$

$$\hat{F}_{2k}^t = \hat{c}_{2k} \hat{\Phi}_{2k}^t. \quad (21)$$

The RNN dynamics can then be formulated in terms of the evolution of Fourier components  $\kappa_r^t$  of  $x^t$ . Taking the Fourier transform of Eq. (1), these dynamics read

$$\kappa_r^{t+1} = \kappa_r^t + \Delta t(-\kappa_r^t + \hat{F}_r^t) \quad r = 0, 1, \dots \quad (22)$$

In particular, the Fourier components  $\kappa_r$  of any fixed point solution  $x^*$  obey

$$\kappa_r = \hat{F}_r \quad r = 0, 1, \dots \quad (23)$$

where  $\hat{F}_r$  depends implicitly on  $x^*$  (Eqs. (20),(21)) and therefore on all its Fourier components. Eq. (23) is therefore a system of an infinite number of coupled equations and hence in general intractable. We next introduce a restricted class of models for which this system becomes finite and tractable.

## 2.5 Low-rank convolutional RNNs

A particular sub-class of ring models is obtained by restricting the connectivity kernel  $c$  to have only a finite number  $K + 1$  of non-zero Fourier terms in Eq. (17). This is the case, for instance, in Ben-Yishai et al. (1995) where only the zero-th and first term are non-zero, so that  $K = 1$ . We call this class of networks *low-rank convolutional RNNs* because their connectivity matrices are of rank  $R = 2K + 1$  (Mastrogiuseppe & Ostojic 2018) (see Appendix B).

For low-rank convolutional RNNs,  $\hat{c}_r = 0$  for  $r > 2K$ , and therefore from at steady-state  $\kappa_r = 0$  for  $r > 2K$ . Eq. (23) then reduces to a system of  $R$  equations for the  $R$  first Fourier components  $\kappa_r$  which we group in a  $R$ -dimensional vector  $\underline{\kappa}$ . To express Eq. (23) explicitly as function of  $\kappa_r$ ,  $r = 0, \dots, R - 1$ , we write the inverse Fourier transform for the fixed-point activation  $x^*$ :

$$x^*(\theta) = \kappa_0 + \sum_{k=1}^K (\kappa_{2k-1} \cos(k\theta) + \kappa_{2k} \sin(k\theta)). \quad (24)$$

Using Eq. (20), for  $r = 2k - 1$  with  $k = 1 \dots R$  we have

$$\begin{aligned}
\hat{F}_{2k-1}(\underline{\kappa}) &= \hat{c}_{2k-1} \frac{1}{2\pi} \int \cos(k\theta) \Phi[x^*(\theta)] d\theta \\
&= \frac{\hat{c}_{2k-1}}{2\pi} \int \cos(k\theta) \Phi \left[ \kappa_0 + \sum_{k'=1}^K \kappa_{2k'-1} \cos(k'\theta) + \kappa_{2k'} \sin(k'\theta) \right] d\theta.
\end{aligned} \tag{25}$$

In Eq. (25) we used the definition of the Fourier transform of  $\Phi^t$  at the steady state (Eq. (20)). In Eq. (25) we replaced  $x^*$  with its inverse Fourier transform given in Eq. (24).

Similarly, from Eq. (20), for  $r = 2k$  with  $k = 1 \dots R$  we have

$$\begin{aligned}
\hat{F}_{2k}(\underline{\kappa}) &= \hat{c}_{2k-1} \frac{1}{2\pi} \int \sin(k\theta) \Phi[x^*(\theta)] d\theta \\
&= \frac{\hat{c}_{2k-1}}{2\pi} \int \sin(k\theta) \Phi \left[ \kappa_0 + \sum_{k'=1}^K \kappa_{2k'-1} \cos(k'\theta) + \kappa_{2k'} \sin(k'\theta) \right] d\theta.
\end{aligned} \tag{26}$$

Inserting Eqs. (25) and (26) into Eq. (23) yields a set of  $R$  coupled non-linear equations for  $\kappa_r$ ,  $r = 0 \dots R-1$ . For special choices of the non-linear function  $\Phi$ , the integrals in Eqs. (25) and (26) can be computed analytically, leading to explicit formulas for the functions  $\hat{F}_r$  (Ben-Yishai et al. 1995).

## 2.6 Fixed-point manifolds in low-rank convolutional RNNs

Restricting the ring model to be of low rank allows us to characterize more explicitly the structure of the fixed point manifolds generated by applying the angular translation operator  $S_\phi$  to a non-trivial fixed point  $x^*$  (Eq. (16)).

The angular translation  $S_\phi$  of  $x^*$  directly induces a linear transformation of its Fourier components.

Directly applying  $S_\phi$  to the inverse Fourier transform of  $x^*$ , we have

$$\begin{aligned}
S_\phi[x^*](\theta) &= x^*(\theta - \phi), \\
&= \kappa_0 + \sum_{k=1}^K [\kappa_{2k-1} \cos(k(\theta - \phi)) + \kappa_{2k} \sin(k(\theta - \phi))],
\end{aligned} \tag{27}$$

$$= \kappa_0 + \sum_{k=1}^K [(\rho_{k,1}(\phi)\kappa_{2k-1} + \rho_{k,2}(\phi)\kappa_{2k}) \cos(k\theta) + (\rho_{k,1}(\phi)\kappa_{2k-1} + \rho_{k,2}(\phi)\kappa_{2k}) \sin(k\theta)]. \tag{28}$$

From Eq. (27) to Eq. (28), we applied elementary trigonometric identities and introduced  $\rho_k(\phi) \in \mathbb{R}^{2 \times 2}$ , the  $2 \times 2$  rotation matrix with angle  $k\phi$

$$\rho_k(\phi) = \begin{pmatrix} \cos(k\phi) & -\sin(k\phi) \\ \sin(k\phi) & \cos(k\phi) \end{pmatrix}. \tag{29}$$

Grouping the Fourier components of  $x^*$  into a vector  $\underline{\kappa} \in \mathbb{R}^R$ , the transformation  $\underline{\kappa}$  under an angular translation is therefore determined by a block-diagonal matrix  $R^K(\phi)$  with  $K+1$  blocks:

$$R^K(\phi) = \begin{pmatrix} \rho_0 & & & \\ & \ddots & & \\ & & \ddots & \\ & & & \rho_K \end{pmatrix}$$

The first block corresponds to the scalar identity  $\rho_0 = 1$ . Each subsequent block is a  $2 \times 2$  rotation matrix with angle  $k\phi$  for  $k = 1 \dots K$ .

Any solution  $\underline{\kappa}$  of Eq. (25)-(26) therefore leads to a manifold of fixed points in Fourier coordinates parametrized by an angle  $\phi$  and given by:

$$\underline{\kappa}(\phi) = R^K(\phi)\underline{\kappa}.$$

## 2.7 The geometry of the fixed-point manifold

A geometric description of the manifold of fixed points can be obtained by interpreting the inverse Fourier transform in Eq. (24) as a linear parametrization of the manifold, where Fourier components provide coordinates of points on the manifold, in a basis formed by Fourier functions. In finite,  $N$ -dimensional networks, the Fourier functions correspond to a set of orthogonal directions in the  $N$ -dimensional activation space. For continuous networks, Fourier functions provide a basis in the infinite-dimensional space of square-integrable functions. In low-rank networks, at most  $R$  of the Fourier components are non-zero, so that the fixed-point manifold is embedded in a finite-dimensional subspace both for finite-dimensional and continuous networks.

The most minimal non-trivial manifold is generated by a fixed point  $\underline{\kappa}$  with zero values everywhere except on a single Fourier component with  $k > 0$ . If Eq. (23) admits such a solution, the corresponding manifold is a ring embedded in two dimensions (Fig. 2 B):

$$x^*(\theta) = \kappa_{2k-1} \cos(k\theta) + \kappa_{2k} \sin(k\theta).$$

More generally, if a fixed point  $\kappa$  has non-zero entries on  $P$  Fourier components, the manifold will be a twisted ring embedded in  $2P$  dimensions (Fig. 3 D).

### 3 Equivariant Recurrent Neural Networks

The formulation of the ring model in the language of geometric deep learning makes clear that the properties of the fixed-point manifolds stem from the following underlying structure: (i) neurons are indexed by elements of a one-dimensional domain  $\Omega$ ; (ii) any element of  $\Omega$  can be mapped onto any other one using an angular translation; (iii) the recurrent input is equivariant under the set  $G$  of all angular translations.

The angular translations in the ring model are a particular type of transformation associated with the ring-like domain  $\Omega$ . Following the blueprint of geometric deep learning (Bronstein et al. 2021), the structure of the ring model can be generalized to a broader class of transformations acting on more general domains  $\Omega$ . This gives rise to a family of models which we call *equivariant RNNs* (*eqRNNs*). This generalization relies on the mathematical formalism of group theory (Kosmann-Schwarzbach 2009). In this section, we introduce equivariant RNNs using group theory in an informal manner. A summary of key concepts in group theory is provided in Appendix A. Specific examples of eqRNNs are developed in the next section.

We start by defining a class of RNNs in which units are indexed by the elements of domain  $\Omega$ . Our central assumption is that this domain is associated with transformations that map any two elements of  $\Omega$  onto each other. The set of these transformations forms a finite or compact group  $G$ . Using a generalized concept of convolution, we define equivariant RNNs as the set of RNNs in which the recurrent input is equivariant under the action of  $G$ . We show that as a consequence, eqRNNs give rise to manifolds of fixed points generated by the action of  $G$ . We then use the concept of group Fourier transform to introduce low-rank eqRNNs. Similarly to low-rank ring models, low-rank eqRNNs lead to explicit parametrizations of fixed-point manifolds based on group representation theory.

#### 3.1 Equivariant recurrent neural networks

We consider a population of neurons indexed by elements  $u$  of a domain  $\Omega$ , that can be either discrete or compact (i.e. continuous, closed and bounded). We assume that  $\Omega$  is associated with a set of transformations  $G$  that form a finite or compact group. Elements of  $G$  are transformations  $g : \Omega \rightarrow \Omega$  equipped with a composition operation which obeys group axioms (Appendix A). The transformations  $g$  play a role analogous to angular translations in the ring model, and group axioms correspond to a generalization of properties outlined in Eqs. (11)-(12).

Our key assumption is that  $\Omega$  is a *homogeneous space* with respect to  $G$ . This means that for any fixed  $u_0 \in \Omega$ , every other element  $w \in \Omega$  can be reached by applying a given  $g_w \in G$  such that  $g_w u_0 = w$ . This defines a mapping from  $G$  to  $\Omega$  that allows us to index elements of  $\Omega$  by elements of  $G$ . In the ring model, any angular translation in  $G$  corresponds to a unique angle in  $\Omega$ , so that  $\Omega$  and  $G$  are isomorphic, which we write as  $\Omega = G$ . Importantly, in general this needs not be the case, as the mapping from  $G$  to  $\Omega$  is not necessarily bijective. In the following, we will systematically distinguish the case where  $\Omega$  and  $G$  are isomorphic and the case where they are not, as the second one is technically more complex than the first.

We next define an RNN with units indexed by elements of  $\Omega$ . As for the ring model, the activation in the network is defined by a function  $x^t : \Omega \rightarrow \mathbb{R}$  that associates to each neuron  $u \in \Omega$ , its activation  $x^t(u)$  at time  $t$ . Analogously, the firing rate and the recurrent input at time  $t$  are defined by two functions  $\Phi^t$  and  $F^t : \Omega \rightarrow \mathbb{R}$ . In accordance with the structure of interactions in RNNs (Eq. (2)), we assume that the recurrent input has the form of an abstract single-layer feed-forward network applied to the activity in the previous time-step, and is therefore defined as  $F_t = \mathcal{F}[x^t]$  where  $\mathcal{F} : L_{\mathbb{R}(\Omega)} \rightarrow L_{\mathbb{R}(\Omega)}$  is a time-independent operator that consists of a point-wise non-linearity followed by a linear operation. The dynamics of  $x^t$  obey Eq. (5).

Since the domain  $\Omega$  is associated with the group  $G$ , any transformation  $g_w \in G$  induces a transformation of any function  $f \in L_{\mathbb{R}(\Omega)}$ . By analogy with Eq. (13), we denote the transformed function as  $S_{g_w}[f]$ , and define it as

$$S_g[f](u) = f(g^{-1}(u)) \quad \forall u \in \Omega. \quad (30)$$

The corresponding operator  $S_{g_w} : L_{\mathbb{R}(\Omega)} \rightarrow L_{\mathbb{R}(\Omega)}$  is called the action of  $g_w$  on  $L_{\mathbb{R}(\Omega)}$ . Applying  $S_{g_w}$  to  $x^t$  or  $F^t$  is analogous to an angular translation of the activations or the recurrent inputs in the ring model.

A central property of the ring model is that the operator  $\mathcal{F}$  defining the recurrent input is equivariant under angular translations, i.e. commutes with their action (Eq. (14)). Our goal here is to define a family of recurrent input operators  $\mathcal{F}$  that extends this property to the more general case of a domain  $\Omega$  that is homogeneous with respect to the group  $G$ .

The equivariance of the recurrent inputs in the ring model is a direct consequence of the convolutional structure of  $\mathcal{F}$  with respect to translations on  $\Omega = [0, 2\pi]$  (Eq. (9)). To generalize this property, we rely on the results of Kondor & Trivedi (2018), who showed that any single-layer feed-forward network is equivariant under the action of a group  $G$  if and only if its linear operation consists of a generalized form of convolution, based on the concept of *group convolution*.

Introducing a kernel function  $c \in L_{\mathbb{R}(\Omega)}$ , by analogy with Eq. (9) we will define the recurrent input operator  $\mathcal{F}$  as the generalized convolution on  $\Omega$  between  $c$  and the firing rate  $\Phi[x]$ :

$$\mathcal{F}[x] = c *_{\Omega} \Phi[x]. \quad (31)$$

The generalized convolution on  $\Omega$  in Eq. (31) is based on the concept of the group convolution on  $G$ , which is defined for functions acting on the elements of  $G$  (rather than  $\Omega$ ). For two functions  $f^1, f^2 : G \rightarrow \mathbb{R}$  the  $G$ -convolution is a function  $G \rightarrow \mathbb{R}$  defined by (Kondor & Trivedi 2018)

$$(f_1 *_G f_2)(g) = \sum_{h \in G} f_1(g^{-1}h) f_2(h) \quad (32)$$

for a discrete group and

$$(f_1 *_G f_2)(g) = \int_G f_1(g^{-1}h) f_2(h) d\mu(h) \quad (33)$$

for a continuous group, where  $\mu$  is the Haar measure on  $G$  (Kondor & Trivedi 2018).

In the case where  $G$  and  $\Omega$  are isomorphic, every element  $u$  in  $\Omega$  corresponds to a unique element  $g_u$  in  $G$ . The group convolution in Eq. (32) then directly defines a convolution of two functions  $f^1, f^2 : \Omega \rightarrow \mathbb{R}$  that we use in Eq. (31).

The recurrent input  $F^t(u)$  to unit  $u$  at time  $t$  is therefore given by

$$\begin{aligned} F^t(u) &= (c *_G \Phi[x])(g_u) \\ &= \sum_{v \in \Omega} c(g_u^{-1}v) \Phi[x^t(v)] \end{aligned} \quad (34)$$

for discrete  $\Omega$  and  $G$ , while in the continuous case

$$F^t(u) = \int_{v \in \Omega} c(g_u^{-1}v) \Phi[x^t(v)] d\mu(v). \quad (35)$$

If  $G$  and  $\Omega$  are not isomorphic, the recurrent input cannot be defined directly in terms of the standard group convolution. Indeed, the group convolution in Eq. (32) is defined on functions on  $G$ , while the recurrent input acts on functions on  $\Omega$ . In such a situation, we follow Kondor & Trivedi (2018), who define a generalized convolution for functions on a domain  $\Omega$  that is homogeneous with respect to  $G$ . Using the fact that  $\Omega$  can be written as a quotient  $G/H$  between  $G$  and another group  $H$ , Kondor & Trivedi (2018) show that their generalized form of convolution inherits the key properties of the standard group convolution. We provide a summary of this construction in Appendix A.8, and a concrete example in Sec. 4.3. We in particular show that defining the recurrent in terms of this generalized convolution reduces precisely to Eq. (34), the only difference being that  $g_u$  is replaced by its representative on the coset  $gH$ .

The definition of the recurrent input  $\mathcal{F}$  in terms of the group convolution (Eq. (31)) directly ensures that  $\mathcal{F}$  satisfies the equivariance property with respect to the group action defined in Eq. (30):

$$\mathcal{F}S_g = S_g \mathcal{F} \quad \forall g \in G. \quad (36)$$

Here we provide the proof for the case where  $G$  and  $\Omega$  are isomorphic. It follows the same steps as for Eq. (14). Indeed,  $\forall x \in L_{\mathbb{R}(\Omega)}$  and  $\forall u, w \in \Omega$ , we have

$$\begin{aligned}
\mathcal{F}[S_{g_w}[x]](u) &= c *_G \Phi[S_{g_w}[x]](g_u) \\
&= \sum_{v \in \Omega} c(g_u^{-1}v) \Phi[S_{g_w}[x](v)] \\
&= \sum_{v \in \Omega} c(g_u^{-1}v) \Phi[x(g_w^{-1}v)] \\
&\quad (\text{change of variables: } v' = g_w^{-1}v, v = g_w v') \\
&= \sum_{v' \in \Omega} c(g_u^{-1}g_w v') \Phi[x(v')] \\
&= \sum_{v' \in \Omega} c((g_w^{-1}g_u)^{-1}v') \Phi[x(v')] \\
&= (c *_G \Phi[x])(g_w^{-1}g_u) \\
&= S_{g_w} \mathcal{F}[x](u).
\end{aligned}$$

In summary, an equivariant RNN is defined by a triplet  $(\Omega, G, c)$  consisting of a domain  $\Omega$ , a group  $G$  acting on it, and a kernel  $c$  that specifies a convolutional recurrent input that is equivariant with respect to the action of  $G$  on  $\Omega$ .

### 3.2 Structure of fixed points

Similarly to the ring model, the equivariance of the recurrent input (Eq. (36)) directly implies the existence of sets of fixed points generated by the action of the group  $G$ . Indeed, an activation  $x^* \in L_{\mathbb{R}(\Omega)}$  is a fixed point of the dynamics (Eq. (5)) if it obeys

$$x^*(u) = \mathcal{F}[x^*](u) \quad \forall u \in \Omega. \quad (37)$$

The equivariance of  $\mathcal{F}$  directly implies that  $\forall g \in G, S_g x^*$  is then also a fixed point. Indeed

$$\begin{aligned}
\mathcal{F}[S_g x^*] &= S_g \mathcal{F}[x^*] \\
&= S_g x^*,
\end{aligned}$$

where the first equality follows from the equivariance property of  $\mathcal{F}$  (Eq. (36)), and the second one follows from the fact that  $x^*$  is a fixed point (Eq. (37)). As in the ring model, the generalized convolutional structure of equivariant RNNs therefore induces a fundamental symmetry in the set of fixed points.

Starting from a fixed point  $x^*$  and applying the group action operators  $S_g$  for  $g \in G$  therefore yields a set of fixed points

$$\mathcal{M}_{x^*} = \{S_g[x^*] \mid g \in G\}. \quad (38)$$

Here we denote  $\mathcal{M}_{x^*}$  as the *manifold of fixed points* originating from  $x^*$  even if  $G$  is finite or discrete, but strictly speaking  $\mathcal{M}_{x^*}$  is a manifold only if  $G$  is a continuous group.

As for the ring model, different seed fixed points  $x^*$  can give rise to different manifolds generated by applying elements of  $G$ . More specifically, defining  $H_{x^*} = \{h \in G \mid S_h[x^*] = x^*\}$ , the subgroup of  $G$  whose action keeps  $x^*$  identical, the manifold  $\mathcal{M}_{x^*}$  is homeomorphic to the quotient  $G/H$ . The intrinsic dimension of  $\mathcal{M}_{x^*}$  is therefore less or equal to the dimension of  $G$ , and depends on the dimension of  $H_{x^*}$ .

Importantly, all fixed points belonging to a given manifold  $\mathcal{M}_{x^*}$  have identical stability properties. This follows from differentiating the equivariance property (Eq. (36)) with respect to  $x$ , which yields

$$\text{Jac}_{S_g x^*} \mathcal{F} = S_g \text{Jac}_{x^*} \mathcal{F} S_g^{-1},$$

where  $\text{Jac}_{x^*} \mathcal{F} = \partial \mathcal{F} / \partial x|_{x^*}$ . This similarity transformation ensures that the Jacobians at all points  $S_g x^* \in \mathcal{M}_{x^*}$  share identical eigenvalues (and therefore identical stability properties). If  $G$  is a continuous, Lie group, and  $\mathcal{M}_{x^*}$  is non-trivial (i.e. not consisting of a single fixed point), each fixed point in  $\mathcal{M}_{x^*}$  will be marginally stable, with zero eigenvalues associated to directions tangent to the manifold.

In summary, the seed fixed point  $x^*$  therefore determines both the dimensionality and the stability of the resulting fixed-point manifold  $\mathcal{M}_{x^*}$ .

### 3.3 The group Fourier transform of equivariant RNNs

For classical ring models, expressing the activity on Fourier components and restricting the number of non-zero components in the connectivity kernel led to an explicit parametrization of the fixed-point manifolds. Here we extend this approach to equivariant RNNs by using the generalization to *group Fourier transforms*. We first introduce group Fourier transforms, and then apply them to equivariant RNNs.

Group Fourier transforms are based on the concept of *irreducible representations*, which play a role analogous to the classical Fourier basis. A  $d$ -dimensional group representation  $\rho$  is a mapping  $G \rightarrow \mathbb{R}^{d \times d}$  which represents each group element  $g$  by a  $d \times d$  invertible matrix, in such a way that the group composition corresponds to matrix multiplication:

$$\rho(g_1 g_2) = \rho(g_1) \rho(g_2). \quad (39)$$

A reducible representation is a representation in which all matrices  $\rho(g)$  for  $g \in G$  can be put in block-diagonal form through a common change of basis. An irreducible representation (irrep) is conversely a representation that cannot be reduced to smaller blocks. A *system of irreps* of a group  $G$  therefore forms its set of elementary representations. Representation theory is a prominent branch of mathematics that has in particular extensively mapped and characterized the irreps of finite or compact groups. In particular, for any compact group, any system of irreps is countable and can therefore be indexed by positive integers (Kosmann-Schwarzbach 2009). We therefore denote a given system of irreps as  $\{\rho_k\}_{k=0,1,\dots}$ .

The group Fourier transform of a function  $f : G \rightarrow \mathbb{R}$  with respect to the group  $G$  is defined by the collection of its *Fourier components* on a system of irreps  $\{\rho_k\}_{k=0,1,\dots}$  of  $G$  (Kondor & Trivedi 2018). For a discrete group, the  $k$ -th Fourier component  $\hat{f}_k$  is a  $d_k \times d_k$  matrix given by

$$\hat{f}_k = \sum_{g \in G} f(g) \rho_k(g), \quad k = 0, 1, 2, \dots \quad (40)$$

where  $\rho_k : G \rightarrow \mathbb{R}^{d_k \times d_k}$  is the  $k$ -th irrep of the considered system. For a continuous, compact group, the sum is replaced by the integral over the Haar measure:

$$\hat{f}_k = \int_{g \in G} f(g) \rho_k(g) d\mu(g). \quad (41)$$

The group Fourier transform obeys properties analogous to the classical Fourier transform. In particular, any function  $f \in L_{\mathbb{R}(G)}$  can be expressed in terms of its inverse Fourier transform (Theorem 4.5 in Kosmann-Schwarzbach (2009)) as

$$f(g) = \frac{1}{|G|} \sum_{k=0}^{\infty} \tilde{d}_k \operatorname{tr} [\hat{f}_k \rho_k^{-1}(g)] \quad \forall g \in \Omega, \quad (42)$$

where  $\tilde{d}_k$  is the dimension of the  $k$ -th complex-valued irreducible representation.

Moreover, the group convolution theorem (Proposition 2 in Kondor & Trivedi (2018)) states that the Fourier components of the convolution  $f^1 *_G f^2$  of two functions  $f^1, f^2 \in L_{\mathbb{R}(G)}$  is given by the product of their Fourier components:

$$\widehat{(f^1 *_G f^2)}_k = \hat{f}^1_k \cdot \hat{f}^2_k, \quad k = 0, 1, 2, \dots \quad (43)$$

In the case where  $G$  and  $\Omega$  are isomorphic, the group Fourier transform on  $G$  directly defines a Fourier transform for functions  $f : \Omega \rightarrow \mathbb{R}$ . When  $G$  and  $\Omega$  are not isomorphic, Kondor et al. (2018) show that a Fourier transform on  $\Omega = G/H$  can be naturally defined by restricting the irreducible representations of  $G$  to specific columns. We sketch this construction in Appendix A.9, and provide a concrete example in Sec. 4.3. For simplicity, in the following we focus on the case where  $G = \Omega$ , so that every element  $u$  in  $\Omega$  corresponds to a unique element  $g_u$  in  $G$ . Eq. (40) then directly defines a generalized Fourier transform for any  $f : G \rightarrow \Omega$ :

$$\hat{f}_k = \sum_{u \in \Omega} f(u) \rho_k(g_u), \quad k = 0, 1, 2, \dots \quad (44)$$

or in the continuous case:

$$\hat{f}_k = \int_{u \in \Omega} f(u) \rho_k(g_u) d\mu(\Omega), \quad k = 0, 1, 2, \dots \quad (45)$$

where  $d\mu(\Omega)$  is the invariant measure on  $\Omega$ .

Analogously to the ring model, we next express in the Fourier space the dynamics of an eqRNN defined on a domain  $\Omega = G$ . We denote as  $\kappa'_k, \hat{\Phi}'_k, \hat{F}'_k, \hat{c}_k$  the  $k$ -th Fourier components of the activation function  $x^t$ , the firing rate  $\Phi^t$ , the recurrent input  $F^t$  and the connectivity kernel  $c$ , with respect to a system of irreps  $\{\rho_k\}_{k=0,1,\dots}$  of  $G$ . In contrast to the classical ring model where the Fourier components were scalar, in the general case the  $k$ -th component is a  $d_k \times d_k$  matrix, where  $d_k$  is the dimension of  $\rho_k$ .

Since  $F^t$  is given by the group convolution between  $c$  and  $\Phi^t$  (Eq. (31)), applying the group convolution theorem we have:

$$\hat{F}'_k = \hat{c}_k \hat{\Phi}'_k, \quad k = 0, 1, 2, \dots \quad (46)$$

Applying the group Fourier transform to Eq. (5) then allows us to express the RNN dynamics in terms of the Fourier components  $\kappa'_k$  of the activation  $x^t$ :

$$\begin{aligned} \kappa'^{t+1}_k &= \kappa'_k + \Delta t (-\kappa'_k + \hat{F}'_k) \\ &= \kappa'_k + \Delta t (-\kappa'_k + \hat{c}_k \hat{\Phi}'_k). \end{aligned} \quad (47)$$

The Fourier components  $\kappa_k$  of any fixed point solution  $x^*$  obey

$$\begin{aligned} \kappa_k &= \hat{F}_k \\ &= \hat{c}_k \hat{\Phi}_k. \end{aligned} \quad (48)$$

As for the classical ring model, Eq. (48) forms in general an infinite system of equations coupled through  $\hat{\Phi}_k$  which depends implicitly on  $x^*$  and therefore all the Fourier components. For general equivariant RNNs, the entries of each equation are however  $d_k \times d_k$  matrices instead of scalars.

### 3.4 Low-rank equivariant RNNs

Following the approach used for ring models, we next define *low-rank eqRNNs* as the subset of eqRNNs for which the Fourier components  $\hat{c}_k$  of the kernel  $c$  are zero for  $k > K$ . For low-rank eqRNNs, from Eq. (46) we have  $\hat{F}'_k = 0$  and therefore  $\kappa_k = 0$  for  $k > K$ . Any steady state  $x^*$  of a low-rank eqRNN is therefore characterized by a set of at most  $K + 1$  non-zero Fourier components. As the  $k$ -th Fourier component is a  $d_k \times d_k$  matrix, this corresponds to at most  $R = \sum_{k=0}^K d_k^2$  scalar values. These  $K + 1$  Fourier components obey  $K + 1$  matrix-valued equations given by Eq. (48).

To express these equations explicitly, we write the inverse Fourier transform (Eq. (42)) for the fixed-point activation  $x^*$ :

$$x^*(u) = \frac{1}{|G|} \sum_{k=0}^K \tilde{d}_k \operatorname{tr} [\kappa_k \rho_k^{-1}(g_u)]. \quad (49)$$

Inserting this expression in Eq. (48) for  $k = 0, \dots, K$ , we get a closed set of fixed point equations for the Fourier components  $\{\kappa_k\}_{k=0,\dots,K}$  of a fixed point:

$$\begin{aligned} \kappa_k &= \hat{F}_k (\kappa_0, \dots, \kappa_K) \\ &= \hat{c}_k \sum_{u \in \Omega} \Phi(x^t(u)) \rho_k(g_u) \end{aligned} \quad (50)$$

$$= \hat{c}_k \sum_{u \in \Omega} \Phi \left( \frac{1}{|G|} \sum_{k'=0}^K \tilde{d}_{k'} \operatorname{tr} [\kappa_{k'} \rho_{k'}^{-1}(g_u)] \right) \rho_k(g_u). \quad (51)$$

In Eq. (50) we used the definition of the group Fourier transform of  $\Phi$ , while in Eq. (51) we replaced  $x^*$  with its inverse Fourier transform (Eq. (49)).

Note that the stability of any fixed point satisfying Eq. (50) is determined by the eigenvalues of the Jacobian  $\partial \hat{F}_k / \partial \kappa_{k'}$ .

### 3.5 Fixed-point manifolds in low-rank equivariant RNNs

Restricting the ring model to be of low rank allows us to characterize more explicitly the structure of the fixed point manifold generated by applying the group action  $S_g$  to a non-trivial fixed point  $x^*$  (Eq. (38)).

The action  $S_g$  on  $x^*$  directly induces a linear transformation of its Fourier components. Indeed, directly applying  $S_g$  to the inverse Fourier transform of  $x^*$  (Eq. (49)), we have

$$\begin{aligned} S_g[x^*](u) &= x^*(g_u^{-1}) \\ &= \frac{1}{|G|} \sum_{k=0}^K d_k \operatorname{tr} [\kappa_k \rho_k^{-1}(g^{-1} g_u)] \\ &= \frac{1}{|G|} \sum_{k=0}^K d_k \operatorname{tr} [\kappa_k \rho_k(g) \rho_k^{-1}(g_u)] \end{aligned} \quad (52)$$

where we used Eq. (39) to write:

$$\rho_k^{-1}(g^{-1} g_u) = \rho_k(g) \rho_k^{-1}(g_u).$$

From Eq. (52), we see that the transformation  $x^* \mapsto S_g x^*$  induces a transformation of Fourier components given by

$$\kappa_k \mapsto \rho_k(g) \kappa_k. \quad (53)$$

Equivalently, grouping the  $K + 1$  Fourier components of  $x^*$  into a block-diagonal matrix  $\underline{\kappa} \in \mathbb{R}^{R \times R}$  defined as

$$\underline{\kappa} = \begin{pmatrix} \kappa_0 & & \\ & \ddots & \\ & & \kappa_R \end{pmatrix}, \quad (54)$$

the transformation of Fourier components is determined by a block-diagonal matrix  $R^K(g)$ :

$$R^K(g) = \begin{pmatrix} \rho_0(g) & & \\ & \ddots & \\ & & \rho_K(g) \end{pmatrix}. \quad (55)$$

The equivariance of the fixed point equation for  $x$  with respect to  $S_g$  directly implies the equivariance of the fixed point equation for  $\underline{\kappa}$  with respect to the matrix  $R^{(K)}(g)$ :

$$\hat{F}(R^{(K)}(g)\underline{\kappa}) = R^{(K)}(g)\hat{F}(\underline{\kappa}) \quad \forall \phi \in \Omega. \quad (56)$$

Starting from a seed fixed point  $x^*$  with Fourier components  $\underline{\kappa}^*$  therefore leads to a manifold of fixed points in Fourier coordinates parametrized by elements of  $G$  and given by:

$$\underline{\kappa}(g) = R^K(g)\underline{\kappa}^*. \quad (57)$$

All fixed points parametrized by Eq. (57) have identical stability properties. This follows from differentiating the equivariance property (Eq. (56)) with respect to  $\underline{\kappa}$ , which yields

$$\operatorname{Jac}_{R^{(K)}(g)\underline{\kappa}} \hat{F} = R^{(K)}(g) \operatorname{Jac}_{\underline{\kappa}} \hat{F} R^{(K)}(g)^{-1}, \quad (58)$$

where  $\operatorname{Jac}_{\underline{\kappa}} \hat{F}$  denotes the Jacobian matrix of  $\hat{F}$  with respect to  $\underline{\kappa}$ . This similarity transformation ensures that the Jacobians at all points  $R^{(K)}(g)\underline{\kappa}$  on the manifold share identical eigenvalues.

### 3.6 The geometry of the fixed-point manifold

Similarly to the ring model, in eqRNNs the inverse Fourier transform in Eq. (49), can be interpreted as a linear parametrization of the fixed-point manifold where the Fourier components provide coordinates in a basis-set provided by the entries of irreducible representations. In low-rank eqRNNs, at most  $R$  of the Fourier components are non-zero, so that the fixed-point manifold is embedded in a finite-dimensional subspace of the full space of square-integrable functions on  $\Omega$ . The embedding dimensionality of a fixed point manifold  $\mathcal{M}_{x^*}$ , i.e. its number of non-zero Fourier components, is determined by the number of non-zero Fourier components of the seed fixed point  $x^*$  through Eq. (57). The intrinsic dimension of  $\mathcal{M}_{x^*}$ , i.e. the minimal number of parameters needed for a non-linear parametrization is instead determined by the dimensionality of the subgroup  $H$  of  $G$  that leaves  $x^*$  invariant. As we will illustrate in the examples, these two properties lead to variety of possible fixed-point manifolds for a given group  $G$ .

## 4 Examples of specific equivariant RNNs

Having laid out the general framework of equivariant RNNs, in this section we provide three specific instantiations that correspond to three different domains  $\Omega$  and associated groups  $G$ . We start by the ring model, reformulating it this time in the group-theoretic language of eqRNNs. We then consider toroidal and spherical RNNs as two more general examples of eqRNNs on higher-dimensional domains  $\Omega$ .

### 4.1 Ring RNNs

In this section, we revisit the ring model introduced in Section 2 and now formulate it within the formalism of group theory presented in Section 3. We first explicitly differentiate between the discrete and continuous versions of the model, and then focus on the continuous case.

#### 4.1.1 Domain structure and symmetry group

In the discrete ring model, neurons are indexed by angles  $u = \theta_i = \frac{2\pi i}{N}$  for  $i = 0, \dots, N-1$ , so that the domain  $\Omega$  forms a discretized circle  $\Omega = \{\theta_i = \frac{2\pi i}{N} | i = 0, \dots, N-1\}$ . The associated group  $G$  consists of the set of angular translations on  $\Omega$ , and is directly isomorphic to  $\Omega$  equipped with addition modulo  $2\pi$ .  $G$  is a finite group known as the cyclic group  $G = \mathbb{Z}_N$ .

In the continuous limit  $N \rightarrow \infty$ , neurons in the ring model are labeled with a continuous angle  $u = \theta$ , so that  $\Omega = [0, 2\pi)$  is homeomorphic to the unit circle  $\mathcal{S}^1$ . The associated continuous, compact group of angular translations is the circle group  $G = \mathbb{S}^1$ , which is isomorphic to the special orthogonal group  $SO(2)$ , to the group of real numbers modulo the integers  $\mathbb{R}/2\pi\mathbb{Z}$ , and to the first unitary group  $U(1)$  (Zee 2016).

In both the discrete and continuous ring models, any element of the group  $G$  corresponds to a unique element in  $\Omega$ , which allows us to identify the group  $G$  with the domain  $\Omega$ .

#### 4.1.2 Group convolution

For the discrete ring model, the recurrent input in Eq. (31) is defined as the  $\mathbb{Z}_N$ -convolution between the kernel function  $c : \Omega \rightarrow \mathbb{R}$  and the firing rate,  $\Phi[x] : \Omega \rightarrow \mathbb{R}$ :

$$F^t(\theta_i) = \frac{1}{N} \sum_{\theta_j \in \frac{2\pi}{N} \mathbb{Z}_N} c(g_{\theta_i}^{-1}(\theta_j)) \Phi[x_t(\theta_j)] = \frac{1}{N} \sum_{j=0}^{N-1} c(\theta_j - \theta_i) \Phi[x^t(\theta_j)]. \quad (59)$$

In the continuous case, as in Eq. (35), the recurrent input is the  $\mathbb{S}^1$ -convolution between  $c, \Phi[x] : \Omega = \mathcal{S}^1 \rightarrow \mathbb{R}$ :

$$F^t(\theta) = \int_0^{2\pi} c(g_{\theta}^{-1}(\phi)) \Phi[x^t(\phi)] \frac{d\phi}{2\pi} = \int_0^{2\pi} c(\phi - \theta) \Phi[x^t(\phi)] \frac{d\phi}{2\pi}, \quad (60)$$

where we integrate with respect to the normalized Haar measure  $d\mu(\mathcal{S}^1) = \frac{d\phi}{2\pi}$ .

#### 4.1.3 Group representations

The groups  $\mathbb{Z}_N$  and  $\mathbb{S}^1$  associated with the discrete and continuous ring models have a well-studied set of irreducible representations (irreps) that directly correspond to the classical discrete and continuous Fourier bases. Working in the real-valued setting, here we provide the standard form of the irreps.

For the discrete ring with  $N$  neurons, the group  $\mathbb{Z}_N$  has  $\lfloor N/2 \rfloor + 1$  distinct irreducible representations, which we denote as  $\rho_k$  with  $k = 0, \dots, \lfloor N/2 \rfloor + 1$ . For  $k = 0$  and  $k = N/2$  (when  $N$  is even),  $\rho_k$  are one-dimensional, and given by

$$\begin{aligned} \rho_0(\theta_j) &= 1 \\ \rho_{N/2}(\theta_j) &= (-1)^j. \end{aligned}$$

For  $k = 1, 2, \dots, \lfloor (N-1)/2 \rfloor$ , the irreps are two-dimensional rotation matrices:

$$\rho_k(\theta_j) = \begin{pmatrix} \cos(k\theta_j) & -\sin(k\theta_j) \\ \sin(k\theta_j) & \cos(k\theta_j) \end{pmatrix}$$

for  $\theta_j = \frac{2\pi j}{N}$ ,  $j = 0 \dots N - 1$ .

In the continuous case, the group  $\mathbb{S}^1$  has a countable set of irreps  $\{\rho_k\}_{k \in \mathbb{N}}$ . For  $k = 0$ ,

$$\rho_0(\theta) = 1, \quad (61)$$

while for  $k \geq 1$ , the irreps are two-dimensional rotation matrices (Feehan & Leness 2020):

$$\rho_k(\theta) = \begin{pmatrix} \cos(k\theta) & -\sin(k\theta) \\ \sin(k\theta) & \cos(k\theta) \end{pmatrix} \quad (62)$$

for  $\theta \in [0, 2\pi)$ .

#### 4.1.4 Group Fourier transform

We next use the real-valued irreps to explicitly write the components  $\hat{f}_k$  of the group Fourier transform defined in Eq. (40) for any function  $f : \Omega \rightarrow \mathbb{R}$ . From this section, we focus on the continuous case, where  $\Omega = G = \mathbb{S}^1$ .

For  $k = 0$ , introducing Eq. (61) into Eq. (40),  $\hat{f}_0$  is a scalar given by

$$\hat{f}_0 = \int_0^{2\pi} f(\theta) \frac{d\theta}{2\pi}, \quad (63)$$

For  $k > 1$ , inserting Eq. (62) into Eq. (40),

$$\begin{aligned} \hat{f}_k &= \int_0^{2\pi} f(\theta) \begin{pmatrix} \cos(k\theta) & -\sin(k\theta) \\ \sin(k\theta) & \cos(k\theta) \end{pmatrix} \frac{d\theta}{2\pi} \\ &= \int_0^{2\pi} \begin{pmatrix} f(\theta) \cos(k\theta) & -f(\theta) \sin(k\theta) \\ f(\theta) \sin(k\theta) & f(\theta) \cos(k\theta) \end{pmatrix} \frac{d\theta}{2\pi} \end{aligned} \quad (64)$$

$$= \begin{pmatrix} \hat{f}_{k,1} & -\hat{f}_{k,2} \\ \hat{f}_{k,2} & \hat{f}_{k,1} \end{pmatrix}. \quad (65)$$

For  $k > 1$ ,  $\hat{f}_k$  is therefore a  $2 \times 2$  matrix, but it contains only two independent elements, which we denote as  $\hat{f}_{k,1}$  and  $\hat{f}_{k,2}$ , with:

$$\begin{aligned} \hat{f}_{k,1} &= \int_0^{2\pi} f(\theta) \cos(k\theta) \frac{d\theta}{2\pi}, \\ \hat{f}_{k,2} &= \int_0^{2\pi} f(\theta) \sin(k\theta) \frac{d\theta}{2\pi}. \end{aligned}$$

These elements are the classical Fourier components introduced in Eq. (17).

#### 4.1.5 Fixed point equations for low-rank models

We now focus on low-rank models, i.e. models for which the matrix-valued Fourier components  $\hat{c}_k$  of the kernel  $c$  are zero for  $k > K$ . As shown in Sec. 3.4, for such models the steady-state activation is described by a finite number of non-zero Fourier components  $\kappa_k$  for  $k \leq K$ . Here we use the expressions for the irreps to write explicitly the fixed-point equation (Eq. (51)) satisfied by the Fourier components  $\kappa_k$  of any steady-state activation  $x^*$ .

Using the Convolution Theorem (Eq. (43)), we get for  $k = 0$ :

$$\hat{F}_0 = \hat{c}_0 \cdot \hat{\Phi}_0 \quad (66)$$

and, for  $k > 1$ :

$$\begin{aligned} \hat{F}_k &= \hat{c}_k \cdot \hat{\Phi}_k = \begin{pmatrix} \hat{c}_{k,1} & -\hat{c}_{k,2} \\ \hat{c}_{k,2} & \hat{c}_{k,1} \end{pmatrix} \begin{pmatrix} \hat{\Phi}_{k,1} & -\hat{\Phi}_{k,2} \\ \hat{\Phi}_{k,2} & \hat{\Phi}_{k,1} \end{pmatrix} \\ &= \begin{pmatrix} \hat{c}_{k,1} \hat{\Phi}_{k,1} - \hat{c}_{k,2} \hat{\Phi}_{k,2} & -\hat{c}_{k,1} \hat{\Phi}_{k,2} - \hat{c}_{k,2} \hat{\Phi}_{k,1} \\ \hat{c}_{k,2} \hat{\Phi}_{k,1} + \hat{c}_{k,1} \hat{\Phi}_{k,2} & -\hat{c}_{k,2} \hat{\Phi}_{k,2} + \hat{c}_{k,1} \hat{\Phi}_{k,1} \end{pmatrix} \\ &= \begin{pmatrix} \hat{F}_{k,1} & -\hat{F}_{k,2} \\ \hat{F}_{k,2} & \hat{F}_{k,1} \end{pmatrix} \end{aligned}$$

where

$$\begin{aligned}\hat{F}_{k,1} &= \hat{c}_{k,1}\hat{\Phi}_{k,1} - \hat{c}_{k,2}\hat{\Phi}_{k,2}, \\ \hat{F}_{k,2} &= \hat{c}_{k,2}\hat{\Phi}_{k,1} + \hat{c}_{k,1}\hat{\Phi}_{k,2}.\end{aligned}$$

To express explicitly  $\hat{F}_{k,1}$  and  $\hat{F}_{k,2}$ , we write  $\hat{\Phi}_k$  in terms of the Fourier components  $\kappa_k$  of the steady-state activation  $x^*$ . For  $k = 0$ , we have

$$\hat{\Phi}_0 = \int_0^{2\pi} \Phi[x^*(\theta)] \frac{d\theta}{2\pi}, \quad (67)$$

while for  $k > 1$ , the independent matrix elements are given by

$$\hat{\Phi}_{k,1} = \int_0^{2\pi} \Phi[x^*(\theta)] \cos(k\theta) \frac{d\theta}{2\pi}, \quad (68)$$

$$\hat{\Phi}_{k,2} = \int_0^{2\pi} \Phi[x^*(\theta)] \sin(k\theta) \frac{d\theta}{2\pi}. \quad (69)$$

We next write the steady-state activation  $x^*$  using the Inverse Fourier Transform (Eq. (42)):

$$\begin{aligned}x(\theta) &= \sum_{k=0}^K \tilde{d}_k \operatorname{tr}(\kappa_k \rho_k^{-1}(\theta)) \\ &= \kappa_0 + \sum_{k=1}^K \operatorname{tr} \left( \begin{pmatrix} \kappa_{k,1} & -\kappa_{k,2} \\ \kappa_{k,2} & \kappa_{k,1} \end{pmatrix} \begin{pmatrix} \cos(k\theta) & \sin(k\theta) \\ -\sin(k\theta) & \cos(k\theta) \end{pmatrix} \right) \\ &= \kappa_0 + \sum_{k=1}^K \operatorname{tr} \left( \begin{pmatrix} \kappa_{k,1} \cos(k\theta) + \kappa_{k,2} \sin(k\theta) & \kappa_{k,1} \sin(k\theta) - \kappa_{k,2} \cos(k\theta) \\ \kappa_{k,2} \cos(k\theta) - \kappa_{k,1} \sin(k\theta) & \kappa_{k,2} \sin(k\theta) + \kappa_{k,1} \cos(k\theta) \end{pmatrix} \right) \\ &= \kappa_0 + \sum_{k=1}^K 2(\kappa_{k,1} \cos(k\theta) + \kappa_{k,2} \sin(k\theta)).\end{aligned} \quad (70)$$

Notice that we include only the  $K + 1$  first Fourier components, because at steady-state  $\kappa_k = 0$  for  $k > K$ .

Inserting Eq. (70) into Eqs. (67), (68) and (69) gives us explicit expressions for  $\hat{\Phi}_0$ ,  $\hat{\Phi}_{k,1}$  and  $\hat{\Phi}_{k,2}$  as function of the set of scalars  $\kappa_0, \kappa_{k,1}, \kappa_{k,2}$  for  $k = 1 \dots K$ .

This leads to a set of  $R = 2K + 1$  fixed point equations for the  $R$  scalar variables  $\kappa_0, \kappa_{k,1}, \kappa_{k,2}$ :

$$\kappa_0 = \hat{c}_0 \int_0^{2\pi} \Phi \left[ \kappa_0 + \sum_{k'=1}^K 2(\kappa_{k',1} \cos(k'\theta) + \kappa_{k',2} \sin(k'\theta)) \right] \frac{d\theta}{2\pi}, \quad (71)$$

$$\kappa_{k,1} = \int_0^{2\pi} (\hat{c}_{k,1} \cos(k\theta) - \hat{c}_{k,2} \sin(k\theta)) \Phi \left[ \kappa_0 + \sum_{k'=1}^K 2(\kappa_{k',1} \cos(k'\theta) + \kappa_{k',2} \sin(k'\theta)) \right] \frac{d\theta}{2\pi}, \quad (72)$$

$$\kappa_{k,2} = \int_0^{2\pi} (\hat{c}_{k,2} \cos(k\theta) + \hat{c}_{k,1} \sin(k\theta)) \Phi \left[ \kappa_0 + \sum_{k'=1}^K 2(\kappa_{k',1} \cos(k'\theta) + \kappa_{k',2} \sin(k'\theta)) \right] \frac{d\theta}{2\pi}. \quad (73)$$

#### 4.1.6 Fixed point manifold

Any solution  $\underline{\kappa}$  of the fixed point equation (71), (72), (73) leads to a manifold of fixed points in Fourier coordinates parametrized by elements of the group  $\mathbb{S}^1$ :

$$\underline{\kappa}(\phi) = \underline{\kappa}R^K(\phi). \quad (74)$$

where  $R^K(\phi)$  is block-diagonal matrix containing at most  $(K + 1)$  rotation matrices that act on the corresponding Fourier components, and given by:

$$R^K(\phi) = \begin{pmatrix} \rho_0(\phi) & & & & \\ & \rho_1(\phi) & & & \\ & & \rho_2(\phi) & & \\ & & & \ddots & \\ & & & & \rho_K(\phi) \end{pmatrix}. \quad (75)$$

#### 4.1.7 Rank two ring model

We now consider the specific instantiation of the ring model with the connectivity kernel

$$c(\theta) = J_1 \cos(\theta),$$

where  $J_1$  is a scalar parameter that modulates the strength of the recurrent connectivity. In this case, the only non-zero Fourier component of the kernel is  $\hat{c}_1$  with

$$\begin{aligned} \hat{c}_{1,1} &= \frac{J_1}{2}, \\ \hat{c}_{1,2} &= 0. \end{aligned}$$

The only potentially non-zero Fourier component of the steady state activation  $x^*$  is the matrix  $\kappa_1$ , so that

$$x^*(\theta) = 2(\kappa_{1,1} \cos(\theta) + \kappa_{1,2} \sin(\theta)). \quad (76)$$

The steady state is therefore described by  $R = 2$  scalar variables, and we denote this instance of the ring model as the *rank two model* because the connectivity matrix in the finite-size network is of rank two (Appendix B).

Eqs. (71)-(73) then reduce to two coupled equations for the scalars  $\kappa_{1,1}$  and  $\kappa_{1,2}$ :

$$\begin{cases} \kappa_{1,1} = \frac{J_1}{2} \int_0^{2\pi} \cos \theta \Phi [2(\kappa_{1,1} \cos \theta + \kappa_{1,2} \sin \theta)] \frac{d\theta}{2\pi} \\ \kappa_{1,2} = \frac{J_1}{2} \int_0^{2\pi} \sin \theta \Phi [2(\kappa_{1,1} \cos \theta + \kappa_{1,2} \sin \theta)] \frac{d\theta}{2\pi}. \end{cases} \quad (77)$$

Using Eq. (74), it follows that any non-zero solution  $\underline{\kappa} = (\kappa_{1,1}, \kappa_{1,2})$  of Eq. (77) leads to a manifold of fixed points in Fourier coordinates parametrized by  $\phi \in [0, 2\pi]$ :

$$\underline{\kappa}(\phi) = R^1(\phi) \underline{\kappa}, \quad (78)$$

where

$$R^1(\phi) = \begin{pmatrix} \cos(\phi) & -\sin(\phi) \\ \sin(\phi) & \cos(\phi) \end{pmatrix}.$$

Setting  $\phi = 0$ , we obtain a particular solution  $\underline{\kappa}(0) = (\kappa_{1,1}, 0)$ . The system (77) then reduces to the one dimensional equation:

$$\kappa_{1,1} = \frac{J_1}{2} \int_0^{2\pi} \Phi(2\kappa_{1,1} \cos \theta) \cos \theta \frac{d\theta}{2\pi}. \quad (79)$$

The stability of the fixed-point is determined by the sign of the derivative of the r.h.s with respect to  $\kappa_{1,1}$ , evaluated at the fixed point. This stability is then inherited by all the fixed points on the resulting manifold.

Eq. (79) equation admits a zero solution  $\kappa_{1,1} = 0$  that is stable for  $J_1$  smaller than a critical coupling  $J_c$ , and unstable for  $J_1 > J_c$ . For  $J_1 > J_c$ , Eq. (79) admits an additional pair of non-zero solutions with opposite signs:  $\kappa_{1,1} = \pm \varrho$  (Fig. 2 A). These solutions are stable, and lead to a manifold of stable fixed points that form a ring embedded in two dimensions (Fig. 2 B). The radius of the ring is given by  $\kappa_{1,1}$ , and increases with  $J_c$ . Note that the two non-zero solutions of Eq. (79) with opposite signs correspond to opposite points  $\phi = 0$  and  $\phi = \pi$  on the ring. Using the inverse Fourier transform (Eq. (76)), the fixed point activation  $x_\phi$  can be expressed as a cosine function centered at  $\phi$ , and of amplitude  $\kappa_{1,1}$  (Fig. 2 C).

More specifically, applying the relation (78) to the particular solution  $\underline{\kappa}(0) = (\varrho, 0)$ , we get a general solution for  $\phi \in [0, 2\pi]$ :

$$\underline{\kappa}(\phi) = (\varrho \cos(\phi), \varrho \sin(\phi)). \quad (80)$$

Inserting Eq. (80) into Eq. (76) results the classical bump-like population activity for a fixed  $\phi$  (Fig. 2C):

$$x_\phi(\theta) = 2\varrho \cos(\theta - \phi). \quad (81)$$

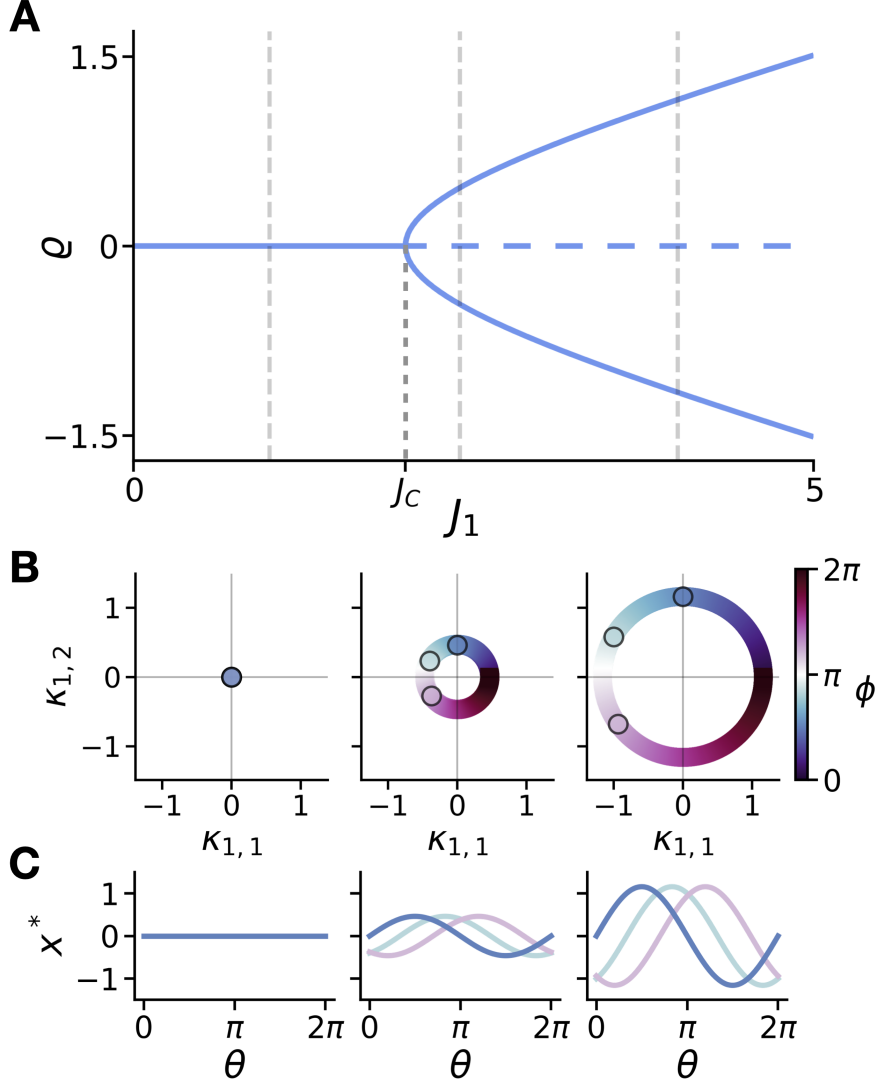


Figure 2: Bifurcation analysis and manifolds in the rank-two ring model. A) Bifurcation diagram showing the emergence of non-zero fixed points ( $\kappa_{1,1}$ ) as a function of coupling strength  $J_1$ . Solid lines represent stable solutions while dashed lines indicate unstable solutions. B) Manifolds of stable fixed points in the  $\kappa_{1,1}$ - $\kappa_{1,2}$  plane at three different values of  $J_1$  (increasing from left to right), color-coded by phase  $\phi$ . Left: At subcritical coupling, only the origin is stable. Middle: Above the bifurcation, a stable ring manifold emerges. Right: At stronger coupling, the ring manifold expands its radius. C) Population activity profiles ( $x^*$ ) corresponding to points on each manifold plotted as function of  $\theta$ . The profiles transition from uniform/null (left) to sinusoidal patterns (middle) to more pronounced bumps (right) as coupling strength increases. Different colors show  $\phi$ -shifted versions of the same solution. **Computational details:** Panel A:  $\varrho$  is computed by numerically solving Eq. (79). The integral is evaluated numerically using a discretized approximation with  $N$  neurons uniformly distributed around the ring. Panel B: Manifolds are generated by applying the rotation (78) to fixed-point solutions from (A). Panel C: Activity profiles from Eq. (81).

#### 4.1.8 Rank five ring model

To illustrate the effect of including a higher number of Fourier components in the connectivity kernel, we next consider the rank five ring model, defined by the kernel

$$c(\theta) = J_0 + J_1 \cos(\theta) + J_2 \cos(2\theta),$$

with  $J_0, J_1$  and  $J_2$  scalar parameters. In this case, the non-zero Fourier components are

$$\begin{aligned}\hat{c}_0 &= J_0 \\ \hat{c}_1 &= \begin{pmatrix} \hat{c}_{1,1} & -\hat{c}_{1,2} \\ \hat{c}_{1,2} & \hat{c}_{1,1} \end{pmatrix} = J_1 \begin{pmatrix} \frac{1}{2} & 0 \\ 0 & \frac{1}{2} \end{pmatrix} \\ \hat{c}_2 &= \begin{pmatrix} \hat{c}_{2,1} & -\hat{c}_{2,2} \\ \hat{c}_{2,2} & \hat{c}_{2,1} \end{pmatrix} = J_2 \begin{pmatrix} \frac{1}{2} & 0 \\ 0 & \frac{1}{2} \end{pmatrix}\end{aligned}$$

while for  $k > 2$

$$\hat{c}_k = \begin{pmatrix} 0 & 0 \\ 0 & 0 \end{pmatrix}.$$

The steady state activation  $x^*(\theta)$  is given by

$$x(\theta) = \kappa_0 + 2(\kappa_{1,1} \cos(\theta) + \kappa_{1,2} \sin(\theta) + \kappa_{2,1} \cos(2\theta) + \kappa_{2,2} \sin(2\theta)). \quad (82)$$

Analogously to the rank two ring model, the fixed point equations (71)-(73) reduce to a set of  $R = 2K + 1 = 5$  coupled equations for the scalars  $\kappa_0, \kappa_{1,1}, \kappa_{1,2}, \kappa_{2,1}, \kappa_{2,2}$ :

$$\begin{cases} \kappa_0 = J_0 \int_0^{2\pi} \Phi [\kappa_0 + 2(\kappa_{1,1} \cos \theta + \kappa_{1,2} \sin \theta + \kappa_{2,1} \cos 2\theta + \kappa_{2,2} \sin 2\theta)] \frac{d\theta}{2\pi} \\ \kappa_{1,1} = \frac{J_1}{2} \int_0^{2\pi} \Phi [\kappa_0 + 2(\kappa_{1,1} \cos \theta + \kappa_{1,2} \sin \theta + \kappa_{2,1} \cos 2\theta + \kappa_{2,2} \sin 2\theta)] \cos \theta \frac{d\theta}{2\pi} \\ \kappa_{1,2} = \frac{J_1}{2} \pi \int_0^{2\pi} \Phi [\kappa_0 + 2(\kappa_{1,1} \cos \theta + \kappa_{1,2} \sin \theta + \kappa_{2,1} \cos 2\theta + \kappa_{2,2} \sin 2\theta)] \sin \theta \frac{d\theta}{2\pi} \\ \kappa_{2,1} = \frac{J_2}{2} \pi \int_0^{2\pi} \Phi [\kappa_0 + 2(\kappa_{1,1} \cos \theta + \kappa_{1,2} \sin \theta + \kappa_{2,1} \cos 2\theta + \kappa_{2,2} \sin 2\theta)] \cos 2\theta \frac{d\theta}{2\pi} \\ \kappa_{2,2} = \frac{J_2}{2} \pi \int_0^{2\pi} \Phi [\kappa_0 + 2(\kappa_{1,1} \cos \theta + \kappa_{1,2} \sin \theta + \kappa_{2,1} \cos 2\theta + \kappa_{2,2} \sin 2\theta)] \sin 2\theta \frac{d\theta}{2\pi} \end{cases} \quad (83)$$

Using Eq. (74), any solution  $\underline{\kappa} = (\kappa_0, \kappa_{1,1}, \kappa_{1,2}, \kappa_{2,1}, \kappa_{2,2})$  of the system (83) leads to a manifold of fixed points in Fourier coordinates, parametrized by element of  $SO(2)$ , but with a higher dimensional representation:

$$\underline{\kappa}(\phi) = R^2(\phi) \underline{\kappa} \quad (84)$$

where  $R^2(\phi) \in \mathbb{R}^{5 \times 5}$  is a block diagonal matrix:

$$R^2(\phi) = \begin{pmatrix} 1 & 0 & 0 & 0 & 0 \\ 0 & \cos(\phi) & -\sin(\phi) & 0 & 0 \\ 0 & \sin(\phi) & \cos(\phi) & 0 & 0 \\ 0 & 0 & 0 & \cos(2\phi) & -\sin(2\phi) \\ 0 & 0 & 0 & \sin(2\phi) & \cos(2\phi) \end{pmatrix}. \quad (85)$$

Setting  $\phi = 0$ , we obtain a particular solution  $\underline{\kappa}(0) = (\kappa_0, \kappa_{1,1}, 0, \kappa_{2,1}, 0)$ . Eq. (83) then reduces to the three dimensional system:

$$\begin{cases} \kappa_0 = J_0 \int_0^{2\pi} \Phi [\kappa_0 + 2(\kappa_{1,1} \cos \theta + \kappa_{2,1} \cos 2\theta)] \frac{d\theta}{2\pi} \\ \kappa_{1,1} = \frac{J_1}{2} \pi \int_0^{2\pi} \Phi [\kappa_0 + 2(\kappa_{1,1} \cos \theta + \kappa_{2,1} \cos 2\theta)] \cos \theta \frac{d\theta}{2\pi} \\ \kappa_{2,1} = \frac{J_2}{2} \pi \int_0^{2\pi} \Phi [\kappa_0 + 2(\kappa_{1,1} \cos \theta + \kappa_{2,1} \cos 2\theta)] \cos 2\theta \frac{d\theta}{2\pi} \end{cases} \quad (86)$$

The stability of each fixed point is determined by the eigenvalues of the Jacobian of the r.h.s, evaluated at the fixed point. This stability is then inherited by all the fixed points on the resulting manifold.

Eqs. (86) admit three types of solutions that lead to different types of manifolds of fixed points in Eq. (82): (i) solutions with  $\kappa_0 = \varrho_0 \neq 0$  and  $\kappa_{1,1} = \kappa_{2,1} = 0$ ; from Eq. (85) such solutions lead to single fixed point; (ii) solutions with  $\kappa_{1,1} = \varrho_1 \neq 0$  and  $\kappa_{2,1} = 0$ , or  $\kappa_{1,1} = 0$  and  $\kappa_{2,1} = \varrho_2 \neq 0$ ; from Eq. (85) such solutions lead to rings of fixed points embedded in two dimensions, i.e. a manifold of intrinsic dimension 1 and embedding dimension 2; (iii) solutions with  $\kappa_{1,1} = \varrho_1 \neq 0$  and  $\kappa_{2,1} = \varrho_2 \neq 0$  lead to a ring of fixed points embedded in four dimensions, i.e. a manifold of intrinsic dimension 1, but embedding dimension 4. The existence of these solutions depend on the values of the parameters  $J_0, J_1, J_2$ . For a fixed set of parameter values, we find that several types of solutions can co-exist, leading to multi-stability between different manifolds of fixed points, some stable and others consisting of saddle points (Fig. 3).

Specifically, applying the relation (84) to the particular solution  $\underline{\kappa}(0) = (\varrho_0, \varrho_1, 0, \varrho_2, 0)$ , the solution for general  $\phi \in [0, 2\pi]$  is:

$$\underline{\kappa}(\phi) = (\varrho_0, \varrho_1 \cos(\phi), \varrho_1 \sin(\phi), \varrho_2 \cos(2\phi), \varrho_2 \sin(2\phi)). \quad (87)$$

Inserting Eq. (87) into Eq. (82) results in the population activity for a fixed  $\phi$  (Fig. 3D, Right):

$$x_\phi(\theta) = \varrho_0 + 2(\varrho_1 \cos(\theta - \phi) + \varrho_2 \cos(2(\theta - \phi))). \quad (88)$$

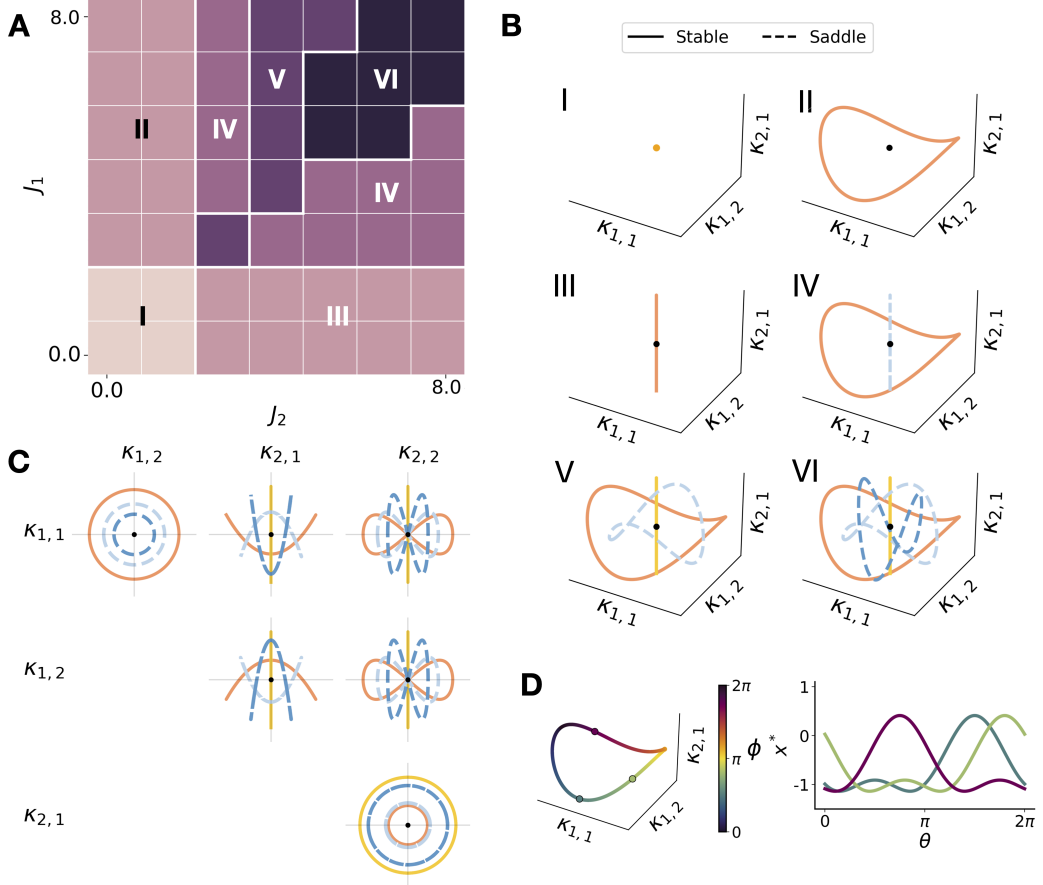


Figure 3: Manifolds of fixed points in the rank five ring model. A) Bifurcation diagram showing six regions of parameters (I-VI) leading to different combinations of co-existing fixed point solutions. Here we vary  $J_1$  and  $J_2$ , while  $J_0 = -1$  is fixed. B) Co-existing manifolds of fixed points within each of the six parameter regions. The manifolds are shown in the three-dimensional space corresponding to the Fourier components  $\kappa_{1,1}, \kappa_{1,2}, \kappa_{2,1}, \kappa_{2,2}$ , while they are actually embedded in four dimensions  $\kappa_{1,1}, \kappa_{1,2}, \kappa_{2,1}, \kappa_{2,2}$ . In this projection, rings in the  $\kappa_{2,1}-\kappa_{2,2}$  plane appear as vertical segments. I: single, stable fixed point; II: unstable single point and a stable 4d-ring; III: unstable single point and stable 2d-ring in the plane  $\kappa_{2,1}-\kappa_{2,2}$ ; IV: unstable single point, a saddle 2d-ring (in the plane  $\kappa_{2,1}-\kappa_{2,2}$ ) and a stable 4d-ring (or vice versa); V: unstable single point, a stable 2d-ring and two 4d-rings (one stable, one saddle); VI: unstable single point and a stable 2d-ring and three 4d-rings (one stable, two saddle). Stable solutions are shown as solid lines, saddles are shown as dashed lines. C) Two-dimensional projections of the manifolds of fixed point in region VI onto planes corresponding to different pairs of Fourier component. D) Left: Three points on a stable solution manifold (type II solution), color-coded by phase  $\phi$ . Right: The corresponding population activity profiles, showing how shifted positions on the manifold correspond to shifted activity profiles.

## 4.2 Toroidal RNNs

A natural extension of the ring models are networks defined on a two-dimensional domain consisting of a product of two one-dimensional ring-like domains. More generally, we can consider domains that are products of  $d$  rings, i.e.  $d$ -dimensional torii. The associated transformations then consist of angular translations along the  $d$  dimensions, and form so-called *toroidal groups*. We denote as *toroidal RNNs* equivariant RNNs defined on such domains and associated toroidal groups. While the ring models generate fixed-point manifolds of intrinsic dimension 1, i.e. parametrized by a single variable, a  $d$ -dimensional toroidal RNN can additionally generate manifolds of intrinsic dimension up to  $d$ . In the following we focus on the simplest toroidal RNN with  $d = 2$ .

### 4.2.1 Domain structure and symmetry group

In a two-dimensional toroidal RNN, neurons are indexed by pairs of angles  $(u_1, u_2) = (\theta_1, \theta_2)$  with  $\theta_1, \theta_2 \in [0, 2\pi]$ . The domain  $\Omega$  is therefore the direct product of two circles  $\Omega = \mathcal{S}^1 \times \mathcal{S}^1$ , forming a two-dimensional torus  $\mathcal{T}^2$ . The symmetry group  $G$  associated with this domain is the set of two-dimensional angular translations on  $\mathcal{T}^2$ .  $G$  is called the 2-dimensional toroidal group  $\mathbb{T}^2$ , and it is isomorphic the group product  $\mathbb{S}^1 \times \mathbb{S}^1$ . This group is isomorphic to  $SO(2) \times SO(2)$ , to  $(\mathbb{R}/2\pi\mathbb{Z})^2$ , and to the product of two unitary groups  $U(1) \times U(1)$ .

We denote the elements of  $G$  as  $g_{\phi_1, \phi_2}$  for  $\phi_1, \phi_2 \in [0, 2\pi]$ . Their action on  $\Omega$  is given by

$$\begin{aligned} g_{\phi_1, \phi_2} : \quad & \Omega \rightarrow \Omega \\ (\theta_1, \theta_2) \mapsto & (\theta_1 + \phi_1 \bmod 2\pi, \theta_2 + \phi_2 \bmod 2\pi). \end{aligned}$$

### 4.2.2 Group convolution

The recurrent input in Eq. (31) is defined as the group convolution between the kernel function  $c : \mathcal{S}^1 \times \mathcal{S}^1 \rightarrow \mathbb{R}$  and the firing rate,  $\Phi[x]$ . Following Eq. (33), it is written as:

$$\begin{aligned} F^t(\theta_1, \theta_2) &= \int_0^{2\pi} \int_0^{2\pi} c(g_{(\theta_1, \theta_2)}^{-1}(\phi_1, \phi_2)) \Phi[x^t(\phi_1, \phi_2)] \frac{d\phi_1 d\phi_2}{4\pi^2} \\ &= \int_0^{2\pi} \int_0^{2\pi} c(\phi_1 - \theta_1, \phi_2 - \theta_2) \Phi[x^t(\phi_1, \phi_2)] \frac{d\phi_1 d\phi_2}{4\pi^2} \end{aligned} \quad (89)$$

where we integrate with respect to the normalized Haar measure  $d\mu(\mathcal{S}^1 \times \mathcal{S}^1) = \frac{d\phi_1 d\phi_2}{4\pi^2}$ .

### 4.2.3 Group representations

The irreps of  $\mathbb{T}^2 = \mathcal{S}^1 \times \mathcal{S}^1$  are therefore indexed by pairs of integers  $(k_1, k_2)$  where  $k_1, k_2 \in \mathbb{Z}$ , and given by  $\rho_{(k_1, k_2)}(\phi_1, \phi_2) = \rho_{k_1}(\phi_1)\rho_{k_2}(\phi_2)$ , with  $\rho_k(\phi)$  an irrep of  $\mathcal{S}^1$  (Eq. (62)). In the real-valued setting, these irreps fall into two categories. For  $k_1 = 0$  and  $k_2 = 0$ , the irrep is one-dimensional:

$$\rho_{(0,0)}(\phi_1, \phi_2) = 1 \quad (90)$$

Otherwise, the irreps are two-dimensional rotation matrices, obtained by matrix multiplication of pairs of  $SO(2)$  irreps (Eq. 15.2 in [Bump \(2013\)](#)):

$$\rho_{(k_1, k_2)}(\phi_1, \phi_2) = \begin{pmatrix} \cos(k_1\phi_1 + k_2\phi_2) & -\sin(k_1\phi_1 + k_2\phi_2) \\ \sin(k_1\phi_1 + k_2\phi_2) & \cos(k_1\phi_1 + k_2\phi_2) \end{pmatrix}, \quad (91)$$

for  $\phi_1, \phi_2 \in [0, 2\pi)$ .

While the irreps of  $\mathbb{T}^2$  are rotational matrices as in the ring model, they depend on two independent indices and two independent angular variables.

### 4.2.4 Group Fourier transform

We next use the irreps in Eqs. (90)-(91) to write the components  $\hat{f}_{k_1, k_2}$  of the group Fourier transform for any function  $f : \Omega \rightarrow \mathbb{R}$ .

For  $k_1 = 0$  and  $k_2 = 0$ , inserting Eq. (90) into Eq. (40),  $\hat{f}_{(0,0)}$  is a scalar given by

$$\hat{f}_{(0,0)} = \int_0^{2\pi} \int_0^{2\pi} f(\theta_1, \theta_2) \frac{d\theta_1 d\theta_2}{4\pi^2}.$$

When  $k_1$  and/or  $k_2$  are not zero, inserting Eq. (91) into Eq. (40), the components  $\hat{f}_{k_1, k_2}$  are  $2 \times 2$  matrices:

$$\begin{aligned} \hat{f}_{(k_1, k_2)} &= \int_0^{2\pi} \int_0^{2\pi} f(\theta_1, \theta_2) \begin{pmatrix} \cos(k_1\theta_1 + k_2\theta_2) & -\sin(k_1\theta_1 + k_2\theta_2) \\ \sin(k_1\theta_1 + k_2\theta_2) & \cos(k_1\theta_1 + k_2\theta_2) \end{pmatrix} \frac{d\theta_1 d\theta_2}{4\pi^2} \\ &= \begin{pmatrix} \hat{f}_{(k_1, k_2), 1} & -\hat{f}_{(k_1, k_2), 2} \\ \hat{f}_{(k_1, k_2), 2} & \hat{f}_{(k_1, k_2), 1} \end{pmatrix} \end{aligned}$$

where:

$$\begin{aligned} \hat{f}_{(k_1, k_2), 1} &= \int_0^{2\pi} \int_0^{2\pi} f(\theta_1, \theta_2) \cos(k_1\theta_1 + k_2\theta_2) \frac{d\theta_1 d\theta_2}{4\pi^2}, \\ \hat{f}_{(k_1, k_2), 2} &= \int_0^{2\pi} \int_0^{2\pi} f(\theta_1, \theta_2) \sin(k_1\theta_1 + k_2\theta_2) \frac{d\theta_1 d\theta_2}{4\pi^2}. \end{aligned}$$

As for the ring model, the matrix-valued Fourier components  $\hat{f}_{(k_1, k_2)}$  have only two independent scalar entries that we denote as  $\hat{f}_{(k_1, k_2), 1}$  and  $\hat{f}_{(k_1, k_2), 2}$ . These elements are the classical two-dimensional Fourier components, corresponding to basis functions on the torus.

#### 4.2.5 Fixed point equations for low-rank networks

We now focus on low-rank networks, i.e. models for which the Fourier components  $\hat{c}_{k_1, k_2}$  of the kernel  $c$  are zero for  $k_1 > K_1$  or  $k_2 > K_2$ . As shown in Sec. 3.4, for such models the steady-state activation is described by a finite number of non-zero Fourier components  $\kappa_{k_1, k_2}$  for  $k_1 \leq K_1$  and  $k_2 \leq K_2$ . Here we use the expressions for the irreps to write explicitly the fixed-point equation (Eq. (51)) satisfied by the Fourier components  $\kappa_{k_1, k_2}$  of any steady-state activation  $x^*$ .

Using the Convolution Theorem (Eq. (43)), we get for  $k_1 = 0$  and  $k_2 = 0$ :

$$\hat{F}_{(0,0)} = \hat{c}_{(0,0)} \cdot \hat{\Phi}_{(0,0)} \quad (92)$$

and, for  $(k_1, k_2) \neq (0, 0)$ :

$$\begin{aligned} \hat{F}_{(k_1, k_2)} &= \hat{c}_{(k_1, k_2)} \cdot \hat{\Phi}_{(k_1, k_2)} \\ &= \begin{pmatrix} \hat{c}_{(k_1, k_2), 1} \hat{\Phi}_{(k_1, k_2), 1} - \hat{c}_{(k_1, k_2), 2} \hat{\Phi}_{(k_1, k_2), 2} & -\hat{c}_{(k_1, k_2), 1} \hat{\Phi}_{(k_1, k_2), 2} - \hat{c}_{(k_1, k_2), 2} \hat{\Phi}_{(k_1, k_2), 1} \\ \hat{c}_{(k_1, k_2), 2} \hat{\Phi}_{(k_1, k_2), 1} + \hat{c}_{(k_1, k_2), 1} \hat{\Phi}_{(k_1, k_2), 2} & -\hat{c}_{(k_1, k_2), 2} \hat{\Phi}_{(k_1, k_2), 2} + \hat{c}_{(k_1, k_2), 1} \hat{\Phi}_{(k_1, k_2), 1} \end{pmatrix} \\ &:= \begin{pmatrix} \hat{F}_{(k_1, k_2), 1} & -\hat{F}_{(k_1, k_2), 2} \\ \hat{F}_{(k_1, k_2), 2} & \hat{F}_{(k_1, k_2), 1} \end{pmatrix} \end{aligned} \quad (93)$$

where

$$\begin{aligned} \hat{F}_{(k_1, k_2), 1} &= \hat{c}_{(k_1, k_2), 1} \hat{\Phi}_{(k_1, k_2), 1} - \hat{c}_{(k_1, k_2), 2} \hat{\Phi}_{(k_1, k_2), 2}, \\ \hat{F}_{(k_1, k_2), 2} &= \hat{c}_{(k_1, k_2), 2} \hat{\Phi}_{(k_1, k_2), 1} + \hat{c}_{(k_1, k_2), 1} \hat{\Phi}_{(k_1, k_2), 2}. \end{aligned}$$

To express explicitly  $\hat{F}_{(k_1, k_2), 1}$  and  $\hat{F}_{(k_1, k_2), 2}$ , we write the expressions for  $\hat{\Phi}_{(k_1, k_2)}$  in terms of the Fourier components  $\kappa_{(k_1, k_2)}$  of the steady-state activation  $x^*$ .

For  $k_1 = 0$  and  $k_2 = 0$ , we have

$$\hat{\Phi}_{(0,0)} = \int_0^{2\pi} \int_0^{2\pi} \Phi[x^*(\theta_1, \theta_2)] \frac{d\theta_1 d\theta_2}{4\pi^2}, \quad (94)$$

while for  $(k_1, k_2) \neq (0, 0)$ , the independent matrix elements are given by

$$\hat{\Phi}_{(k_1, k_2), 1} = \int_0^{2\pi} \int_0^{2\pi} \Phi [x^*(\theta_1, \theta_2)] \cos(k_1 \theta_1 + k_2 \theta_2) \frac{d\theta_1 d\theta_2}{4\pi^2}, \quad (95)$$

$$\hat{\Phi}_{(k_1, k_2), 2} = \int_0^{2\pi} \int_0^{2\pi} \Phi [x^*(\theta_1, \theta_2)] \sin(k_1 \theta_1 + k_2 \theta_2) \frac{d\theta_1 d\theta_2}{4\pi^2}. \quad (96)$$

We next write the steady-state activation  $x^*$  using the Inverse Fourier Transform (Eq. (42)):

$$\begin{aligned} x^*(\theta_1, \theta_2) &= \sum_{k_1=0, k_2=0}^{K_1, K_2} \tilde{d}_{(k_1, k_2)} \operatorname{tr}(\kappa_{(k_1, k_2)} \rho_{(k_1, k_2)}^{-1}(\theta_1, \theta_2)) \\ &= \kappa_{(0,0)} + \sum_{\substack{k_1=0, k_2=0 \\ (k_1, k_2) \neq (0,0)}}^{K_1, K_2} \operatorname{tr} \left( \begin{pmatrix} \kappa_{(k_1, k_2), 1} & -\kappa_{(k_1, k_2), 2} \\ \kappa_{(k_1, k_2), 2} & \kappa_{(k_1, k_2), 1} \end{pmatrix} \begin{pmatrix} \cos(k_1 \theta_1 + k_2 \theta_2) & \sin(k_1 \theta_1 + k_2 \theta_2) \\ -\sin(k_1 \theta_1 + k_2 \theta_2) & \cos(k_1 \theta_1 + k_2 \theta_2) \end{pmatrix} \right) \\ &= \kappa_{(0,0)} + \sum_{\substack{k_1=0, k_2=0 \\ (k_1, k_2) \neq (0,0)}}^{K_1, K_2} 2 (\kappa_{(k_1, k_2), 1} \cos(k_1 \theta_1 + k_2 \theta_2) + \kappa_{(k_1, k_2), 2} \sin(k_1 \theta_1 + k_2 \theta_2)). \end{aligned} \quad (97)$$

Here we include only the Fourier components up to  $K_1$  and  $K_2$ , because at steady-state  $\kappa_{(k_1, k_2)} = 0$  for  $k_1 > K_1$  or  $k_2 > K_2$ .

Inserting Eq. (97) into Eqs. (94), (95) and (96) gives us explicit expressions for  $\hat{\Phi}_{(0,0)}$ ,  $\hat{\Phi}_{(k_1, k_2), 1}$  and  $\hat{\Phi}_{(k_1, k_2), 2}$  as functions of the set of scalars  $\kappa_{(0,0)}$ ,  $\kappa_{(k_1, k_2), 1}$ ,  $\kappa_{(k_1, k_2), 2}$  for  $k_1 = 1 \dots K_1$  and  $k_2 = 1 \dots K_2$ .

This leads to the following fixed point equations:

$$\kappa_{(0,0)} = \hat{c}_0 \int_0^{2\pi} \int_0^{2\pi} \Phi \left[ \kappa_{(0,0)} + \sum_{\substack{k_1=0, k_2=0 \\ (k_1, k_2) \neq (0,0)}}^{K_1, K_2} 2 (\kappa_{(k_1, k_2), 1} \cos(k_1 \theta_1 + k_2 \theta_2) + \kappa_{(k_1, k_2), 2} \sin(k_1 \theta_1 + k_2 \theta_2)) \right] \frac{d\theta_1 d\theta_2}{4\pi^2}, \quad (98)$$

$$\kappa_{(k_1, k_2), 1} = \int_0^{2\pi} \int_0^{2\pi} \Phi \left[ \kappa_{(0,0)} + \sum_{\substack{k'_1=0, k'_2=0 \\ (k'_1, k'_2) \neq (0,0)}}^{K_1, K_2} 2 (\kappa_{(k'_1, k'_2), 1} \cos(k'_1 \theta_1 + k'_2 \theta_2) + \kappa_{(k'_1, k'_2), 2} \sin(k'_1 \theta_1 + k'_2 \theta_2)) \right] \frac{d\theta_1 d\theta_2}{4\pi^2}, \quad (99)$$

$$\times (\hat{c}_{(k_1, k_2), 1} \cos(k_1 \theta_1 + k_2 \theta_2) - \hat{c}_{(k_1, k_2), 2} \sin(k_1 \theta_1 + k_2 \theta_2)) \frac{d\theta_1 d\theta_2}{4\pi^2}, \quad (100)$$

$$\kappa_{(k_1, k_2), 2} = \int_0^{2\pi} \int_0^{2\pi} \Phi \left[ \kappa_{(0,0)} + \sum_{\substack{k'_1=0, k'_2=0 \\ (k'_1, k'_2) \neq (0,0)}}^{K_1, K_2} 2 (\kappa_{(k'_1, k'_2), 1} \cos(k'_1 \theta_1 + k'_2 \theta_2) + \kappa_{(k'_1, k'_2), 2} \sin(k'_1 \theta_1 + k'_2 \theta_2)) \right] \frac{d\theta_1 d\theta_2}{4\pi^2}. \quad (101)$$

$$\times (\hat{c}_{(k_1, k_2), 2} \cos(k_1 \theta_1 + k_2 \theta_2) + \hat{c}_{(k_1, k_2), 1} \sin(k_1 \theta_1 + k_2 \theta_2)) \frac{d\theta_1 d\theta_2}{4\pi^2}. \quad (102)$$

#### 4.2.6 Fixed point manifold

Any solution  $\underline{\kappa}$  of the fixed point equation (98), (99), (101) therefore leads to a manifold of fixed points in Fourier coordinates parametrized by elements of the group  $\mathbb{S}^1 \times \mathbb{S}^1$ :

$$\underline{\kappa}(\phi_1, \phi_2) = R^{K_1, K_2}(\phi_1, \phi_2) \underline{\kappa}. \quad (103)$$

where  $R^{K_1, K_2}(\phi_1, \phi_2)$  is block-diagonal containing at most  $(K_1+1)(K_2+1)$  rotation matrices that act on the corresponding Fourier components:

$$R^{K_1, K_2}(\phi_1, \phi_2) = \begin{pmatrix} \rho_{(0,0)}(\phi_1, \phi_2) & & & & \\ & \rho_{(1,0)}(\phi_1, \phi_2) & & & \\ & & \rho_{(0,1)}(\phi_1, \phi_2) & & \\ & & & \rho_{(1,1)}(\phi_1, \phi_2) & \\ & & & & \ddots \\ & & & & \rho_{(K_1, K_2)}(\phi_1, \phi_2) \end{pmatrix}. \quad (104)$$

#### 4.2.7 Rank five toroidal RNN

As a concrete example, we consider the rank five toroidal model, which we explicitly contrast with the rank five ring model described in Sec. 4.1.8. The rank five toroidal model is defined by the connectivity kernel

$$c(\theta_1, \theta_2) = J_0 + J_1 \cos(\theta_1) + J_2 \cos(\theta_2),$$

where  $J_0, J_1$  and  $J_2$  are scalar parameters. In this case, the non-zero Fourier components are

$$\begin{aligned} \hat{c}_{(0,0)} &= J_0 \\ \hat{c}_{(1,0)} &= \begin{pmatrix} \hat{c}_{(1,0)1} & -\hat{c}_{(1,0)2} \\ \hat{c}_{(1,0)2} & \hat{c}_{(1,0)1} \end{pmatrix} = J_1 \begin{pmatrix} \frac{1}{2} & 0 \\ 0 & \frac{1}{2} \end{pmatrix} \\ \hat{c}_{(0,1)} &= \begin{pmatrix} \hat{c}_{(0,1)1} & -\hat{c}_{(0,1)2} \\ \hat{c}_{(0,1)2} & \hat{c}_{(0,1)1} \end{pmatrix} = J_2 \begin{pmatrix} \frac{1}{2} & 0 \\ 0 & \frac{1}{2} \end{pmatrix} \end{aligned}$$

while for  $k_1 \geq 1$  and  $k_2 \geq 1$ :

$$\hat{c}_{(k_1, k_2)} = \begin{pmatrix} 0 & 0 \\ 0 & 0 \end{pmatrix}.$$

The Fourier components of the kernel are zero for  $k_1 \geq 1$  and  $k_2 \geq 1$ , resulting in a rank 5 model. From Eq. (97), the steady state activation  $x^*(\theta_1, \theta_2)$  is given by

$$x(\theta_1, \theta_2) = \kappa_{(0,0)} + 2(\kappa_{(1,0),1} \cos(\theta_1) + \kappa_{(1,0),2} \sin(\theta_1) + \kappa_{(0,1),1} \cos(\theta_2) + \kappa_{(0,1),2} \sin(\theta_2)). \quad (105)$$

The fixed point equations (98)-(101) reduce to a set of 5 coupled equations for the scalars  $\kappa_{(0,0)}, \kappa_{(1,0),1}, \kappa_{(1,0),2}, \kappa_{(0,1),1}, \kappa_{(0,1),2}$ :

$$\begin{cases} \kappa_{(0,0)} = J_0 \int_0^{2\pi} \Phi [\kappa_{(0,0)} + 2(\kappa_{(1,0),1} \cos(\theta_1) + \kappa_{(1,0),2} \sin(\theta_1) + \kappa_{(0,1),1} \cos(\theta_2) + \kappa_{(0,1),2} \sin(\theta_2))] \frac{d\theta_1 d\theta_2}{4\pi^2}, \\ \kappa_{(1,0),1} = \frac{J_1}{2} \int_0^{2\pi} \Phi [\kappa_{(0,0)} + 2(\kappa_{(1,0),1} \cos(\theta_1) + \kappa_{(1,0),2} \sin(\theta_1) + \kappa_{(0,1),1} \cos(\theta_2) + \kappa_{(0,1),2} \sin(\theta_2))] \cos(\theta_1) \frac{d\theta_1 d\theta_2}{4\pi^2}, \\ \kappa_{(1,0),2} = \frac{J_1}{2} \int_0^{2\pi} \Phi [\kappa_{(0,0)} + 2(\kappa_{(1,0),1} \cos(\theta_1) + \kappa_{(1,0),2} \sin(\theta_1) + \kappa_{(0,1),1} \cos(\theta_2) + \kappa_{(0,1),2} \sin(\theta_2))] \sin(\theta_1) \frac{d\theta_1 d\theta_2}{4\pi^2}, \\ \kappa_{(0,1),1} = \frac{J_2}{2} \int_0^{2\pi} \Phi [\kappa_{(0,0)} + 2(\kappa_{(1,0),1} \cos(\theta_1) + \kappa_{(1,0),2} \sin(\theta_1) + \kappa_{(0,1),1} \cos(\theta_2) + \kappa_{(0,1),2} \sin(\theta_2))] \cos(\theta_2) \frac{d\theta_1 d\theta_2}{4\pi^2}, \\ \kappa_{(0,1),2} = \frac{J_2}{2} \int_0^{2\pi} \Phi [\kappa_{(0,0)} + 2(\kappa_{(1,0),1} \cos(\theta_1) + \kappa_{(1,0),2} \sin(\theta_1) + \kappa_{(0,1),1} \cos(\theta_2) + \kappa_{(0,1),2} \sin(\theta_2))] \sin(\theta_2) \frac{d\theta_1 d\theta_2}{4\pi^2}. \end{cases} \quad (106)$$

Using Eq. (103), any solution  $\underline{\kappa} := (\kappa_{(0,0)}, \kappa_{(1,0),1}, \kappa_{(1,0),2}, \kappa_{(0,1),1}, \kappa_{(0,1),2})$  of the system (106) leads to a manifold of fixed points in Fourier coordinates, parametrized by elements of  $SO(2) \times SO(2)$ :

$$\underline{\kappa}(\phi_1, \phi_2) = R^{(1,1)}(\phi_1, \phi_2) \underline{\kappa}. \quad (107)$$

Here,  $R^{(1,1)}(\phi_1, \phi_2)$ , is a block diagonal 5D matrix containing independent rotation matrices:

$$R^{(1,1)}(\phi_1, \phi_2) = \begin{pmatrix} 1 & 0 & 0 & 0 & 0 \\ 0 & \cos(\phi_1) & -\sin(\phi_1) & 0 & 0 \\ 0 & \sin(\phi_1) & \cos(\phi_1) & 0 & 0 \\ 0 & 0 & 0 & \cos(\phi_2) & -\sin(\phi_2) \\ 0 & 0 & 0 & \sin(\phi_2) & \cos(\phi_2) \end{pmatrix}. \quad (108)$$

Setting  $\phi_1 = 0$  and  $\phi_2 = 0$ , we obtain a particular solution  $\underline{\kappa}(0, 0) = (\kappa_{(0,0)}, \kappa_{(1,0),1}, 0, \kappa_{(0,1),1}, 0)$ . The system (106) then reduces to the three-dimensional system:

$$\begin{cases} \kappa_{(0,0)} = J_0 \int_0^{2\pi} \Phi [\kappa_{(0,0)} + 2(\kappa_{(1,0),1} \cos(\theta_1) + \kappa_{(0,1),1} \cos(\theta_2))] \frac{d\theta_1 d\theta_2}{4\pi^2}, \\ \kappa_{(1,0),1} = \frac{J_1}{2} \int_0^{2\pi} \Phi [\kappa_{(0,0)} + 2(\kappa_{(1,0),1} \cos(\theta_1) + \kappa_{(0,1),1} \cos(\theta_2))] \cos(\theta_1) \frac{d\theta_1 d\theta_2}{4\pi^2}, \\ \kappa_{(0,1),1} = \frac{J_2}{2} \int_0^{2\pi} \Phi [\kappa_{(0,0)} + 2(\kappa_{(1,0),1} \cos(\theta_1) + \kappa_{(0,1),1} \cos(\theta_2))] \cos(\theta_2) \frac{d\theta_1 d\theta_2}{4\pi^2}. \end{cases} \quad (109)$$

The stability of each fixed-point is determined by the eigenvalues of the Jacobian of the r.h.s, evaluated at the fixed point. This stability is then inherited by all the fixed points on the resulting manifold.

Eqs. (109) admit three types of solutions that lead to different types of manifolds of fixed points in Eq. (105): (i) solutions with  $\kappa_{(0,0)} = \varrho_0 \neq 0$  and  $\kappa_{(1,0),1} = \kappa_{(1,0),2} = 0$ ; from Eq. (108) such solutions lead to single fixed point, i.e. a manifold of intrinsic dimension 0; (ii) solutions with  $\kappa_{(1,0),1} = \varrho_1 \neq 0$  and  $\kappa_{(1,0),2} = 0$ , or  $\kappa_{(1,0),2} = \varrho_2 \neq 0$  and  $\kappa_{(1,0),1} = 0$ ; from Eq. (108) each such solution leads to a ring of fixed points embedded in two dimensions, i.e. a manifold of intrinsic dimension 1 and embedding dimension 2; (iii) solutions with  $\kappa_{(1,0),1} = \varrho_1 \neq 0$  and  $\kappa_{(1,0),2} = \varrho_2 \neq 0$  lead to a torus of fixed points embedded in four dimensions, i.e. a manifold of intrinsic dimension 2, and embedding dimension 4. The existence of these solutions depends on the values of the parameters  $J_0, J_1, J_2$ . For a fixed set of parameter values, we find that several types of solutions can co-exist, leading to multi-stability between fixed points manifolds of various intrinsic and embedding dimensions, some stable others consisting of saddle points (Fig. 4).

Specifically, applying the relation (107) to particular solution  $\underline{\kappa}(0, 0) = (\varrho_0, \varrho_1, 0, \varrho_2, 0)$ , the general solution for  $(\phi_1, \phi_2) \in [0, 2\pi] \times [0, 2\pi]$  is:

$$\underline{\kappa}(\phi_1, \phi_2) = (\varrho_0, \varrho_1 \cos(\phi_1), \varrho_1 \sin(\phi_1), \varrho_2 \cos(\phi_2), \varrho_2 \sin(\phi_2)). \quad (110)$$

Inserting Eq. (110) into Eq. (105) results in the population activity for fixed  $(\phi_1, \phi_2)$  (Fig. 4D):

$$x_{(\phi_1, \phi_2)}(\theta_1, \theta_2) = \varrho_0 + 2(\varrho_1 \cos(\theta_1 - \phi_1) + \varrho_2 \cos(\theta_2 - \phi_2)). \quad (111)$$

The rank five toroidal eqRNN and the rank five ring model are both five-dimensional models, in the sense that at most five Fourier components of the steady state can be simultaneously non-zero. The matrices determining the fixed point manifolds have a similar block structure, with the key difference that for the toroidal model the rotation matrix depends on two independent angles (Eq. (108)), while for the ring model the blocks depend on a single angle and its double (Eq. (85)). This leads to an important difference in the resulting fixed-point manifolds. While both models can generate ring manifolds embedded in two dimensions, toroidal eqRNNs generate torii embedded in four-dimensions, while the ring model generates ring manifolds embedded in four dimensions.

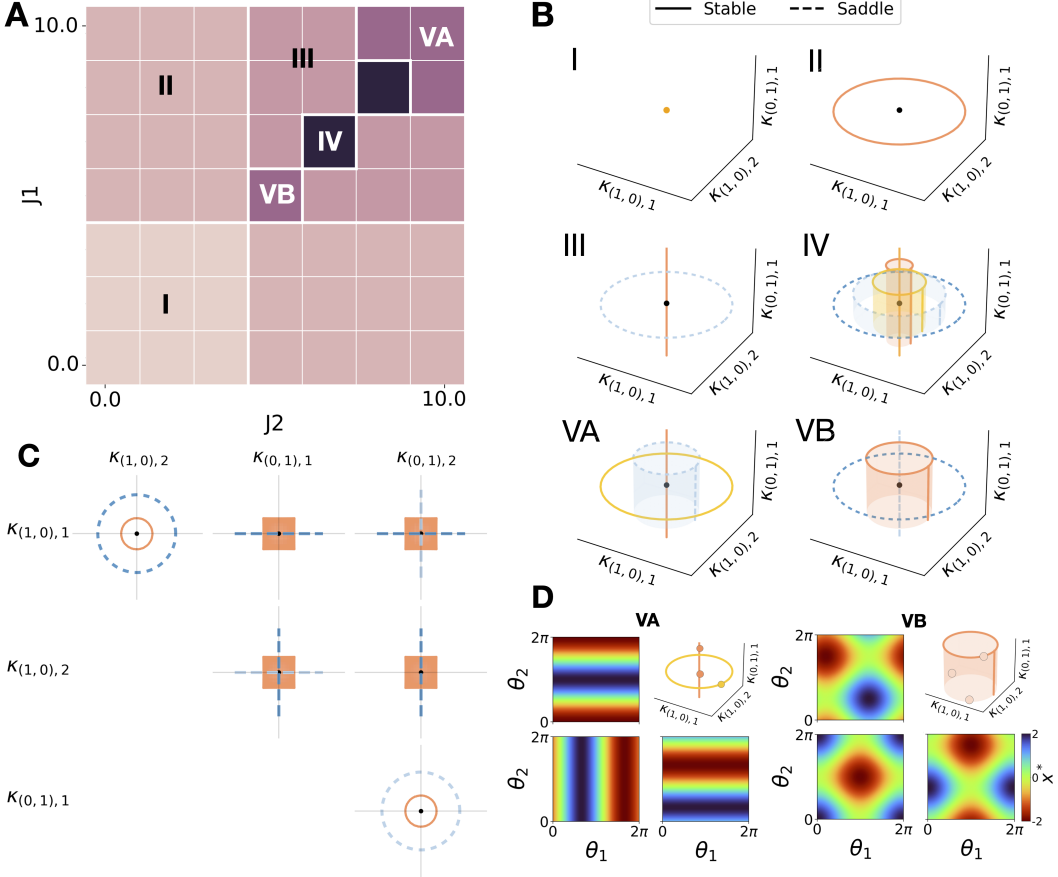


Figure 4: Manifolds of fixed points in the rank five toroidal RNN. A) Bifurcation diagram showing five regions of parameters (I-V) leading to different combinations of co-existing fixed point solutions. Here we vary  $J_1$  and  $J_2$ , while  $J_0 = -3$  is fixed. B) Illustration of co-existing manifolds of fixed points within each of the five parameter regions. The manifolds are shown in the three-dimensional space corresponding to the Fourier components  $K_{(1,0),1}, K_{(1,0),2}, K_{(0,1),1}$ , while they are actually embedded in four dimensions  $K_{(1,0),1}, K_{(1,0),2}, K_{(0,1),1}, K_{(0,1),2}$ . In this projection, torii appear as cylinders, and rings in the  $K_{(0,1),1} - K_{(0,1),2}$  plane as vertical segments. I: single, stable fixed point; II: unstable single and a stable 2d-ring; III: unstable single point and two 2d-rings in the planes  $K_{(1,0),1} - K_{(1,0),2}$  (saddle) and  $K_{(0,1),1} - K_{(0,1),2}$  (stable); IV: unstable single point, two stable 2d-rings (in the planes  $K_{(1,0),1} - K_{(1,0),2}$  and  $K_{(0,1),1} - K_{(0,1),2}$ ) and three tori (one stable, two saddles); V: unstable single point, two stable 2d-rings and one saddle torus (or vice versa). Stable solutions are shown as solid lines, saddles are shown as dashed lines. C) Two-dimensional projections of the manifolds of fixed point in region VB onto planes corresponding to different pairs of Fourier component  $K_{(1,0),1}, K_{(1,0),2}, K_{(0,1),1}, K_{(0,1),2}$ . The projection of a torus (orange) leads to circles in the planes  $K_{(1,0),1} - K_{(1,0),2}$  and  $K_{(0,1),1} - K_{(0,1),2}$ , and squares in the other planes. D) Left: Population activity profiles corresponding to the union of two stable orthogonal 2d-ring manifolds, displaying a band pattern. Right: Population activity profiles corresponding to the stable torus manifold, displaying a localized bump pattern.

### 4.3 Spherical RNNs

While toroidal RNNs are a generalization of the ring model to a higher-dimensional domain with a product structure, the framework of eqRNNs allows us to extend ring models to more general higher-dimensional domains. The simplest two-dimensional domain without a product structure is the two-dimensional sphere, which leads to a class of models we call *spherical RNNs*. These models are an instance of the situation where the domain  $\Omega$  and the associated group  $G$  are not isomorphic, and we use this example to illustrate how the eqRNN framework extends to that case.

### 4.3.1 Domain structure and symmetry group

In spherical RNNs, neurons are indexed by points on the 2-dimensional sphere  $\mathcal{S}^2$ . The domain is therefore  $\Omega = \mathcal{S}^2$ , and each unit is parametrized by a pair of angles  $(u_1, u_2) = (\theta, \phi)$  with  $\theta \in [0, \pi]$  (longitude) and  $\phi \in [0, 2\pi]$  (colatitude). Importantly,  $\mathcal{S}^2$  does not itself form a group. The group associated with  $\mathcal{S}^2$  is instead  $G = SO(3)$ , the group of all rotations in  $\mathbb{R}^3$ . Elements of  $SO(3)$  are parametrized by three parameters, and we denote them as  $g_{\alpha, \beta, \gamma}$ , where  $\alpha, \beta, \gamma$  are the Euler angles with  $\alpha, \gamma \in [0, 2\pi]$  and  $\beta \in [0, \pi]$ . Any point  $(\theta, \phi) \in \mathcal{S}^2$  can be mapped onto any other point  $(\theta', \phi') \in \mathcal{S}^2$  by applying an element  $g_{\alpha, \beta, \gamma} \in SO(3)$  such that  $g_{\alpha, \beta, \gamma}(\theta, \phi) = (\theta', \phi')$ . The sphere  $\mathcal{S}^2$  is therefore a homogeneous space under the action of  $SO(3)$  (Kondor & Trivedi 2018, Bekkers 2019, Cohen, Geiger & Weiler 2018). However, in contrast to the two previous examples,  $\mathcal{S}^2$  and  $SO(3)$  are not isomorphic, because the element of  $SO(3)$  mapping  $(\theta, \phi)$  onto  $(\theta', \phi')$  is in general not unique. Indeed, while  $g_{\alpha, \beta, \gamma}$  describes all possible rotations of a rigid body in  $\mathbb{R}^3$  using three parameters, on the sphere  $\mathcal{S}^2$  only two angles are necessary to describe any point. This is because, the third Euler angle  $\gamma$  represents a rotation of a rigid body around the local axis defined by  $(\alpha, \beta)$ , which does not change the position of a point on the sphere. A bijective mapping between  $\mathcal{S}^2$  and  $SO(3)$  is therefore obtained by fixing  $\gamma = 0$ . More formally, this amounts to identifying  $\mathcal{S}^2$  with the quotient  $SO(3)/SO(2)$ .

Spherical RNNs are therefore an example of a model in which the domain  $\Omega$  is not a group, but can be formulated as a quotient  $G/H$  of two groups  $G$  and  $H$ . Kondor & Trivedi (2018) show how, in such a situation, the concepts of group convolution and group Fourier transform can be extended based on the irreducible representations of  $G$  and  $H$ . Here we follow their construction in the case  $G = SO(3)$  and  $H = SO(2)$ .

### 4.3.2 Spherical convolution

A convolution with respect to a group  $G$  is habitually defined on functions  $G \rightarrow \mathbb{R}$  (Eq. (32)). To construct a convolutional RNN defined on a domain  $\Omega$ , we instead need to define the recurrent input as a convolution of functions  $\Omega \rightarrow \mathbb{R}$ . In previous examples, we had  $\Omega = G$ , so this was not an issue, but for spherical RNNs  $\Omega$  and  $G$  are not isomorphic. Following Kondor and Trivedi, we define the convolution on  $\Omega = G/H$  by lifting the convolution from  $G/H$  to  $G$  (see Appendix A.8).

For  $\Omega = SO(3)/SO(2)$ , this is equivalent to defining the recurrent input in terms of the *spherical convolution* (Bekkers 2019, Kondor et al. 2018, Kennedy et al. 2011, Roddy & McEwen 2021). For a connectivity kernel  $c : \mathcal{S}^2 \rightarrow \mathbb{R}$ , and the firing rate  $\Phi : \mathcal{S}^2 \rightarrow \mathbb{R}$ , the recurrent input  $F^t : \mathcal{S}^2 \rightarrow \mathbb{R}$  at time step  $t$  is defined as

$$F^t(\theta, \phi) = \int_0^{2\pi} \int_0^\pi c(g_{(\theta, \phi, \gamma=0)}^{-1}(\theta', \phi')) \Phi(x_t(\theta', \phi')) \frac{\sin \theta' d\theta' d\phi'}{4\pi}, \quad (112)$$

where we integrate with respect to the normalized Haar measure  $d\mu(\mathcal{S}^2) = \frac{\sin \theta' d\theta' d\phi'}{4\pi}$ .

### 4.3.3 Representations of $SO(3)$ and their restriction to $\mathcal{S}^2$

The habitual definition of the group Fourier transform for functions  $G \rightarrow \mathbb{R}$  relies on the irreducible representations of  $G$  (Eq. (40)). To define low-rank networks on  $\Omega$ , we instead need a Fourier transform for functions  $\Omega \rightarrow \mathbb{R}$ . For  $\Omega = G/H$ , Kondor and Trivedi show that a Fourier transform on  $\Omega$  is naturally defined by restricting the irreps of  $G$  to  $G/H$ , which amounts to keeping only specific columns of each irrep of  $G$ . While the group Fourier transform consists of matrix-valued components (Eq. (40)), the Fourier transform on  $\Omega = G/H$  has instead vector-valued components. Here we follow the construction of Kondor and Trivedi for  $G = SO(3)$  and  $H = SO(2)$ . This approach provides a direct relation between the irreps of  $SO(3)$  and spherical harmonics that are habitually used to define the Fourier transform on  $\mathcal{S}^2$  (Kondor et al. 2018, Kennedy et al. 2011).

The irreducible representations of  $SO(3)$  are indexed by a parameter  $\ell \in \mathbb{N}$ . For a given  $\ell$ , the representation  $\rho_\ell(g_{\alpha, \beta, \gamma})$  of a group element  $g_{\alpha, \beta, \gamma} \in SO(3)$ , is a  $(2\ell + 1) \times (2\ell + 1)$  matrix called the  $2\ell + 1$  dimensional Wigner  $D$ -matrix (Cohen & Welling 2014, Kosmann-Schwarzbach 2009, Cohen, Geiger, Köhler & Welling 2018):

$$\rho_\ell(g_{\alpha, \beta, \gamma}) = D^\ell(\alpha, \beta, \gamma).$$

Restricting  $SO(3)$  to  $SO(3)/SO(2)$  corresponds to setting  $\gamma = 0$  in  $\rho_\ell(g_{\alpha, \beta, \gamma})$ . This amounts to selecting the central column of the Wigner matrix  $D^\ell$ , which contains a  $(2\ell + 1)$ -dimensional vector called the spherical harmonic  $\underline{Y}_\ell$ .

For  $\ell = 0$ ,  $Y_0$  is a scalar given by:

$$Y_0(\theta, \phi) = 1,$$

while for  $\ell > 0$ , the elements  $Y_\ell^m$  for  $m = -\ell, \dots, \ell$  of  $\underline{Y}_\ell$  are given by

$$Y_{\ell m}(\theta, \phi) = \begin{cases} (-1)^m \sqrt{2} \sqrt{(2\ell+1) \frac{(\ell-|m|)!}{(\ell+|m|)!}} P_\ell^{|m|}(\cos \theta) \sin(|m|\phi), & \text{if } m < 0, \\ \sqrt{(2\ell+1)} P_\ell^m(\cos \theta), & \text{if } m = 0, \\ (-1)^m \sqrt{2} \sqrt{(2\ell+1) \frac{(\ell-m)!}{(\ell+m)!}} P_\ell^m(\cos \theta) \cos(m\phi), & \text{if } m > 0 \end{cases}$$

where  $P_\ell^m : [-1, 1] \rightarrow \mathbb{R}$  are the associated Legendre polynomials (Kosmann-Schwarzbach 2009).

#### 4.3.4 Spherical Fourier transform

Using the restriction of  $SO(3)$  irreps, the Fourier transform for a function  $f : \mathcal{S}^2 \rightarrow \mathbb{R}$  consists of vector-valued components indexed by  $\ell \in \mathbb{N}$  and obtained by projecting  $f$  on spherical harmonics.

For  $\ell = 0$ , the Fourier component  $\hat{f}_0$  is a scalar given by

$$\hat{f}_0 = \int_0^{2\pi} \int_0^\pi f(\theta, \phi) Y_0(\theta, \phi) \frac{\sin \theta d\theta d\phi}{4\pi}, \quad (113)$$

while for  $\ell > 0$ ,  $\hat{f}_\ell \in \mathbb{R}^{2\ell+1}$  is a vector containing  $(2\ell+1)$  elements  $\hat{f}_{\ell,m}$ ,  $m = -\ell, \dots, \ell$ , given by:

$$\hat{f}_{\ell,m} = \int_0^{2\pi} \int_0^\pi f(\theta, \phi) Y_{\ell,m}(\theta, \phi) \frac{\sin \theta d\theta d\phi}{4\pi}.$$

The function  $f$  can be reconstructed from its Fourier components using the real-valued spherical harmonic expansion, which is equivalent to the inverse Fourier transform on  $\mathcal{S}^2$  (Kondor et al. 2018):

$$f(\theta, \phi) = \sum_{\ell=0}^{\infty} \sum_{m=-\ell}^{\ell} \hat{f}_{\ell,m} Y_{\ell,m}(\theta, \phi).$$

#### 4.3.5 Fixed point equations for low-rank models

We now focus on low-rank models on the sphere, i.e., models where the Fourier coefficients  $\hat{c}_{\ell,m}$  of the kernel  $c(\theta, \phi)$  are zero for  $\ell > L$ . As shown in Sec. 3.4, for such models the steady-state activation is described by a finite number of non-zero Fourier components  $\kappa_{\ell,m}$  for  $\ell \leq L$  and  $-\ell \leq m \leq \ell$ . Here we use the expressions for the irreps to write explicitly the fixed-point equation (Eq. (51)) satisfied by the Fourier coefficients  $\kappa_{\ell,m}$  of any steady-state activation  $x^*$ .

Using the Convolution Theorem (Eq. (43)), we get for  $\ell = 0$  (and  $m = 0$ ):

$$\hat{F}_0 = \hat{c}_0 \cdot \hat{\Phi}_0 \quad (114)$$

For  $\ell > 0$ ,  $m \in [-\ell, \ell]$ :

$$\hat{F}_{\ell,m} = \hat{c}_{\ell,m} \cdot \hat{\Phi}_{\ell,m}. \quad (115)$$

To express explicitly  $\hat{F}_0$  and  $\hat{F}_{\ell,m}$ , we write the expressions for  $\hat{\Phi}_0$  and  $\hat{\Phi}_{\ell,m}$  in terms of the Fourier components  $\kappa_{\ell,m}$  of the steady-state activation  $x^*$ .

For  $\ell = 0$  (and  $m = 0$ ), we have the scalar

$$\hat{\Phi}_0 = \int_0^{2\pi} \int_0^\pi \Phi[x(\theta, \phi)] Y_0(\theta, \phi) \frac{\sin \theta d\theta d\phi}{4\pi}, \quad (116)$$

while for  $\ell > 0$ , the Fourier components are vectors which elements are given by

$$\hat{\Phi}_{\ell,m} = \int_0^{2\pi} \int_0^\pi \Phi[x(\theta, \phi)] Y_{\ell,m}(\theta, \phi) \frac{\sin \theta d\theta d\phi}{4\pi}. \quad (117)$$

We next write the steady-state activation  $x(\theta, \phi)$  using the Inverse Fourier Transform:

$$\begin{aligned}
x(\theta, \phi) &= \sum_{\ell=0}^L \sum_{m=-\ell}^{\ell} \kappa_{\ell,m} Y_{\ell,m}(\theta, \phi) \\
&= \kappa_0 Y_0(\theta, \phi) + \sum_{\ell=1}^L \sum_{m=-\ell}^{\ell} \kappa_{\ell,m} Y_{\ell,m}(\theta, \phi) \\
&= \kappa_0 + \sum_{\ell=1}^L \sum_{m=-\ell}^{\ell} \kappa_{\ell,m} Y_{\ell,m}(\theta, \phi).
\end{aligned} \tag{118}$$

Notice that we include only the  $L$  first Fourier components, because at steady-state  $\kappa_{\ell,m} = 0$  for  $\ell > L$ .

Inserting Eq. (118) into Eqs. (116) and (117) gives us explicit expressions for  $\hat{\Phi}_0$  and  $\hat{\Phi}_{\ell,m}$  as function of the set of  $2\ell + 1$  scalars  $\kappa_0$  and  $\kappa_{\ell,m}$ .

This leads to the explicit form of the fixed point equations:

$$\kappa_0 = \hat{c}_0 \int_0^{2\pi} \int_0^\pi \Phi \left[ \kappa_0 + \sum_{\ell=1}^L \sum_{m=-\ell}^{\ell} \kappa_{\ell,m} Y_{\ell,m}(\theta, \phi) \right] \frac{\sin \theta d\theta d\phi}{4\pi}, \tag{119}$$

$$\kappa_{\ell,m} = \hat{c}_{\ell,m} \int_0^{2\pi} \int_0^\pi \Phi \left[ \kappa_0 + \sum_{\ell'=1}^L \sum_{m'=-\ell'}^{\ell'} \kappa_{\ell',m'} Y_{\ell',m'}(\theta, \phi) \right] Y_{\ell,m}(\theta, \phi) \frac{\sin \theta d\theta d\phi}{4\pi}. \tag{120}$$

#### 4.3.6 Fixed point manifold

Because of the equivariance of recurrent inputs with respect to rotations in three dimensions, any steady state activation  $x^*$  leads to a manifold of fixed points given by  $S_g x^*$  for  $g \in SO(3)$ .

As shown in Eq. (53), applying the group action  $S_g$  to  $x^*$  leads to a linear transformation of its Fourier components determined by the corresponding irreducible representations of  $G$ . In this case  $G = SO(3)$ , so that

$$\kappa_l \mapsto \kappa_l D^\ell(\alpha, \beta, \gamma). \tag{121}$$

where  $D^\ell(\alpha, \beta, \gamma)$  is the  $\ell$ -th Wigner matrix associated with  $g \in SO(3)$  (Cohen, Geiger, Köhler & Welling 2018), and  $\kappa_l$  is a  $(2\ell + 1)$ -dimensional vector of Fourier components. Since  $x^*$  is a function on  $S^2$ , we can moreover set  $\gamma = 0$ , which amounts to parametrizing the fixed point manifold by elements of  $SO(3)/SO(2)$ .

In a low-rank spherical RNN, we have at most  $K + 1$  non-zero vector-valued Fourier components. Grouping them in a single vector  $\underline{\kappa}$  of dimension  $R = \sum_{\ell=0}^K 2\ell + 1$ , the manifold of fixed points in Fourier coordinates is given by

$$\underline{\kappa}(\alpha, \beta) = R^K(\alpha, \beta) \underline{\kappa}, \tag{122}$$

where  $R^K(\alpha, \beta)$  is block-diagonal, with each block corresponding to a Wigner  $D$ -matrix  $D^\ell(\alpha, \beta, 0)$  of increasing dimension  $2\ell + 1$ , for  $\ell = 0, 1, \dots, K$ .

#### 4.3.7 Rank three spherical RNN

We now consider the specific instantiation of the sphere model with the connectivity kernel

$$c(\theta, \phi) = J_1(\sin \theta \sin \phi + \cos \theta + \sin \theta \cos \phi),$$

where  $J_1$  is a scalar parameter that modulates the strength of the connectivity kernel. In this case, the only non-zero Fourier components of the kernel are for  $\ell = 1$ , with  $m = -1, 0, 1$ .

These components are given by:

$$\hat{c}_{1,-1} = \frac{J_1}{\sqrt{3}}, \quad \hat{c}_{1,0} = \frac{J_1}{\sqrt{3}}, \quad \hat{c}_{1,1} = \frac{J_1}{\sqrt{3}},$$

where the  $\ell = 0$  normalized real spherical harmonics are used:

$$Y_{1,-1}(\theta, \phi) = \sqrt{3} \sin \theta \sin \phi, \quad Y_{1,0}(\theta, \phi) = \sqrt{3} \cos \theta, \quad Y_{1,1}(\theta, \phi) = \sqrt{3} \sin \theta \cos \phi.$$

The only potentially non-zero Fourier components of the steady-state activation  $x^*$  are  $\kappa_{1,-1}, \kappa_{1,0}, \kappa_{1,1}$ , so that

$$\begin{aligned} x^*(\theta, \phi) &= \sum_{m=-1}^1 \kappa_{1,m} Y_{1,m}(\theta, \phi), \\ &= \kappa_{1,-1} Y_{1,-1}(\theta, \phi) + \kappa_{1,0} Y_{1,0}(\theta, \phi) + \kappa_{1,1} Y_{1,1}(\theta, \phi), \\ &= \sqrt{3} (\kappa_{1,-1} \sin \theta \sin \phi + \kappa_{1,0} \cos \theta + \kappa_{1,1} \sin \theta \cos \phi). \end{aligned} \quad (123)$$

In this case, Eqs. (119)-(120) reduce to three coupled equations for the scalars  $\kappa_{1,-1}, \kappa_{1,0}, \kappa_{1,1}$

$$\begin{aligned} \kappa_{1,-1} &= \frac{J_1}{\sqrt{3}} \int_0^{2\pi} \int_0^\pi \Phi \left[ \sum_{m=-1}^1 \kappa_{1,m} Y_{1,m}(\theta, \phi) \right] Y_{1,-1}(\theta, \phi) \frac{\sin \theta d\theta d\phi}{4\pi}, \\ \kappa_{1,0} &= \frac{J_1}{\sqrt{3}} \int_0^{2\pi} \int_0^\pi \Phi \left[ \sum_{m=-1}^1 \kappa_{1,m} Y_{1,m}(\theta, \phi) \right] Y_{1,0}(\theta, \phi) \frac{\sin \theta d\theta d\phi}{4\pi}, \\ \kappa_{1,1} &= \frac{J_1}{\sqrt{3}} \int_0^{2\pi} \int_0^\pi \Phi \left[ \sum_{m=-1}^1 \kappa_{1,m} Y_{1,m}(\theta, \phi) \right] Y_{1,1}(\theta, \phi) \frac{\sin \theta d\theta d\phi}{4\pi}. \end{aligned} \quad (124)$$

Any non-zero solution  $\underline{\kappa} = (\kappa_{1,-1}, \kappa_{1,0}, \kappa_{1,1})$  of these equations leads to a manifold of fixed points in Fourier coordinates, parametrized by elements of  $SO(3)$  (Zhengwei Su n.d., Blanco et al. 1997, Pinchon & Hoggan 2007):

$$\underline{\kappa}(\alpha, \beta) = R^1(\alpha, \beta) \underline{\kappa}, \quad (125)$$

where

$$R^1(\alpha, \beta) = \begin{pmatrix} \cos \alpha & \sin \alpha \sin \beta & \sin \alpha \cos \beta \\ 0 & \cos \beta & -\sin \beta \\ -\sin \alpha & \cos \alpha \sin \beta & \cos \alpha \cos \beta \end{pmatrix}.$$

Setting  $\alpha, \beta = 0, 0$ , we obtain a particular solution  $\underline{\kappa}(0, 0) = (0, \kappa_{1,0}, 0)$ . The system (124) then reduces to the one dimensional equation:

$$\kappa_{1,0} = \frac{J_1}{\sqrt{3}} \int_0^{2\pi} \int_0^\pi \Phi [\kappa_{1,0} Y_{1,0}(\theta, \phi)] Y_{1,0}(\theta, \phi) \frac{\sin \theta d\theta d\phi}{4\pi} \quad (126)$$

The stability of each fixed-point is determined by the sign of the derivative of the r.h.s with respect to  $\kappa_{1,0}$ , evaluated at the fixed point. This stability is then inherited by all the fixed points on the resulting manifold.

Eq. (126) admits a zero solution  $\kappa_{1,0} = 0$  that is stable for  $J_1 < J_c$ , and unstable for  $J_1 > J_c$ . For  $J_1 > J_c$ , Eq. (126) admits an additional pair of non-zero solutions with opposite signs  $\kappa_{1,0} = \pm \rho$  (Fig. 5 A). These solutions are stable, and lead to a manifold of stable fixed points that form a sphere embedded in three dimensions (Fig. 5 B). The radius of the sphere increases with  $J_1$ . Note that the two non-zero solutions of Eq. (126) with opposite signs correspond to antipodal points on the sphere.

Specifically, applying the relation (125) to the particular solution  $\underline{\kappa}(0, 0) = (0, \rho, 0)$ , leads to the general solution for  $(\alpha, \beta) \in [0, 2\pi] \times [0, \pi)$ :

$$\underline{\kappa}(\alpha, \beta) = (\rho \sin \alpha \sin \beta, \rho \cos \beta, \rho \cos \alpha \sin \beta). \quad (127)$$

Inserting (127) into Eq. (123) results in the population activity for fixed values of  $(\alpha, \beta)$  (Fig. 5C):

$$x_{\alpha, \beta}(\theta, \phi) = \sqrt{3} \rho \left( \sin \beta \sin \theta \cos(\phi - \alpha) + \cos \beta \cos \theta \right). \quad (128)$$

Note that, unlike the ring and the torus, the sphere does not admit a regular discretization that preserves (discretized) three-dimensional rotations. We provide an example of a discretization in the Appendix B.3. In general, a discretized version of the spherical RNN leads to at most two exact fixed points, but the rest of spherical manifold forms slow points, on which the speed of dynamics depends on the exact discretization (Fig. 7).

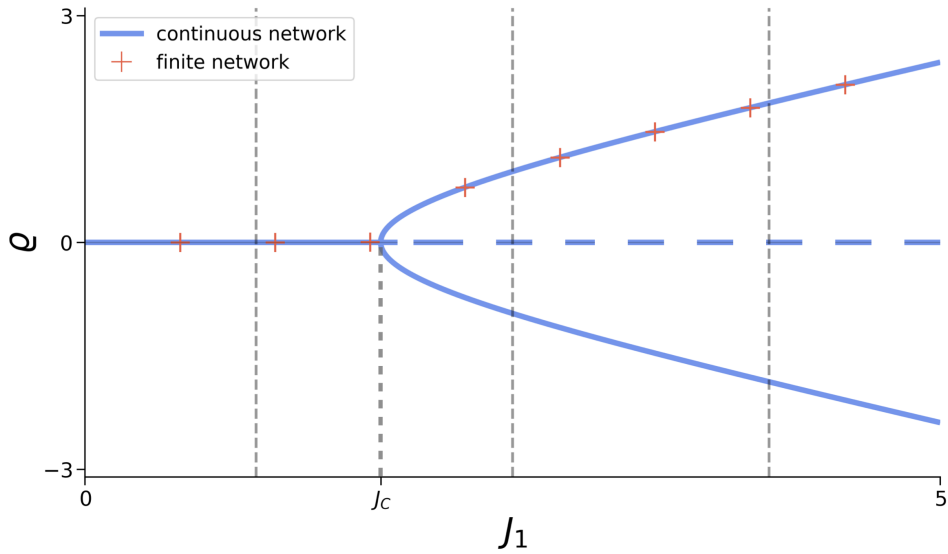
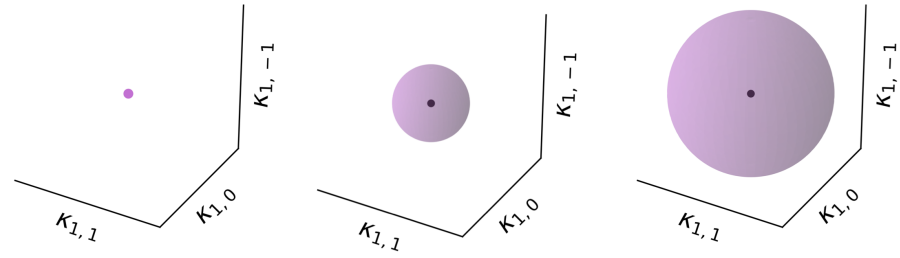
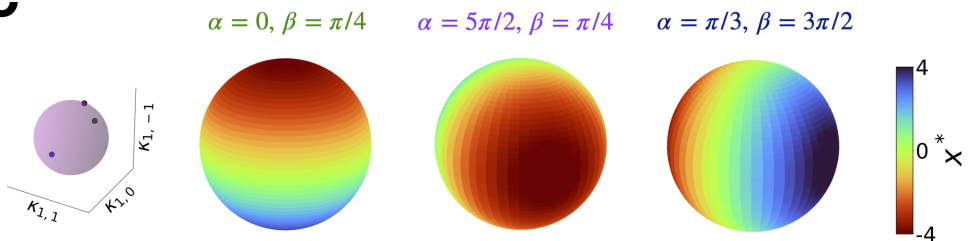
**A****B****C**

Figure 5: Bifurcation analysis and manifolds in the rank three spherical model. A) Bifurcation diagram showing the emergence of non-zero fixed points  $\kappa_{0,1}$  as a function of coupling strength  $J_1$ . Solid blue lines represent stable solutions while the dashed blue line indicates an unstable solution. Crosses show simulations of finite size network ( $N=1000$ , see appendix B.3). B) Fixed-point manifolds for three different coupling strengths indicated by vertical dashed lines in panel A. Left: At subcritical coupling, only a single fixed point exists. Middle: for  $J_1 > J_c$ , a spherical manifold of stable fixed points emerges. Right: At stronger coupling, the radius of the spherical manifold increases. C) Population activity patterns for three different fixed points on the spherical manifold for  $J = 1.1$ , corresponding to three different sets of coordinates  $(\alpha, \beta)$  indicated in the leftmost panel. Each color plot shows the fixed point neural activity  $x_{\alpha, \beta}^*(\theta, \phi)$ , as function of the coordinates  $(\theta, \phi)$  of neurons on  $\Omega = S^2$ , for a fixed set of  $(\alpha, \beta)$  values.

## Discussion

In this study, we adopted an abstract, mathematical approach to formulate a broad set of models that we call equivariant recurrent neural networks. This class of models provides a unified framework that relates the symmetries in the connectivity matrix of a recurrent network to the symmetries of its set of fixed points. Various particular instances of equivariant RNNs have been previously used in computational neuroscience as models of specific brain phenomena. The most central example is of course the classical ring model (Amari 1977), which is a standard model of orientation selectivity in the visual cortex (Ben-Yishai et al. 1995), head direction signals (Zhang 1996), place cells (Tsodyks & Sejnowski 1995, Samsonovich & McNaughton 1997, Tsodyks 1999) or working memory (Compte et al. 2000). Several recent works have applied the formalism of group theory to ring models (Zhang et al. 2022, Zuo et al. 2023, 2024). The rank two version of the ring model was originally introduced in Ben-Yishai et al. (1995) in networks of threshold-linear units, and analyzed using a decomposition on Fourier components. The discrete version, consisting of a small number of neurons, has attracted renewed attention recently (Noorman et al. 2024), with the discovery of the head-direction system in the fly (Kim et al. 2017) and the zebrafish (Petrucco et al. 2023). The class of models we call toroidal RNNs have been previously studied in several contexts. The equivalent of our rank five toroidal RNN with multi-stable ring attractors has been used as a model of storing multiple spatial maps in the navigation system (Romani & Tsodyks 2010, Si et al. 2014). More general toroidal RNNs leading to two-dimensional toroidal manifolds correspond to classical models of grid cells in the entorhinal cortex (Burak & Fiete 2009, Gardner et al. 2022). The original model of Burak & Fiete (2009) was based on a Gaussian connectivity kernel, while the rank five model used here keeps only the first two non-uniform Fourier components of the kernel. Note that, while the rank five toroidal RNN studied in Sec. 4.2.7 gives rise to toroidal manifolds, the individual neurons exhibit square rather than hexagonal tuning patterns (Sorscher et al. 2023, Khona et al. 2025). One way to generate hexagonal tuning patterns is to modify the underlying domain  $\Omega$  by introducing a twist, which effectively gives rise to a twisted torus (Guanella et al. 2007, Spalla et al. 2019). In absence of such a twist, identifying the conditions under which low-rank toroidal RNNs generate hexagonal grid cells is an interesting question for a future study.

Spherical RNNs analyzed in Sec. 4.3 provide a potential model for neural systems in charge of navigation in three dimensions (Stella et al. 2013, Spezialetti et al. 2020), such as the head orientation system in bats (Finkelstein et al. 2014). Such models have been comparatively less studied as they present two complications (Spezialetti et al. 2020). First, the relation between spherical variables and the corresponding set of symmetries, rotations in three dimensions, is less direct than for two-dimensional variables. More specifically, the set of points on a sphere does not form a group, and the associated group of three-dimensional rotations is three-dimensional rather than two-dimensional. As a consequence, the manifold of fixed points in the spherical RNN is not directly indexed by group elements, and therefore does not form a Lie group in contrast to the ring and toroidal models. Second, unlike the ring and the torus, the sphere and the associated symmetry group do not admit a regular discretization that preserves a set of discretized three-dimensional rotational symmetries (Cohen, Geiger, Köhler & Welling 2018, Kondor et al. 2018). Because of that, a discretized version of the spherical RNN leads in general to at most two exact fixed points (Appendix B.3) rather than an extensive number as in the ring and toroidal RNN. While the symmetry, and the resulting fixed-point manifold, are recovered in the continuum limit, finite-size models instead exhibit a spherical manifold of slow points (Fig. 7).

Our work is closely related to recent studies that have proposed practical recipes for constructing continuous attractor models with arbitrary topologies (Machens & Brody 2008, Darshan & Rivkind 2022, Pollock & Jazayeri 2020, Claudi & Branco 2022, Claudi et al. 2025, Barak & Romani 2021). In particular, studies in Claudi & Branco (2022), Claudi et al. (2025) have highlighted the challenges of modelling memory (Claudi & Branco 2022) and integration (Claudi et al. 2025) on complex topologies that extend beyond the ring, introducing methods from differential geometry to overcome these limitations. Our mathematical approach, based on group theory and Fourier transforms, offers a complementary perspective on this problem. The formalism of group theory, applied within the framework of geometric deep learning, allows us to precisely identify and control the symmetries embedded in the connectivity and activity of these networks. Group Fourier transforms, together with related tools from the framework of low-rank recurrent neural networks, enable us to derive explicit parameterizations and equations for the emergent manifold, from which both dynamical (e.g., stability) and geometric (e.g., embedding dimensionality) properties can be directly controlled. A key insight obtained from our approach is the importance of stability considerations: for a connectivity with a given symmetry, depending on parameters, several manifolds with different symmetry subgroups and different stability properties can coexist.

The mathematical formalism in this study is directly inspired by Geometric Deep Learning, a broad approach that applies group theory tools to various types of deep networks (Bronstein et al. 2021). A distinct line of research has used group theory to study the implications of symmetries on dynamical systems (Golubitsky & Stewart 2003, Chossat 2012). Since recurrent networks are a particular sub-class of dynamical systems, the present manuscript naturally bears similarities to that line of work, but adopts a distinct point of view. The general theory of symmetry in dynamical systems considers flow fields defined on  $\mathbb{R}^N$  that are symmetric, e.g. equivariant, with respect to a set of transformations

of  $\mathbb{R}^N$  that form a subgroup of  $GL(N)$ . That theory then seeks to derive general results for the symmetry of individual solutions, and the change of those symmetries at bifurcation points, i.e. symmetry breaking. In the present manuscript, we consider recurrent networks where units are indexed by an underlying domain  $\Omega$  that is associated with a symmetry group  $G$ . While an  $N$ -dimensional RNN is a dynamical system on  $\mathbb{R}^N$ , we formally define the state of the system as a function  $\Omega \rightarrow \mathbb{R}$ , so that the dynamics in the RNN correspond to dynamics within the space of such functions. Models of this type are usually referred to as neural mass or neural field models (Coombes et al. 2014). Although group theoretical approaches to neural field models have been previously developed (Bressloff et al. 2001), we are unaware of previous works in that literature focusing on connectivity based on group convolutions and the resulting manifolds of fixed points. The relationship between the present study and the broader field of symmetrical dynamical systems certainly merits further investigations.

The connectivity in equivariant RNNs is based on the generalized notion of group convolution. Using the concept of group Fourier transforms, we introduced low-rank RNNs as the subset of models in which the connectivity kernel has a finite number of non-zero Fourier components. For finite networks, this leads to a connectivity matrix that is of a rank determined by the number of non-zero Fourier components (Appendix B). Low-rank equivariant RNNs are therefore a subset of the broader class of low-rank RNNs (Mastrogiosse & Ostoic 2018, Schuessler et al. 2019, Beiran et al. 2021, Dubreuil et al. 2022, Logiaco et al. 2021, Pezon et al. 2024, Schmutz et al. 2025), and correspond to a specific case of the situation where the low-rank connectivity components are indexed by an underlying domain  $\Omega$  (Pezon et al. 2024). For both finite and continuous low-rank equivariant RNNs, the dynamics can be exactly reduced to a finite number of variables, similarly to more general low-rank RNNs. An important ingredient in the definition of the group Fourier transform is the notion of irreducible representations. While group representation theory has extensively mapped systems of irreducible representations for compact groups (Kosmann-Schwarzbach 2009), this theory has been generally developed for representations on complex numbers. To avoid defining complex-valued connectivity, here we instead used representations on real numbers, but strictly speaking this might lead to technical difficulties in certain cases because the set of real numbers is not algebraically closed in contrast to the set of complex numbers.

A central assumption in the class of equivariant RNNs is that the connectivity is defined as an exact convolution with a fixed connectivity kernel. While this ingredient induces the equivariance property of the fixed point equations, and therefore the existence of fixed point manifolds, such an exact symmetry is a very strong, and arguably unrealistic constraint for a biological network. Recent works have shown that this strong constraint is not a necessary condition for the appearance of fixed point manifolds. Statistical symmetries in the distribution of connectivity parameters can lead to continuous attractors in the limit of infinitely large networks (Mastrogiosse & Ostoic 2018, Beiran et al. 2021, 2023, Clark et al. 2025). In finite networks, fluctuations in connectivity (or in discretization, see Appendix B.3) typically lead to a breakdown of the manifold into a finite number of stable fixed points. Nevertheless, the dynamics remain very slow on the entirety of the original manifold, so that the fixed point manifold is effectively replaced by a *slow manifold* - a region in state space to which the dynamics are quickly attracted, but then slowly evolve on it. This empirical observation can be made mathematically more precise, by showing that finite networks remain in the vicinity of continuous attractors when considered in the parameter space (Ságoi et al. 2024). On the timescales of experimental recordings, such slow manifolds may in practice behave in a manner very similar to continuous attractors. Alternatively, it is often possible to fine-tune connectivity parameters to recover exact continuous attractors even in finite networks without full continuous symmetry (Darshan & Rivkind 2022, Noorman et al. 2024). Extending the theory of equivariant RNNs to statistically symmetric connectivity, or finite, disordered networks, is an important direction for future work.

## Acknowledgments

This work was supported by the CRCNS project PIND (ANR-19-NEUC-0001-01), the Simons Collaboration on the Global Brain (AN-NC-GB-Culmination-00003154-05), the program “Ecole Universitaire de Recherche” launched by the French Government and implemented by the ANR, with the reference ANR-17-EURE-0017.

## References

Amari, S. (1977), 'Dynamics of pattern formation in lateral-inhibition type neural fields', *Biol. Cybern.* **27**(2), 77–87.

Barak, O. & Romani, S. (2021), 'Mapping low-dimensional dynamics to high-dimensional neural activity: A derivation of the ring model from the neural engineering framework', *Neural Comput.* **33**(3), 827–852.

Beiran, M., Dubreuil, A., Valente, A., Mastrogiosse, F. & Ostoicic, S. (2021), 'Shaping Dynamics With Multiple Populations in Low-Rank Recurrent Networks', *Neural Computation* **33**(6), 1572–1615.

Beiran, M., Meirhaeghe, N., Sohn, H., Jazayeri, M. & Ostoicic, S. (2023), 'Parametric control of flexible timing through low-dimensional neural manifolds', *Neuron* **111**(5), 739–753.e8.

Bekkers, E. J. (2019), 'B-spline CNNs on lie groups', *arXiv [cs.LG]* .

Ben-Yishai, R., Bar-Or, R. L. & Sompolinsky, H. (1995), 'Theory of orientation tuning in visual cortex.', *Proceedings of the National Academy of Sciences* **92**(9), 3844–3848.

Blanco, M. A., Flórez, M. & Bermejo, M. (1997), 'Evaluation of the rotation matrices in the basis of real spherical harmonics', *Theochem* **419**(1-3), 19–27.

Blumenfeld, B., Bibitchkov, D. & Tsodyks, M. (2006), 'Neural network model of the primary visual cortex: from functional architecture to lateral connectivity and back', *J Comput Neurosci* **20**(2), 219–241.

Blundell, S. J. (2017), 'Group theory in a nutshell for physicists, by a. zee', *Contemp. Phys.* **58**(2), 197–198.

Bracewell, R. & Kahn, P. B. (1966), 'The fourier transform and its applications', *American Journal of Physics* **34**(8), 712–712.

Bressloff, P. C., Cowan, J. D., Golubitsky, M., Thomas, P. J. & Wiener, M. C. (2001), 'Geometric visual hallucinations, euclidean symmetry and the functional architecture of striate cortex', *Philos. Trans. R. Soc. Lond. B Biol. Sci.* **356**(1407), 299–330.

Bronstein, M. M., Bruna, J., Cohen, T. & Velickovic, P. (2021), 'Geometric deep learning: Grids, groups, graphs, geodesics, and gauges', *CoRR* **abs/2104.13478**.

Bump, D. (2013), *Lie Groups*, Graduate texts in mathematics, 2 edn, Springer, New York, NY.

Burak, Y. & Fiete, I. R. (2009), 'Accurate path integration in continuous attractor network models of grid cells', *PLoS Comput. Biol.* **5**(2), e1000291.

Chaudhuri, R., Gercek, B., Pandey, B., Peyrache, A. & Fiete, I. (2019), 'The intrinsic attractor manifold and population dynamics of a canonical cognitive circuit across waking and sleep', *Nature Neuroscience* **22**(9), 1512–1520.

Chossat, P. (2012), *Dynamics, bifurcation and symmetry: New trends and new tools*, Vol. 437, Springer Science & Business Media.

Chung, S. & Abbott, L. (2021), 'Neural population geometry: An approach for understanding biological and artificial neural networks', *Current Opinion in Neurobiology* **70**, 137–144.

Churchland, M. M., Cunningham, J. P., Kaufman, M. T., Foster, J. D., Nuyujukian, P., Ryu, S. I. & Shenoy, K. V. (2012), 'Neural population dynamics during reaching', *Nature* **487**(7405), 51–56.

Clark, D. G., Abbott, L. F. & Sompolinsky, H. (2025), 'Symmetries and continuous attractors in disordered neural circuits', *bioRxiv* .

Claudi, F. & Branco, T. (2022), 'Differential geometry methods for constructing manifold-targeted recurrent neural networks', *Neural Comput.* **34**(8), 1790–1811.

Claudi, F., Chandra, S. & Fiete, I. R. (2025), 'A theory and recipe to construct general and biologically plausible integrating continuous attractor neural networks'.

Cohen, T., Geiger, M. & Weiler, M. (2018), 'A general theory of equivariant CNNs on homogeneous spaces', *arXiv [cs.LG]* .

Cohen, T. S., Geiger, M., Köhler, J. & Welling, M. (2018), 'Spherical cnns', *arXiv preprint arXiv:1801.10130* .

Cohen, T. S. & Welling, M. (2014), 'Transformation properties of learned visual representations', *arXiv [cs.LG]* .

Cohen, T. S. & Welling, M. (2016), 'Group equivariant convolutional networks', *arXiv [cs.LG]* pp. 2990–2999.

Compte, A., Brunel, N., Goldman-Rakic, P. & Wang, X.-J. (2000), 'Synaptic mechanisms and network dynamics underlying spatial working memory in a cortical network model', *Cereb. Cortex* **10**(9), 910–923.

Coombes, S., Graben, P. B., Potthast, R. & Wright, J. (2014), 'Neural fields: theory and applications'.

Couey, J. J., Witoelar, A., Zhang, S.-J., Zheng, K., Ye, J., Dunn, B. A., Czajkowski, R., Moser, M., Moser, E., Roudi, Y. & Witter, M. (2013), 'Recurrent inhibitory circuitry as a mechanism for grid formation', *Nat. Neurosci.* **16**, 318–324.

Cueva, C. J., Ardalan, A., Tsodyks, M. & Qian, N. (2021), 'Recurrent neural network models for working memory of continuous variables: activity manifolds, connectivity patterns, and dynamic codes', *arXiv [q-bio.NC]* .

Darshan, R. & Rivkind, A. (2022), 'Learning to represent continuous variables in heterogeneous neural networks', *Cell Rep.* **39**(1), 110612.

Dipoppa, M., Nogueira, R., Bugeon, S., Friedman, Y., Reddy, C. B., Harris, K. D., Ringach, D. L., Miller, K. D., Carandini, M. & Fusi, S. (2025), 'Adaptation shapes the representational geometry in mouse V1 to efficiently encode the environment', *bioRxiv.org* p. 2024.12. 11.628035.

Dubreuil, A. M., Valente, A., Beirán, M., Mastrogiovanni, F. & Ostoic, S. (2022), 'The role of population structure in computations through neural dynamics', *Nature Neuroscience* **25**, 783 – 794.

Duncker, L. & Sahani, M. (2021), 'Dynamics on the manifold: Identifying computational dynamical activity from neural population recordings', *Curr. Opin. Neurobiol.* **70**, 163–170.

Feehan, P. M. N. & Leness, T. G. (2020), 'Virtual morse-bott index, moduli spaces of pairs, and applications to topology of smooth four-manifolds', *arXiv [math.DG]* .

Finkelstein, A., Derdikman, D., Rubin, A., Foerster, J. N., Las, L. & Ulanovsky, N. (2014), 'Three-dimensional head-direction coding in the bat brain', *Nature* **517**(7533), 159–164.

Gallego, J. A., Perich, M. G., Miller, L. E. & Solla, S. A. (2017), 'Neural manifolds for the control of movement', *Neuron* **94**(5), 978–984.

Gardner, R., Hermansen, E., Pachitariu, M., Burak, Y., Baas, N., Dunn, B., Moser, M. & Moser, E. (2022), 'Toroidal topology of population activity in grid cells', *Nature* **602**(7895), 123–128.

Gerstner, W., Kistler, W. M., Naud, R. & Paninski, L. (2014), *Neuronal dynamics: From single neurons to networks and models of cognition*, Cambridge University Press.

Golubitsky, M. & Stewart, I. (2003), 'The symmetry perspective: from equilibrium to chaos in phase space and physical space', **200**.

González, Á. (2010), 'Measurement of areas on a sphere using fibonacci and latitude–longitude lattices', *Mathematical geosciences* **42**(1), 49–64.

Guanella, A., Kiper, D. & Verschure, P. (2007), 'A model of grid cells based on a twisted torus topology', *International journal of neural systems* **17**(04), 231–240.

Hermansen, E., Klindt, D. A. & Dunn, B. A. (2024), 'Uncovering 2-d toroidal representations in grid cell ensemble activity during 1-d behavior', *Nat. Commun.* **15**(1), 5429.

Jazayeri, M. & Ostoic, S. (2021), 'Interpreting neural computations by examining intrinsic and embedding dimensionality of neural activity', *Curr. Opin. Neurobiol.* **70**, 113–120.

Keller, T. A. (2025), 'Flow equivariant recurrent neural networks', *arXiv preprint arXiv:2507.14793* .

Kennedy, R. A., Lamahewa, T. A. & Wei, L. (2011), 'On azimuthally symmetric 2-sphere convolution', *Digit. Signal Process.* **21**(5), 660–666.

Khona, M., Chandra, S. & Fiete, I. (2025), 'Global modules robustly emerge from local interactions and smooth gradients', *Nature* pp. 1–10.

Khona, M. & Fiete, I. R. (2022), 'Attractor and integrator networks in the brain', *Nat. Rev. Neurosci.* **23**(12), 744–766.

Kim, S. S., Rouault, H., Druckmann, S. & Jayaraman, V. (2017), 'Ring attractor dynamics in the drosophila central brain', *Science* **356**(6340), 849–853.

Kondor, R., Lin, Z. & Trivedi, S. (2018), 'Clebsch-gordan nets: A fully fourier space spherical convolutional neural network', *arXiv [stat.ML]* .

Kondor, R. & Trivedi, S. (2018), On the generalization of equivariance and convolution in neural networks to the action of compact groups, in J. Dy & A. Krause, eds, 'Proceedings of the 35th International Conference on Machine Learning', Vol. 80 of *Proceedings of Machine Learning Research*, PMLR, pp. 2747–2755.

Kosmann-Schwarzbach, Y. (2009), *Groups and Symmetries*, Springer, New York, NY.

Langdon, C., Genkin, M. & Engel, T. A. (2023), 'A unifying perspective on neural manifolds and circuits for cognition', *Nat. Rev. Neurosci.* **24**(6), 363–377.

Logiaco, L., Abbott, L. F. & Escola, S. (2021), 'Thalamic control of cortical dynamics in a model of flexible motor sequencing', *Cell Rep.* **35**(9), 109090.

Machens, C. K. & Brody, C. D. (2008), 'Design of continuous attractor networks with monotonic tuning using a symmetry principle', *Neural Comput.* **20**(2), 452–485.

Mastrogiossepe, F. & Ostoic, S. (2018), 'Linking connectivity, dynamics, and computations in low-rank recurrent neural networks', *Neuron* **99**(3), 609–623.e29.

Monti, F., Boscaini, D., Masci, J., Rodola, E., Svoboda, J. & Bronstein, M. M. (2017), Geometric deep learning on graphs and manifolds using mixture model CNNs, in '2017 IEEE Conference on Computer Vision and Pattern Recognition (CVPR)', IEEE, pp. 5115–5124.

Noorman, M., Hulse, B. K., Jayaraman, V., Romani, S. & Hermundstad, A. M. (2024), 'Maintaining and updating accurate internal representations of continuous variables with a handful of neurons', *Nat. Neurosci.* **27**(11), 2207–2217.

Ostoic, S. & Fusi, S. (2024), 'Computational role of structure in neural activity and connectivity', *Trends Cogn. Sci.* **28**(7), 677–690.

Perich, M. G., Narain, D. & Gallego, J. A. (2025), 'A neural manifold view of the brain', *Nat. Neurosci.* **28**(8), 1582–1597.

Petrucco, L., Lavian, H., Wu, Y. K., Svara, F., Štih, V. & Portugues, R. (2023), 'Neural dynamics and architecture of the heading direction circuit in zebrafish', *Nat. Neurosci.* **26**(5), 765–773.

Pezon, L., Schmutz, V. & Gerstner, W. (2024), 'Linking neural manifolds to circuit structure in recurrent networks', *bioRxiv*.

Pinchon, D. & Hoggan, P. E. (2007), 'Rotation matrices for real spherical harmonics: general rotations of atomic orbitals in space-fixed axes', *J. Phys. A Math. Theor.* **40**(7), 1597–1610.

Pollock, E. & Jazayeri, M. (2020), 'Engineering recurrent neural networks from task-relevant manifolds and dynamics', *PLoS computational biology* **16**(8), e1008128.

Roddy, P. J. & McEwen, J. D. (2021), 'Sifting convolution on the sphere', *IEEE Signal Process. Lett.* **28**, 304–308.

Romani, S. & Tsodyks, M. (2010), 'Continuous attractors with morphed/correlated maps', *PLoS Comput. Biol.* **6**(8).

Rubin, A., Sheintuch, L., Brande-Eilat, N., Pinchasof, O., Rechavi, Y., Geva, N. & Ziv, Y. (2019), 'Revealing neural correlates of behavior without behavioral measurements', *Nat. Commun.* **10**(1), 4745.

Samsonovich, A. & McNaughton, B. (1997), 'Path integration and cognitive mapping in a continuous attractor neural network model', *J. Neurosci.* **17**(15), 5900–5920.

Scarselli, F., Gori, M., Tsoi, A. C., Hagenbuchner, M. & Monfardini, G. (2009), 'The graph neural network model', *IEEE Trans. Neural Netw.* **20**(1), 61–80.

Schmutz, V., Haydaroglu, A., Wang, S., Feng, Y., Carandini, M. & Harris, K. D. (2025), 'High-dimensional neuronal activity from low-dimensional latent dynamics: a solvable model', *bioRxiv* org p. 2025.06. 03.657632.

Schuessler, F., Dubreuil, A., Mastrogiossepe, F., Ostoic, S. & Barak, O. (2019), 'Dynamics of random recurrent networks with correlated low-rank structure', *arXiv [q-bio.NC]*.

Segol, N. & Lipman, Y. (2020), 'On universal equivariant set networks'.

Seung, H. S. (1996), 'How the brain keeps the eyes still', *Proc. Natl. Acad. Sci. U. S. A.* **93**(23), 13339–13344.

Seung, H. S., Lee, D. D., Reis, B. Y. & Tank, D. W. (2000), 'Stability of the memory of eye position in a recurrent network of conductance-based model neurons', *Neuron* **26**(1), 259–271.

Si, B., Romani, S. & Tsodyks, M. (2014), 'Continuous attractor network model for conjunctive position-by-velocity tuning of grid cells', *PLoS Comput. Biol.* **10**(4), e1003558.

Sorscher, B., Mel, G. C., Ocko, S. A., Giocomo, L. M. & Ganguli, S. (2023), 'A unified theory for the computational and mechanistic origins of grid cells', *Neuron* **111**(1), 121–137.e13.

Spalla, D., Cornacchia, I. M. & Treves, A. (2021), 'Continuous attractors for dynamic memories', *Elife* **10**, e69499.

Spalla, D., Dubreuil, A., Rosay, S., Monasson, R. & Treves, A. (2019), 'Can grid cell ensembles represent multiple spaces?', *Neural computation* **31**(12), 2324–2347.

Spezialetti, R., Stella, F., Marcon, M., Silva, L., Salti, S. & Di Stefano, L. (2020), 'Learning to orient surfaces by self-supervised spherical cnns', *Advances in Neural information processing systems* **33**, 5381–5392.

Stella, F., Si, B., Kropff, E. & Treves, A. (2013), 'Grid cells on the ball', *Journal of Statistical Mechanics: Theory and Experiment* **2013**(03), P03013.

Stringer, S. M., Trappenberg, T. P., Rolls, E. T. & de Araujo, I. E. T. (2002), ‘Self-organizing continuous attractor networks and path integration: one-dimensional models of head direction cells’, *Network* **13**(2), 217–242.

Ságodi, A., Martin-Sánchez, G., Sokol, P. & Park, I. M. (2024), ‘Back to the continuous attractor’, *Neural Inf Process Syst* **37**, 66856–66906.

Trettel, S. G., Trimper, J. B., Hwaun, E., Fiete, I. R. & Colgin, L. L. (2019), ‘Grid cell co-activity patterns during sleep reflect spatial overlap of grid fields during active behaviors’, *Nat. Neurosci.* **22**(4), 609–617.

Tsodyks, M. (1999), ‘Attractor neural network models of spatial maps in hippocampus’, *Hippocampus* **9**(4), 481–489.

Tsodyks, M. & Sejnowski, T. (1995), ‘Associative memory and hippocampal place cells’, *Int. J. Neural Syst.* **6**, 81–86.

Vyas, S., Golub, M. D., Sussillo, D. & Shenoy, K. V. (2020), ‘Computation through neural population dynamics’, *Annu. Rev. Neurosci.* **43**(1), 249–275.

Wimmer, K., Nykamp, D. Q., Constantinidis, C. & Compte, A. (2014), ‘Bump attractor dynamics in prefrontal cortex explains behavioral precision in spatial working memory’, *Nat. Neurosci.* **17**(3), 431–439.

Wu, S., Wong, K. Y. M., Fung, C. C. A., Mi, Y. & Zhang, W. (2016), ‘Continuous attractor neural networks: Candidate of a canonical model for neural information representation’, *F1000Res.* **5**, 156.

Xie, X., Hahnloser, R. H. R. & Seung, H. S. (2002), ‘Double-ring network model of the head-direction system’, *Phys. Rev. E Stat. Nonlin. Soft Matter Phys.* **66**(4 Pt 1), 041902.

Zee, A. (2016), *Group theory in a nutshell for physicists*, Princeton University Press.

Zhang, K. (1996), ‘Representation of spatial orientation by the intrinsic dynamics of the head-direction cell ensemble: a theory’, *Journal of Neuroscience* **16**(6), 2112–2126.

Zhang, W. H., Wu, Y. N. & Wu, S. (2022), Translation-equivariant representation in recurrent networks with a continuous manifold of attractors, in S. Koyejo, S. Mohamed, A. Agarwal, D. Belgrave, K. Cho & A. Oh, eds, ‘Advances in Neural Information Processing Systems 35 - 36th Conference on Neural Information Processing Systems, NeurIPS 2022’, Vol. 35 of *Advances in Neural Information Processing Systems*, Neural information processing systems foundation.

Zhengwei Su, P. C. (n.d.), ‘Rotation of real spherical harmonics’. Accessed: 2025-8-21.

Zuo, J., Liu, X., Wu, Y. N., Wu, S. & Zhang, W. (2023), ‘A recurrent neural circuit mechanism of temporal-scaling equivariant representation’, *Advances in Neural Information Processing Systems* **36**, 62682–62695.

Zuo, J., Wu, Y. N., Wu, S. & Zhang, W.-H. (2024), ‘The motion planning neural circuit in goal-directed navigation as lie group operator search’, *Neural Inf Process Syst* **37**, 110369–110387.

## A Group Theory

Here we summarize the main elements of group theory based on [Kosmann-Schwarzbach \(2009\)](#), [Blundell \(2017\)](#). The approach for extending group convolutions and group Fourier transforms to homogeneous spaces is based on [Kondor & Trivedi \(2018\)](#).

### A.1 Groups

A **group**  $G$  is a set equipped with a binary operation  $\cdot : G \times G \rightarrow G$  that satisfies the following axioms:

1. **Closure:** For all  $g_1, g_2 \in G$ ,  $g_1 \cdot g_2 \in G$ .
2. **Associativity:** For all  $g_1, g_2, g_3 \in G$ , we have  $(g_1 \cdot g_2) \cdot g_3 = g_1 \cdot (g_2 \cdot g_3)$ .
3. **Identity:** There exists an element  $e \in G$  such that  $e \cdot g = g \cdot e = g$  for all  $g \in G$ .
4. **Inverse:** For each  $g \in G$ , there exists an element  $g^{-1} \in G$  such that  $g \cdot g^{-1} = g^{-1} \cdot g = e$ .

When  $G$  is a finite set of cardinality  $n$ , we say that  $G$  is a **finite group** and that its **order** is  $n$ . If  $G$  is an infinite set, then it is an **infinite group**, with infinite order.

Furthermore, the elements of a group can be a numerable set, in which case they form a **discrete group**. If the set is not numerable, instead, the group is said to be **continuous** and the elements depend on a number of continuous parameters, referred to as **dimension of the group**. If the group is discrete, we say that its dimension is 0.

Throughout this paper, we focus primarily on compact groups, which are groups that are also compact topological spaces with continuous group operations.

## A.2 Group Actions

An **action** of a group  $G$  on a set  $\Omega$  is a map  $\cdot : G \times \Omega \rightarrow \Omega$  satisfying:

1.  $e \cdot \omega = \omega$  for all  $\omega \in \Omega$ , where  $e$  is the identity element of  $G$ .
2.  $(g_1 \cdot g_2) \cdot \omega = g_1 \cdot (g_2 \cdot \omega)$  for all  $g_1, g_2 \in G$  and  $\omega \in \Omega$ .

Any action of  $G$  on  $\Omega$  induces an action of  $G$  on the set of functions  $\Omega \rightarrow \mathbb{R}$ . For any function  $f : \Omega \rightarrow \mathbb{R}$ , a group element  $g \in G$  induces a transformation denoted  $S_g[f]$  and defined by:

$$S_g[f](\omega) = f(g^{-1} \cdot \omega) \quad \forall \omega \in \Omega. \quad (129)$$

We call the resulting operator  $S_g$  the **action** of  $g$  on the function space  $L_{\mathbb{R}}(\Omega)$ .

## A.3 Cosets and Quotient Spaces

Given a group  $G$ , a subgroup  $H \subseteq G$ , and an element  $g \in G$ , the *left and right cosets* are defined as

$$gH = \{gh \mid h \in H\} \quad (130)$$

$$Hg = \{hg \mid h \in H\}. \quad (131)$$

The cosets partition  $G$  in such a way that each element of  $G$  belongs to only one left or right coset.

The set of all left (resp. right) cosets forms the left quotient space  $G/H$  (resp. right quotient space  $H/G$ ). If the left and right quotient spaces are equal,  $H$  is called a normal subgroup of  $G$  and the quotient space  $G/H = H/G$  forms a group.

## A.4 Homogeneous Spaces

A set  $\Omega$  is called a **homogeneous space** with respect to a group  $G$  if for any two points  $\omega_1, \omega_2 \in \Omega$ , there exists a group element  $g \in G$  such that  $g \cdot \omega_1 = \omega_2$ . Fixing an origin  $\omega_0 \in \Omega$ , any  $\omega \in \Omega$  can be reached as  $\omega = g \cdot \omega_0$  for some  $g \in G$ . This element  $g$  is however not necessarily unique, in particular when  $\Omega$  is not itself a group (Kondor & Trivedi 2018). In that case, the set of elements of  $G$  that fix the origin forms a subgroup  $H = \{h \in G \mid h\omega_0 = \omega_0\}$ , and  $\Omega$  can be identified with the left quotient space  $G/H$ . This identification then defines a map  $g \mapsto [g]_{G/H}$  that maps each element of  $G$  to a unique coset representative within  $G/H = \Omega$ .

## A.5 Haar Measure and Integration on Groups

For a locally compact topological group  $G$ , the **Haar measure**  $d\mu(g)$  is a measure that is invariant under the group action. Specifically, for any  $h \in G$ , and for any integrable function  $f$ , the Haar measure satisfies

$$\int_G f(hg) d\mu(g) = \int_G f d\mu(g).$$

We moreover require that  $\mu$  satisfies the normalization condition

$$\int_G d\mu(g) = 1.$$

Every locally compact group admits a unique invariant Haar measure.

The concept of Haar measure extends beyond groups to homogeneous spaces  $\Omega = G/H$ . When both  $G$  and  $H$  are compact, the group action on  $\Omega$  induces a unique  $G$ -invariant measure  $d\mu(\Omega)$ , and normalized so that  $\int_{\Omega} d\mu(\Omega) = 1$ .

## A.6 Group Representations

A **representation** of a group  $G$  is a homomorphism  $\rho : G \rightarrow GL(V)$ , where  $GL(V)$  is the general linear group of a vector space  $V$ . In concrete terms, a  $d$ -dimensional representation assigns to each group element  $g \in G$  a  $d \times d$  invertible matrix  $\rho(g)$  such that:

$$\rho(g_1 \cdot g_2) = \rho(g_1) \cdot \rho(g_2) \quad (132)$$

for all  $g_1, g_2 \in G$ .

## A.7 Reducible and Irreducible Representations

A representation  $\rho$  is **reducible** if the vector space  $V$  can be decomposed into proper subspaces that are invariant under the action of all  $\rho(g)$  for  $g \in G$ . Otherwise, the representation is **irreducible** (or an **irrep**).

Mathematically, a representation  $\rho$  is reducible if there exists a change of basis such that all matrices  $\rho(g)$  for  $g \in G$  can be simultaneously expressed in block-diagonal form:

$$P^{-1}\rho(g)P = \begin{pmatrix} \rho_1(g) & 0 & \cdots & 0 \\ 0 & \rho_2(g) & \cdots & 0 \\ \vdots & \vdots & \ddots & \vdots \\ 0 & 0 & \cdots & \rho_k(g) \end{pmatrix} \quad (133)$$

where  $P$  is an invertible matrix representing the change of basis, and each  $\rho_i(g)$  is a lower-dimensional representation of  $G$ . This block-diagonal structure corresponds to a decomposition of the vector space  $V$  into proper invariant subspaces  $V = V_1 \oplus V_2 \oplus \cdots \oplus V_k$ , where each subspace  $V_i$  is preserved under the action of  $G$ , meaning that for any  $v \in V_i$  and any  $g \in G$ , we have  $\rho(g)v \in V_i$ .

For compact groups, **Maschke's theorem** ensures that any finite-dimensional representation can be decomposed as a direct sum of irreducible representations, i.e. it is completely reducible. The set of all irreducible representations of a compact group  $G$  is countable.

## A.8 Group convolutions and their extension to homogeneous spaces

For two functions  $f^1, f^2 : G \rightarrow \mathbb{R}$  the  $G$ -convolution is a function  $G \rightarrow \mathbb{R}$  defined by

$$(f_1 *_G f_2)(g) = \sum_{h \in G} f_1(g^{-1}h) f_2(h). \quad (134)$$

To extend this concept of convolutions to functions  $f^1, f^2 : \Omega \rightarrow \mathbb{R}$ , where  $\Omega$  is a homogeneous space with respect to  $G$ , we follow [Kondor & Trivedi \(2018\)](#). For  $f : \Omega \rightarrow \mathbb{R}$ , we first introduce its *lifting* to  $G$  as the function  $f^\dagger : \Omega \rightarrow \mathbb{R}$  defined as

$$f^\dagger(g) = f([g]_\Omega) \quad \forall g \in G, \quad (135)$$

where  $[g]_\Omega = [g]_{G/H}$  is the representative of  $g$  on  $\Omega$ , or equivalently on  $G/H$ . The convolution between  $f^1, f^2 : \Omega \rightarrow \mathbb{R}$  can then be defined as a function  $G \rightarrow \mathbb{R}$  such that

$$(f_1 *_G f_2)(g) = \sum_{h \in G} f_1^\dagger(g^{-1}h) f_2^\dagger(h) \quad (136)$$

$$= \sum_{h \in G} f_1([g^{-1}h]_\Omega) f_2([h]_\Omega). \quad (137)$$

Since the arguments of  $f_1$  and  $f_2$  are representatives of elements of  $G$  on  $\Omega$ , and therefore elements of  $\Omega$ , the sum effectively runs over  $\Omega$ , and the convolution itself is effectively a function on  $\Omega$ .

## A.9 Group Fourier Transforms and their extension to homogeneous spaces

For a compact group  $G$  with a system of irreducible representations  $\{\rho_k\}_{k=0,1,\dots}$ , the **group Fourier transform** of a function  $f : G \rightarrow \mathbb{R}$  is defined as the collection of Fourier components:

$$\hat{f}_k = \int_G f(g) \rho_k(g) d\mu(g) \quad (138)$$

where  $d\mu(g)$  is the normalized Haar measure on  $G$ . For finite groups, the integral is replaced by a sum.

The **Peter-Weyl theorem** states that any function  $f : G \rightarrow \mathbb{R}$  can be reconstructed from its **inverse Fourier transform**:

$$f(g) = \sum_{k=0}^{\infty} \tilde{d}_k \text{tr}(\hat{f}_k \rho_k^{-1}(g)) \quad (139)$$

where  $\tilde{d}_k$  is the dimension of the  $k$ -th complex-valued irreducible representation.

A fundamental property is the **convolution theorem** for group Fourier transforms:

$$\widehat{f^1 *_G f^2}_k = \widehat{f^1}_k \cdot \widehat{f^2}_k \quad (140)$$

where  $*_G$  denotes the group convolution.

Following [Kondor & Trivedi \(2018\)](#), the Group Fourier transform can be directly extended to functions  $f : \Omega \rightarrow \mathbb{R}$ , where  $\Omega$  is a homogeneous space with respect to  $G$  by using the lifting  $f^\dagger$  of  $f$  to  $G$  (Eq. (135)):

$$\widehat{f}_k = \int_G f^\dagger(g) \rho_k(g) d\mu(g) \quad (141)$$

$$= \int_G f([g]_{\Omega=G/H}) \rho_k(g) d\mu(g). \quad (142)$$

[Kondor & Trivedi \(2018\)](#) show that this is in general equivalent to integrating over  $G/H$  while restricting the irreps  $\rho_k$  to specific columns.

## B Finite networks

In this appendix, we provide finite-size, discretized expressions of the recurrent input, the connectivity matrix and the connectivity vectors for the ring model, the toroidal RNN and the spherical RNN.

### B.1 Ring model

The ring  $\Omega = \mathcal{S}^1$  is parametrized by the angle  $\theta \in [0, 2\pi)$ . We discretize the ring using  $N$  equally-spaced points with spacing  $\Delta\theta = \frac{2\pi}{N}$ :

$$\theta_i = i \cdot \Delta\theta = \frac{2\pi i}{N}, \quad i = 0, 1, \dots, N-1. \quad (143)$$

The discrete measure at each point is  $\Delta\mu_i = \frac{\Delta\theta}{2\pi} = \frac{1}{N}$ , ensuring that  $\sum_{i=0}^{N-1} \Delta\mu_i = 1$ .

The continuous convolution in Eq. (60) is then discretized as follows:

$$F^t(\theta_i) = \frac{1}{N} \sum_{j=0}^{N-1} c(g_{\theta_i}^{-1}(\theta_j)) \Phi[x^t(\theta_j)] = \frac{1}{N} \sum_{j=0}^{N-1} c(\theta_j - \theta_i) \Phi[x^t(\theta_j)] \quad (144)$$

where the group action is described by angular translations:  $g_{\theta_i}^{-1}(\theta_j) = \theta_j - \theta_i$ .

The connectivity matrix  $J \in \mathbb{R}^{N \times N}$  has entries

$$J_{ij} = \frac{1}{N} c(\theta_j - \theta_i). \quad (145)$$

The kernel  $c(\theta)$  can be expressed via the Inverse group Fourier transform Eq. (42):

$$c(\theta) = \hat{c}_0 + \sum_{k=1}^K 2(\hat{c}_{k,1} \cos(k\theta) + \hat{c}_{k,2} \sin(k\theta)), \quad (146)$$

where  $\hat{c}_0, \hat{c}_{k,1}, \hat{c}_{k,2}$  are the Fourier components of the kernel, and in the hypothesis of an even kernel, the terms  $\hat{c}_{k,2} = 0$  for each  $k$ . The elements of the connectivity matrix are then given by:

$$J_{ij} = \frac{1}{N} \left[ \hat{c}_0 + \sum_{k=0}^K 2\hat{c}_{k,1} \cos(k(\theta_i - \theta_j)) \right] \quad (147)$$

$$= \frac{1}{N} \left[ \hat{c}_0 + \sum_{k=0}^K 2\hat{c}_{k,1} (\cos(k\theta_i) \cos(k\theta_j) + \sin(k\theta_i) \sin(k\theta_j)) \right] \quad (148)$$

$$= \frac{1}{N} \sum_{k=0}^{2K} z_i^{(k)} z_j^{(k)} \quad (149)$$

where we define the **connectivity vectors**  $z_i^{(k)}$  as (Mastrogiovanni & Ostoic 2018):

$$z_i^{(0)} = \sqrt{\hat{c}_0} \quad (150)$$

$$z_i^{(2k-1)} = \sqrt{2\hat{c}_{k,1}} \cos(k\theta_i), \quad k = 1, \dots, K \quad (151)$$

$$z_i^{(2k)} = \sqrt{2\hat{c}_{k,1}} \sin(k\theta_i), \quad k = 1, \dots, K. \quad (152)$$

The rank of the connectivity matrix is therefore at most  $2K + 1$ .

In the 2D ring model, the kernel is  $c(\theta) = J_1 \cos(\theta)$  (Figure 6A):

$$J_{ij} = \frac{1}{N} J_1 \cos(\theta_i - \theta_j) \quad (153)$$

which can be decomposed as  $J_{ij} = \frac{1}{N} \sum_{k=1}^2 z_i^k z_j^k$ , where the connectivity vectors are

$$z_i^1 = \sqrt{J_1} \cos(\theta_i), \quad z_i^2 = \sqrt{J_1} \sin(\theta_i). \quad (154)$$

In the 5D ring model, the kernel is  $c(\theta) = J_0 + J_1 \cos(\theta) + J_2 \cos(2\theta)$  (Figure 6B):

$$J_{ij} = \frac{1}{N} [J_0 + J_1 \cos(\theta_i - \theta_j) + J_2 \cos(2(\theta_i - \theta_j))] \quad (155)$$

which can be decomposed as  $J_{ij} = \frac{1}{N} \sum_{k=0}^4 z_i^k z_j^k$ , with connectivity vectors

$$z_i^0 = \sqrt{J_0}, \quad z_i^1 = \sqrt{J_1} \cos(\theta_i), \quad z_i^2 = \sqrt{J_1} \sin(\theta_i), \quad z_i^3 = \sqrt{J_2} \cos(2\theta_i), \quad z_i^4 = \sqrt{J_2} \sin(2\theta_i). \quad (156)$$

## B.2 Toroidal RNNs

The torus  $\Omega = \mathcal{T}^2 = \mathcal{S}^1 \times \mathcal{S}^1$  is the product of two rings, parametrized by  $(\theta_1, \theta_2) \in [0, 2\pi] \times [0, 2\pi]$ . The discretization follows directly from the ring case by applying it independently to each angular coordinate. We use a grid of  $N_1 \times N_2$  equally-spaced points, with spacings:

$$\Delta\theta_1 = \frac{2\pi}{N_1} \quad (157)$$

$$\Delta\theta_2 = \frac{2\pi}{N_2}. \quad (158)$$

For a total of  $N$  neurons, we typically set  $N_1 = N_2 = \sqrt{N}$ .

Each neuron  $i \in 0 \dots N - 1$  is indexed by a pair of indices  $(i_1, i_2)$  such that

$$i = i_1 \cdot N_2 + i_2. \quad (159)$$

The index pair  $(i_1, i_2)$  corresponds to the position of the neuron on the two-dimensional grid:

$$\theta_{i_1} = i_1 \cdot \Delta\theta_1, \quad i_1 = 0, 1, \dots, N_1 - 1 \quad (160)$$

$$\theta_{i_2} = i_2 \cdot \Delta\theta_2, \quad i_2 = 0, 1, \dots, N_2 - 1. \quad (161)$$

The discrete measure at each grid point is given by  $\Delta\mu_{i_1, i_2} = \frac{\Delta\theta_1}{2\pi} \cdot \frac{\Delta\theta_2}{2\pi} = \frac{1}{N}$ , ensuring that  $\sum_{i_1=0}^{N_1-1} \sum_{i_2=0}^{N_2-1} \Delta\mu_{i_1, i_2} = 1$ .

The continuous convolution in Eq. (89) is then discretized as a double sum:

$$F^t(\theta_{i_1}, \theta_{i_2}) = \frac{1}{N} \sum_{j_1=0}^{N_1-1} \sum_{j_2=0}^{N_2-1} c(\theta_{i_1} - \theta_{j_1}, \theta_{i_2} - \theta_{j_2}) \Phi[x^t(\theta_{j_1}, \theta_{j_2})]. \quad (162)$$

The connectivity matrix  $J \in \mathbb{R}^{N \times N}$  has entries

$$J_{i,j} = J_{(i_1, i_2)(j_1, j_2)} \quad (163)$$

$$= \frac{1}{N} c(\theta_{j_1} - \theta_{i_1}, \theta_{j_2} - \theta_{i_2}). \quad (164)$$

Following the procedure outlined for the ring model, an even kernel  $c(\theta_1, \theta_2)$ , is expressed via the Inverse group Fourier transform as:

$$c(\theta_{i1}, \theta_{i2}) = \hat{c}_{(0,0)} + \sum_{\substack{k'_1=0, k'_2=0 \\ (k'_1, k'_2) \neq (0,0)}}^{K_1, K_2} 2(\hat{c}_{(k_1, k_2), 1} \cos(k_1 \theta_{i1} + k_2 \theta_{i2})) \quad (165)$$

where  $\hat{c}_{(k_1, k_2)}$ ,  $\hat{c}_{(k_1, k_2), 1}$ ,  $\hat{c}_{(k_1, k_2), 2}$  are the Fourier components and  $K_1, K_2$  are the numbers of non-zero components along each dimension.

The elements of the connectivity matrix are then given by:

$$J_{i,j} = J_{(i_1, i_2)(j_1, j_2)} \quad (166)$$

$$= \frac{1}{N} c(\theta_{i_1} - \theta_{j_1}, \theta_{i_2} - \theta_{j_2}) \quad (167)$$

$$= \frac{1}{N} \left[ \hat{c}_{(0,0)} + \sum_{\substack{k_1=0, k_2=0 \\ (k_1, k_2) \neq (0,0)}}^{K_1, K_2} 2\hat{c}_{(k_1, k_2), 1} \cos(k_1(\theta_{i_1} - \theta_{j_1}) + k_2(\theta_{i_2} - \theta_{j_2})) \right] \quad (168)$$

$$= \frac{1}{N} \left[ \hat{c}_{(0,0)} + \sum_{\substack{k_1=0, k_2=0 \\ (k_1, k_2) \neq (0,0)}}^{K_1, K_2} 2\hat{c}_{(k_1, k_2), 1} (\cos(k_1 \theta_{i_1} + k_2 \theta_{i_2}) \cos(k_1 \theta_{j_1} + k_2 \theta_{j_2}) \right. \\ \left. + \sin(k_1 \theta_{i_1} + k_2 \theta_{i_2}) \sin(k_1 \theta_{j_1} + k_2 \theta_{j_2})) \right] \quad (169)$$

$$= \frac{1}{N} \sum_{r=0}^R z_{(i_1, i_2)}^{(r)} z_{(j_1, j_2)}^{(r)} \quad (170)$$

where  $R = 2(K_1 + 1) \cdot (K_2 + 1) - 1$  and the **connectivity vectors** are defined as:

$$z_{(i_1, i_2)}^{(0)} = \sqrt{\hat{c}_{(0,0)}} \quad (171)$$

$$z_{(i_1, i_2)}^{(2k-1)} = \sqrt{2\hat{c}_{(k_1, k_2), 1}} \cos(k_1 \theta_{i_1} + k_2 \theta_{i_2}), \quad k = 1, \dots, \tilde{K} \quad (172)$$

$$z_{(i_1, i_2)}^{(2k)} = \sqrt{2\hat{c}_{(k_1, k_2), 1}} \sin(k_1 \theta_{i_1} + k_2 \theta_{i_2}), \quad k = 1, \dots, \tilde{K} \quad (173)$$

where to each  $k$  corresponds to a pair  $(k_1, k_2)$ :

$$k = k_1 + k_2 * K_1. \quad (174)$$

In the rank-five toroidal model, the kernel is  $c(\theta_1, \theta_2) = J_0 + J_1 \cos(\theta_1) + J_2 \cos(\theta_2)$ :

$$J_{(i_1, i_2)(j_1, j_2)} = \frac{1}{N} [J_0 + J_1 \cos(\theta_{i_1} - \theta_{j_1}) + J_2 \cos(\theta_{i_2} - \theta_{j_2})] \quad (175)$$

which can be decomposed as  $J_{(i_1, i_2)(j_1, j_2)} = \frac{1}{N} \sum_{k=0}^4 z_{(i_1, i_2)}^{(k)} z_{(j_1, j_2)}^{(k)}$ , where the connectivity vectors are:

$$z_{(i_1, i_2)}^{(0)} = \sqrt{J_0}, \quad z_{(i_1, i_2)}^{(1)} = \sqrt{J_1} \cos(\theta_{i_1}), \quad z_{(i_1, i_2)}^{(2)} = \sqrt{J_1} \sin(\theta_{i_1}), \quad z_{(i_1, i_2)}^{(3)} = \sqrt{J_2} \cos(\theta_{i_2}), \quad z_{(i_1, i_2)}^{(4)} = \sqrt{J_2} \sin(\theta_{i_2}) \quad (176)$$

resulting in a rank-5 connectivity matrix (Figure 6C).

### B.3 Spherical RNNs

The sphere  $\Omega = \mathcal{S}^2$  is parametrized by spherical coordinates  $(\theta, \phi)$  where  $\theta \in [0, \pi]$  is the polar angle and  $\phi \in [0, 2\pi]$  is the azimuthal angle. In contrast to  $\mathcal{S}^1$ , the sphere and the related rotation group do not admit a regular discretization that preserves exact symmetries. Here, we employ Fibonacci lattice sampling, which generates  $N$  points that are approximately uniformly distributed by surface area (González 2010). The Fibonacci lattice uses the golden angle  $\theta_{\text{golden}} = \pi(\sqrt{5} - 1)$  and constructs points via:

$$y_i = 1 - \frac{2i}{N-1}, \quad \theta_i = \arccos(y_i), \quad \phi_i = i \cdot \theta_{\text{golden}} \bmod 2\pi, \quad i = 0, \dots, N-1. \quad (177)$$

The key property of Fibonacci sampling is that each point represents approximately equal surface area. Since the total unnormalized surface area is  $4\pi$ , partitioning into  $N$  approximately equal patches gives each point an unnormalized area  $\sin \theta_i \Delta \theta_i \Delta \phi_i \approx \frac{4\pi}{N}$ . Therefore, the discrete normalized measure for each point is:

$$\Delta \mu_i = \frac{\sin \theta_i \Delta \theta_i \Delta \phi_i}{4\pi} \approx \frac{1}{N}. \quad (178)$$

The convolution Eq. (112) is discretized as:

$$F^t(\theta_i, \phi_i) = \frac{1}{N} \sum_{j=0}^{N-1} c(g_{(\theta_i, \phi_i, 0)}^{-1}(\theta_j, \phi_j)) \Phi(x_t(\theta_j, \phi_j)). \quad (179)$$

The connectivity matrix  $J \in \mathbb{R}^{N \times N}$  has entries:

$$J_{ij} = \frac{1}{N} c(g_{(\theta_i, \phi_i, 0)}^{-1}(\theta_j, \phi_j)). \quad (180)$$

The kernel  $c(\theta, \phi)$  can be expressed via the Inverse group Fourier transform Eq. (42):

$$c(\theta, \phi) = \hat{c}_0 + \sum_{\ell=1}^L \sum_{m=-\ell}^{\ell} \hat{c}_{\ell,m} Y_{\ell,m}(\theta, \phi), \quad (181)$$

where  $\hat{c}_0, \hat{c}_{\ell,m}$  are the Fourier components of the kernel.

Combining Eqs. (180) and (181), the connectivity matrix can be written as:

$$J_{ij} = \frac{1}{N} \left[ \hat{c}_0 + \sum_{\ell=1}^L \sum_{m=-\ell}^{\ell} \hat{c}_{\ell,m} Y_{\ell,m}(g_{(\theta_i, \phi_i, 0)}^{-1}(\theta_j, \phi_j)) \right] \quad (182)$$

$$= \frac{1}{N} \left[ \hat{c}_0 + \sum_{\ell=1}^L \sum_{m=-\ell}^{\ell} \hat{c}_{\ell,m} Y_{\ell,m}((\theta_j, \phi_j)) Y_{\ell,m}((\theta_i, \phi_i)) \right] \quad (183)$$

$$= \frac{1}{N} \sum_{k=0}^K z_i^{(k)} z_j^{(k)} \quad (184)$$

where  $K = \sum_{\ell=0}^L (2\ell + 1)$  is the total number of spherical harmonic modes up to degree  $L$ , and the **connectivity vectors**  $z_i^{(k)}$  are given by:

$$z_i^{(0)} = \sqrt{\hat{c}_0} \quad (185)$$

$$z_i^{(k)} = \sqrt{\hat{c}_{\ell,m}} Y_{\ell,m}(\theta_i, \phi_i), \quad \text{for } k \text{ indexing } (\ell, m) \text{ with } \ell = 1, \dots, L, m = -\ell, \dots, \ell \quad (186)$$

resulting in a connectivity matrix  $J$  with rank at most  $\sum_{\ell=0}^L (2\ell + 1)$ .

For the rank-3 spherical model, the kernel is

$$c(\theta, \phi) = J_1(\sin \theta \sin \phi + \cos \theta + \sin \theta \cos \phi). \quad (187)$$

The resulting connectivity matrix is rank 3 (Figure 6D):

$$J_{ij} = \frac{J_1}{N} \sqrt{3} (\sin \theta_i \cos \phi_i \sin \theta_j \cos \phi_j + \sin \theta_i \sin \phi_i \sin \theta_j \sin \phi_j + \cos \theta_i \cos \theta_j), \quad (188)$$

$$= \frac{1}{N} \sum_{k=1}^3 z_i^{(k)} z_j^{(k)} \quad (189)$$

where the connectivity vectors correspond to

$$z_i^{(1)} = \sqrt{J_1} Y_{1,-1}(\theta_i, \phi_i), \quad z_i^{(2)} = \sqrt{J_1} Y_{1,0}(\theta_i, \phi_i), \quad z_i^{(3)} = \sqrt{J_1} Y_{1,1}(\theta_i, \phi_i). \quad (190)$$

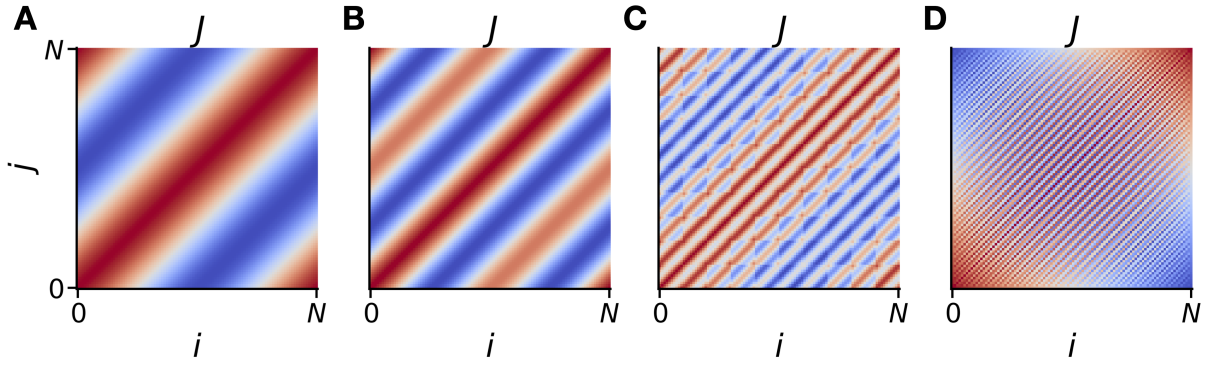


Figure 6: Illustration of connectivity matrices in finite-size networks. A) Rank two ring model; B) Rank five ring model; C) Rank five toroidal model; D) Rank three sphere model.

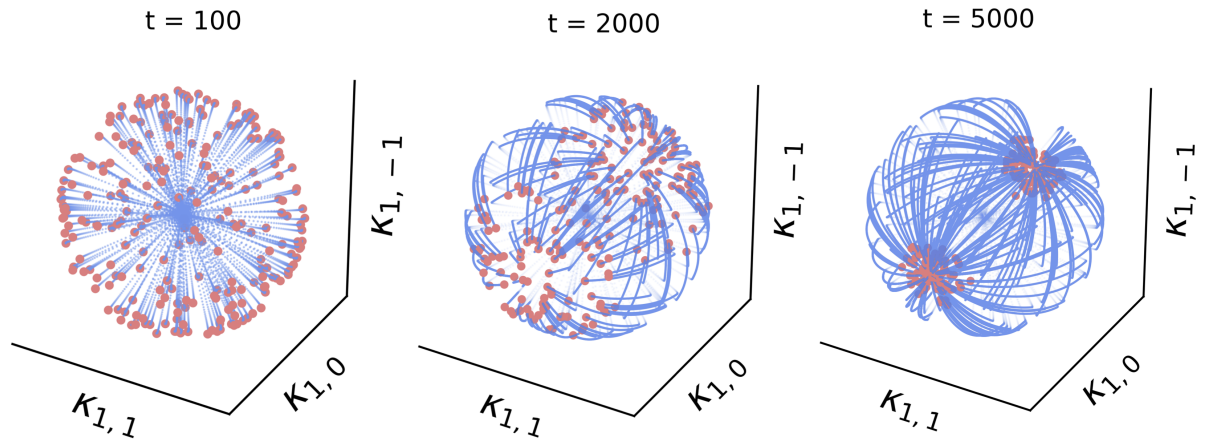


Figure 7: Dynamics in a finite-size spherical RNN with  $N=500$  neurons. Trajectories (light blue) starting from 200 random initial conditions and their position (light red) at  $t = 100, 2000$ , and  $5000$ , showing convergence from random initial conditions to a slow spherical manifold in the  $(\kappa_{1,-1}, \kappa_{1,0}, \kappa_{1,1})$  latent space, and then two fixed points on the slow manifold.